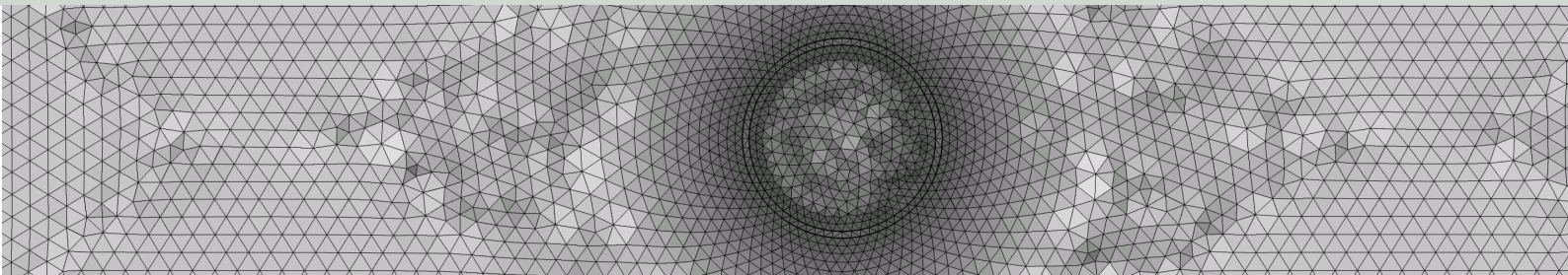




Schweizerische Eidgenossenschaft  
Confédération suisse  
Confederazione Svizzera  
Confederaziun svizra

Swiss Confederation

Eidgenössisches Nuklearsicherheitsinspektorat ENSI  
Inspection fédérale de la sécurité nucléaire IFSN  
Ispettorato federale della sicurezza nucleare IFSN  
Swiss Federal Nuclear Safety Inspectorate ENSI



# Evaluation of a gas experiment Phase I, Final Report – Literature review and scoping calculations

Expertenbericht

im Rahmen der Beurteilung des Vorschlags von mindestens zwei geologischen Standortgebieten pro Lagertyp, Etappe 2, Sachplan geologische Tiefenlager

G. Román-Ross

A. Idiart

F. Grandia

O. Silva

L. Duro

Amphos<sup>21</sup> Consulting S.L.

November 2015

*Disclaimer:*

*Die im Bericht dokumentierten Ansichten und Schlussfolgerungen sind diejenigen der Autoren und stimmen nicht notwendigerweise mit denen des ENSI überein.*

---

# Evaluation of a gas experiment - Phase I Final report

Literature review and scoping  
calculations

**Gabriela Román-Ross**




**Andrés Idiart**

**Fidel Grandia**

**Orlando Silva**

**Lara Duro**

November 2015,

Written by: Gabriela Román-Ross Andrés Idiart 	Reviewed by: Fidel Grandia 	Validated by: Lara Duro 
--	---	---

---

# Table of Contents

<b>1. INTRODUCTION.....</b>	<b>3</b>
<b>2. STATE OF THE ART .....</b>	<b>5</b>
2.1 H <sub>2</sub> GENERATION .....	5
2.1.1 Metal Corrosion.....	5
2.1.2 Radiolysis.....	22
2.2 H <sub>2</sub> CONSUMPTION.....	22
2.2.1 In situ H <sub>2</sub> ad/absorption.....	24
2.2.2 Mineral transformation in clays barriers.....	25
2.2.3 H <sub>2</sub> adsorption in clays.....	28
2.2.4 Reaction catalysed by microbes .....	30
2.3 GAS MIGRATION IN CLAYS .....	33
2.3.1 Data for Opalinus clay.....	34
2.3.2 Data for bentonite .....	37
2.4 UNCERTAINTIES .....	38
2.4.1 Gas generation and consumption by chemical reactions.....	38
2.4.2 Gas transport .....	39
<b>3. SUMMARY OF RELEVANT GEOCHEMICAL PROCESSES.....</b>	<b>40</b>
<b>4. SCOPING CALCULATIONS .....</b>	<b>42</b>
4.1 CALCULATION OF THE TIME NEEDED TO FORM A FREE GAS PHASE .....	42
4.1.1 Results without H <sub>2</sub> consumption by chemical reactions.....	47
4.1.2 Results considering H <sub>2</sub> consumption by chemical reactions.....	49
4.2 ASSESSMENT OF WATER AVAILABILITY FOR THE CORROSION PROCESS .....	51
4.3 EFFECT OF HYDROGEN CONSUMPTION BY CHEMICAL REACTIONS .....	57
4.3.1 Base Case: no consumption .....	59
4.3.2 Hydrogen consumption by pyrite to pyrrhotite reduction .....	63
4.3.3 Hydrogen consumption by microbial activity .....	66
<b>5. CONCLUSIONS OF THE SCOPING CALCULATIONS AND PERSPECTIVES.....</b>	<b>72</b>
<b>6. REFERENCES.....</b>	<b>74</b>

---

# 1. Introduction

In a deep geological disposal facility of high level radioactive waste, various amounts of gas can be generated by different processes. The accurate estimation of the gas generation and accumulation rates for each type of waste depends not only on the waste components, but also on the detailed repository design. Among four possible ways of gas generation (microbial degradation of organic matter, radiolysis, radioactive decay, and corrosion of metal components) the anaerobic corrosion of iron-based elements is reported to generate hydrogen, which is considered to be the major contributor to repository gases (Rodwell et al., 1999, 2003; Volckaert and Mallants, 1999; Johnson, 2006, Duro et al., 2014). The generation, accumulation and release of gases from the disposal facility may significantly influence the long-term radiological safety of the repository via a number of processes (Nuclear Energy Agency, 2001). Therefore, to ensure the long-term safety and performance efficiency of bentonite buffers and host rock, research activities focusing on both experimental and numerical modelling of reactive gas transport through compacted clays are essential.

Prior to gas generation, uniform saturation of the bentonite buffer can be considered, with all the voids filled with water, causing a reduction of the permeability of the buffer to the generated gases. Anaerobic corrosion of metallic canisters and consequent generation of hydrogen gas could initiate before the buffer becomes fully saturated. Senger and co-workers (2008) reported that the corrosion processes start at a relative humidity (RH) of 60% and importantly increases at a RH of 90%, the corresponding values of the degree of saturation are 50% and 90%. Once generated, the flow of H<sub>2</sub> through a saturated buffer could undergo various geochemical processes. As bentonite clay buffers contain significant amounts of chemical species and minerals, gas-chemical/geochemical interactions are of great importance. A number of processes able to consume H<sub>2</sub> such as Fe(III) and pyrite reduction, H<sub>2</sub> adsorption onto clays, and sulphate reduction, have been described in the literature.

ENSI has been a partner in the Mont Terri Project during the past 8 years, mainly aimed at assessing hydro-mechanical aspects of Opalinus Clay. ENSI is currently interested in gas-related issues of the HLW-repository evolution and is evaluating the need and feasibility of conducting a new gas experiment at Mont Terri.

The present document contains a literature review and a set of scoping calculations focused on the chemical aspects of hydrogen gas generation and consumption, as well as on the main features of diffusive gas transport in the pore water of Opalinus clay and compacted bentonite. The scoping calculations performed are listed below:

<i>Scoping calculation</i>	<i>Type</i>
a) Time scale: determine the time needed for the formation of a free gas-phase assuming several chemical reactions for the corrosion leading to gas formation and consumption. The effect of temperature is also analysed	1D axisymmetric diffusion model
b) Assessment of water availability and impact on the hydrogen generation due to steel corrosion	1D axisymmetric fluid flow model
c) H <sub>2</sub> adsorption on mineral surfaces in the bentonite clay	Not considered – lack of data
d) H <sub>2</sub> consumption due to bacteria in the bentonite clay	1D reactive transport model
e) Consumption of H <sub>2</sub> due to reduction of pyrite into pyrrhotite in the system (iron system from the generation of H <sub>2</sub> due to steel corrosion included)	1D reactive transport model

The results of the scoping calculations can be used to categorize the processes to be considered in future field and/or laboratory experiments.

This report provides a general description of the different geochemically relevant processes able to impact on the sources and sinks of hydrogen in the context of the Swiss HLW geological disposal. The main uncertainties associated with the reported data are briefly discussed.

---

## 2. State of the art

### 2.1 H<sub>2</sub> generation

#### 2.1.1 Metal Corrosion

According to the IUPAC recommendations (Heusler et al., 1989), *corrosion is an irreversible interfacial reaction of a material (metal, ceramic, polymer) with its environment, which results in consumption of the material or in dissolution into the material of a component of the environment. Often, but not necessarily, corrosion results in effects detrimental to the usage of the material considered. Exclusively physical or mechanical processes, such as melting or evaporation, abrasion or mechanical fracture are not included in the term corrosion.*

Wastes and their containers, as well as reinforcement steel used in the construction of the repository, are the principal source of gas generation *via* metal corrosion reactions. Main metals to be used and disposed in repositories include carbon and stainless steel, zircalloy, zinc and aluminium. Among all the possible reactions, anoxic corrosion of steel is widely recognized as the main source of hydrogen in this system.

Zero-valent iron is unstable in water (see Figure 1) and corrodes by forming an oxide-type surface layer. During the initial period after closure of the geological repositories, the environment will be oxic, as large volumes of air will be trapped in pores and voids due to the excavation works and the construction of the repository. During this period, no significant amounts of gas will be produced as a reaction product of the corrosion of the metallic overpack (Masum et al., 2012). The trapped oxygen will be consumed by a number of mechanisms, one being oxic metal corrosion. The environmental conditions in the repository will therefore change progressively and become anoxic. Once all oxygen has been exhausted, other oxidants will become active, following the redox ladder shown in Figure 2. When all oxidant species are depleted, corrosion will proceed via water reduction, thus the formation of hydrogen gas will begin to be relevant.

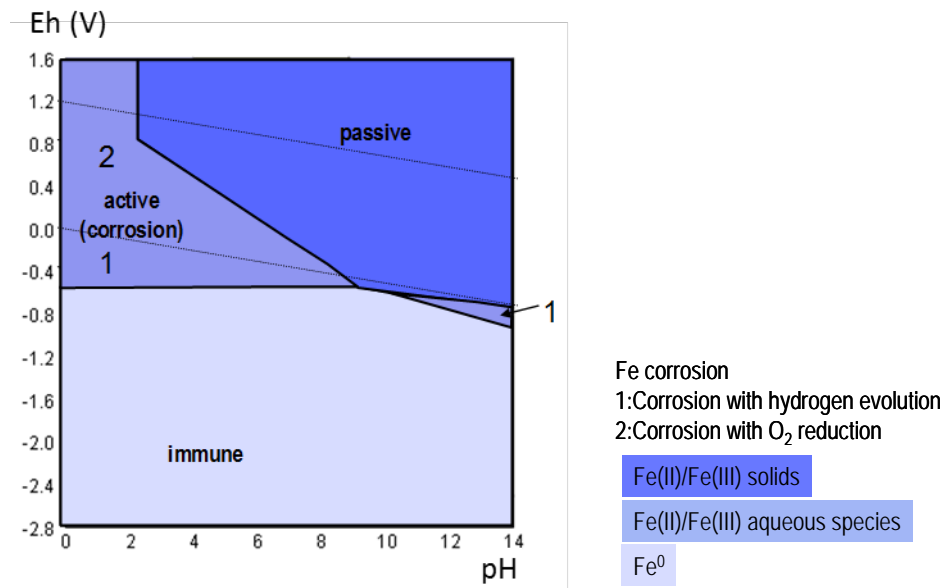


**Figure 1.** Pourbaix diagram of iron, showing the field of stability of iron and its thermodynamic instability in water (dashed lines represent the stability limits of water). The area labelled “immune” covers those conditions where metallic iron is stable and does not corrode, corresponding to very reducing conditions; the area labelled “passive” covers conditions where iron is corroded and forms protective corrosion products on the surface, minimizing the access of oxidants to its surface and then slowing down the corrosion; finally, area labelled “active” covers those conditions under which corrosion occurs more actively. Two different zones can be differentiated in the active area: 1) which indicates that corrosion produces hydrogen evolution, given that it occurs at expenses of water reduction (those areas are out of the stability limit of water) and 2) which stands for those conditions where corrosion involves oxygen reduction.



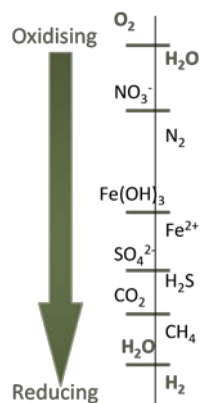


**Figure 2.** Redox ladder showing the oxidation sequence. Oxidants in the left and reductants in the right. Once oxygen is depleted, other oxidants become important. When all oxidising species are absent or inert, water can act as an oxidant, producing hydrogen due to its reduction.

### 2.1.1.1 Corrosion rates and corrosion products under aerobic conditions

The corrosion of carbon steel under aerated conditions in the initial aerobic stage after repository closure is relatively rapid. However, the extent of this process will be closely related to the oxygen availability in the repository environment. Calculations performed for the Swiss design concept under the assumption that  $O_2$  is consumed entirely by steel corrosion at fully saturated conditions indicate timescales for oxygen depletion of about 20-50 years (Wersin, 2003). Similar results have been reported for other geological waste disposals. Wersin and co-workers (1994) calculated timescales for the vertical KBS-3 design on the basis of the reaction of  $O_2$  with pyrite in the bentonite to range from 7 to 290 years. In addition, microbially-mediated and/or inorganic reactions in the host rock are expected to accelerate  $O_2$  consumption rates, as was shown in the REX experiment at Äspö (Puigdomenech et al. 2001) and by the experimental study of Rivas Perez et al. (2005). From all these considerations, the timescale for  $O_2$  depletion is likely to be a few years to a few decades, a very short time period in the long- time frame of a geological disposal.

Under *oxic* conditions, oxygen is the main oxidant producing metallic corrosion. Oxygen reduces itself, gaining electrons, and the oxide ( $O^{2-}$ ) form is produced ( $OH^-$ ). The zerovalent metal loses electrons, being oxidised to  $M^{n+}$ . These two generic oxidation and reduction processes can be exemplified by the following two semireactions:

- Oxidation (anodic reaction):



- Reduction (cathodic reaction):



The metallic cations ( $\text{M}^{n+}$ ) generated in the anodic reaction undergo hydrolysis in the presence of water and precipitate in the form of oxy-hydroxides, the metal corrosion products according to the following reactions (written for the case of iron):



The overall redox reaction can be obtained as follows:



Although oxygen is one of the strongest oxidants in an oxic environment, other species can also cause the corrosion of metals, depending on the environmental conditions.

A large number of studies have been devoted to study the composition and structure of the films formed on Fe and steel under aerobic conditions. King and Stoes-Gascoyne (2000) reviewed these studies and summarized the whole process in the sketch shown in Figure 3. A more detailed explanation about the intermediate products and reactions can be found in King (2008).

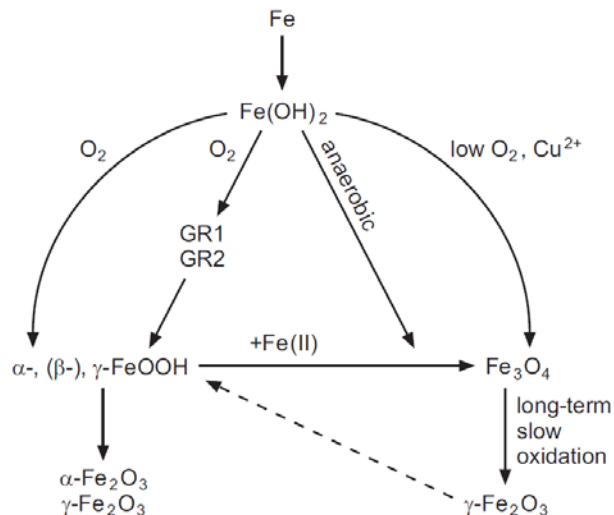


**Figure 3.** Scheme for the formation and transformation of corrosion product films on C-steel (from King and Stores-Gascoyne, 2000). Initial oxidation of Fe in neutral and slightly alkaline solutions leads to the formation of  $\text{Fe}(\text{OH})_2$  which, in turn and under oxidizing conditions, will be oxidized to produce Fe(III)-

---

containing corrosion products. Under anaerobic conditions, complete oxidation of Fe(II) to Fe(III) is very low and mixed FeII/III solid phases are formed. The exact nature and identity of these films is uncertain but the most likely composition is Fe<sub>3</sub>O<sub>4</sub> (Smart et al., 2001). In the presence of high carbonate concentrations and/or bentonite, FeCO<sub>3</sub> prevails (King 2008 and references therein).

The rate at which steel corrosion corrodes under oxic conditions depends on many different parameters, among others: i) initial oxygen concentration, ii) volume of water in contact with metallic surfaces, iii) temperature, iv) pH and v) composition of water.

Figure 4 shows different rates of uniform corrosion measured for stainless steel covered with a passive film under *oxic* conditions (Blackwood et al., 2002; Kursten et al., 2003). As it can be observed, temperature has a noticeable effect on the corrosion rate whereas the system does not seem to be very sensitive to pH changes between 6 and 13. Under hyperalkaline conditions the corrosion rate should be around 0.03 μm/y. Values reported for carbon steel in the same conditions are around 0.08 μm/y (Chambers et al., 1995).

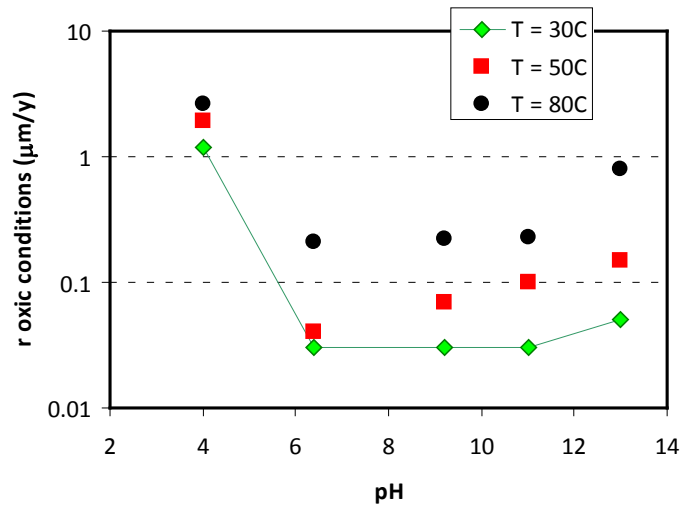


**Figure 4.** Passive corrosion rates for 316L stainless steel covered with a passive film under *oxic* conditions, from (Duro et al., 2012). Data from Blackwood et al. (2002) in Kursten et al. (2003).

---

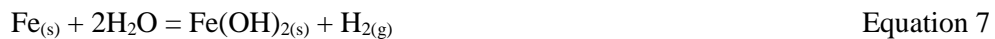
In the frame of the corrosion studies that NAGRA is carrying out in Mont Terri, an *in situ* experiment is currently scheduled in order to investigate aerobic corrosion specifically for carbon steel in contact with bentonite (Diomidis, pers. comm., ENSI Meeting, March 2014). Given that the aerobic corrosion of carbon steel does not produce H<sub>2</sub>, this process is relevant here only because an aerobic period precedes the anaerobic phase and the initial state of the iron-based materials could be modified.

#### 2.1.1.2 Corrosion rates and corrosion products under anaerobic conditions

Zerovalent metals are normally stable under very reducing conditions. However, most transition metals, such as Fe, are not thermodynamically stable in the presence of water, so that its oxidation (corrosion) is the process thermodynamically expected to occur in the presence of humidity (Figure 1). Water can itself act as a metallic oxidant and be reduced by some metals and form hydrogen according to the following semireaction:



The corrosion of iron by water under anaerobic conditions produces hydrogen and iron(II) hydroxide, according to the following reaction:



Fe(OH)<sub>2(s)</sub> is metastable and evolves with time towards the formation of a spinel-like structure oxide, exemplified by magnetite (Figure 3):



The composition of the magnetite film formed on the surface of iron is not exactly known, although it has been suggested that it consists of an oxide Fe<sub>3-x</sub>O<sub>4</sub> with a spinel-like structure varying in composition from Fe<sub>3</sub>O<sub>4</sub> (magnetite), in oxygen-free solutions (Stumm and Morgan 1996). At this point, it should be noticed that the generation of corrosion products may cause an increase of the volume of the metallic wastes stabilised in cement. This process can create mechanical stresses and produce cracks thus enhancing the contact of water with the wastes through the generation of preferential flowpaths. A more effective evacuation of the gases generated due to anoxic corrosion could then occur. A plot of the relative molar volume of the different corrosion products formed under oxic (OX) and anoxic (AN) conditions is presented in

---

Figure 5, from where the increase of the volume of the system and/or the stress generation can be induced.

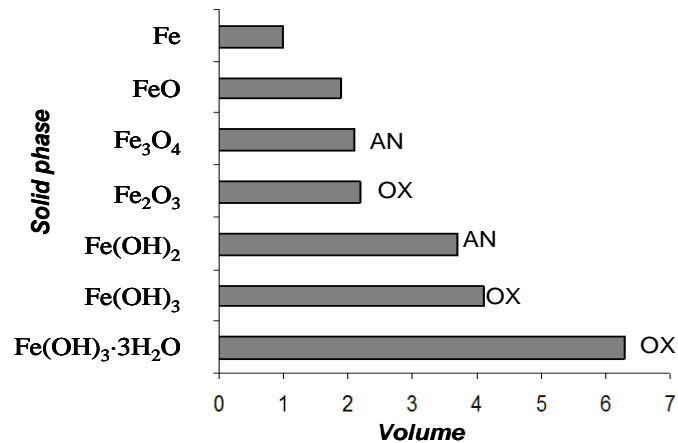


**Figure 5.** Relative molar volume for different iron solid phases. AN: most likely formed from corrosion under anoxic conditions; OX: most likely formed under oxidic conditions (from García Gutierrez et al., 2007).

Iron/steel corrosion can also occur in the presence of carbonates and sulphides. In this case, the corrosion products may change from magnetite to iron sulphides and/or carbonates (siderite), and in the presence of chloride other phases such as the so-called green rusts may form (King, 2008 and reference therein).

Although gaseous hydrogen is written in the chemical reactions, whether a gaseous phase of hydrogen will or not be produced will depend, among other parameters, on the activity of hydrogen generated, the overall pressure of the system and the ability of dissolved hydrogen to diffuse out of the confined system. The global reaction (eq. 8) for the transformation of iron into magnetite indicates that 4 moles of water will be needed for the oxidation of 3 moles of iron, and 4 moles of hydrogen will be produced (Agg, 1993). However, an accurate estimation of the rate of generation of H<sub>2</sub> and Fe(II) corrosion products, requires a value for the rate of anaerobic corrosion. An extensive review on the corrosion of carbon steel under anaerobic conditions has been published by King (2008). In that work, based on a compilation of several studies, the authors highlight that the corrosion rate decreases with increasing length of exposure.

---

It should be pointed out that corrosion rates reported in the nuclear waste management literature are typically determined from either the weight loss or from measurement of the rate of H<sub>2</sub> evolution. Because of the decrease in rate with time due to film formation, the rates determined from these two techniques are not strictly comparable. Weight-loss corrosion rates are averaged over the entire duration of the exposure period, and the measured rates tend to be overestimated. Rates measured from the evolution of H<sub>2</sub> are more representative of “instantaneous” corrosion rates characteristic of the rate of corrosion at the time of measurement. This method is very sensitive and allows monitoring corrosion rate evolution. However, even rates determined from H<sub>2</sub> evolution are only an approximation of the instantaneous corrosion rate as the rate is derived from the amount of H<sub>2</sub> evolved between successive measurements and H<sub>2</sub> can be consumed in the process (e.g. reduction of Fe(III)). Corrosion rates can also be determined electrochemically. This is a quick method that can provide information on mechanisms. However, it is difficult to properly account for the effects of time-dependent film formation and the corrosion rate can be overestimated (King, 2008, Diomidis, ENSI Meeting, March 2014).

Smart and co-workers have performed a number of studies on the anaerobic corrosion of C-steel and cast-iron for SKB (Smart et al., 2001, 2002a, b, 2004). These experiments showed that anaerobic corrosion rates declined from the initial values of 10-30 µm/y to low values of 0.1 µm/y upon growth of a protective magnetite layer. The long-term corrosion rates of carbon steel determined in presence of compacted bentonite saturated with NaCl at pH 8.4 showed no significant influence of temperature within the range of 30-85 °C.

A number of relevant corrosion studies were performed as part of the Nagra’s programs in the 1980’s (Kreis and Simpson 1992, Schenk 1988, Simpson 1984, Simpson and Valloton 1986, Simpson and Weber 1992, Simpson et al. 1985) by using a combination of mass-loss and H<sub>2</sub>-generation measurements. Various natural and synthetic groundwaters, as well as NaCl solutions of different pH values (controlled by addition of HCO<sub>3</sub><sup>-</sup>/CO<sub>3</sub><sup>2-</sup>) were used at test temperatures between 25°C and 140°C. All the reported rate measurements evidence a variety of behaviour depending on the experiment. The whole results suggest a mean corrosion rate of C-steel of 1-3 µm y<sup>-1</sup> for the short-term (8-16 days) H<sub>2</sub> generation rates and 0.1 µm y<sup>-1</sup> for the long-term (45 days) corrosion rates. Under near-neutral conditions, the corrosion rate reached a maximum value at temperature between 50 and 80 °C. Natural and synthetic groundwater solutions produced

---

higher corrosion rates than saline concentrations. However, a correlation between corrosion rate and Cl concentrations have not been found.

The Japan Nuclear Cycle Development Institute (JNC) published a compilation of anaerobic corrosion rates for C-steel as part of the H-12 project (Taniguchi et al., 2004 and 2010). As in other studies, the corrosion rate was found to decrease significantly with increasing time of exposure. The corrosion experiments were performed by immersion in saline (19880 ppm Cl) solution and in saturated compacted bentonite, at pH from 7.9 to 9.4 and between 50 and 90°C. Conversion of the time-averaged mass loss rates to instantaneous rate gives rates of 1-2  $\mu\text{m y}^{-1}$  after 10 years of exposure.

Carbon steel has been a candidate canister material in the Belgian program for a number of years and has been considered in a number of different repository designs. Corrosion studies have been performed in the laboratory and *in situ* in an underground research laboratory. In laboratory testing, mass-loss corrosion rates of  $< 2 \mu\text{m yr}^{-1}$  were observed for various C-steel coupons exposed to de-aerated interstitial water at a temperature of 170°C (De Bruyn et al. 1991, Kursten and Van Iseghem 1999, Kursten et al. 1996).

#### *2.1.1.3 Corrosion rates and corrosion products under anaerobic condition in the presence of bentonite*

In compacted clay systems the corrosion rate is lower compared with that determined without clays and steady-state conditions are reached in a period of 2-4 years. In bulk solutions the corrosion rate is stabilised in a period of approximately six months (King, 2008). There is a significant body of evidence that indicates an anaerobic corrosion rate of the order of 1-2  $\mu\text{m yr}^{-1}$  in systems containing compacted clay. The protective films tend to be carbonate-based rather than magnetite-based (King, 2008). The findings of Smart and co-workers (2004) in systems exposed to de-aerated bentonite slurry at different temperatures indicate that corrosion rates were slightly higher initially than those observed in groundwater solutions, but the long-term rate after  $\sim 1.5$  y was similar ( $\leq 1 \mu\text{m y}^{-1}$ ). The studies performed by Nagra provide corrosion rates for cast steel of the order of 8-12  $\mu\text{m y}^{-1}$  for the higher density bentonite and 14-29  $\mu\text{m y}^{-1}$  at the lower density (Simpson and Valloton., 1986). Xia et al. (2005), who also performed corrosion studies in compacted bentonite, yielded low corrosion rates of 0.1  $\mu\text{m}$  over a corrosion period of 5 months. Taniguchi et al.(2004) conclude that the anaerobic corrosion rate of C-steel in compacted

---

bentonite was  $\leq 1 \mu\text{m y}^{-1}$  at 80 °C and  $2 \mu\text{m y}^{-1}$  at 50°C. The long-term corrosion test for carbon steel performed in situ with probes inserted in direct contact with the Boom clay produced rates in the range of 2-9  $\mu\text{m y}^{-1}$ . The corrosion rates increased with increasing temperature but decreased with increasing exposure time.

In order to solve some discrepancies in the results obtained from different experiments, in the frame of the FORGE project, several experiments were focused on the measurement of hydrogen evolution from carbon steel plates in anaerobic conditions at different temperatures under contact with compacted bentonite (Bhuha et al., 2010). It was found that the corrosion rate, and consequently hydrogen generation rate, of carbon steel in anaerobic environment depends on a large number of factors, such as temperature, the ratio of amount of water to metal or contact of bentonite with metal, geochemical conditions being affected also by corrosion itself. Contrary to some previous work (Vokál et al., 2007), it was not possible to conclude that corrosion rate will decrease or will be constant all the time after the first decrease caused by the creation of a protective corrosion layer on the surface of metal. The results suggest that due to the change of the nature of the corrosion product layers due to the change of geochemical conditions, hydrogen evolution rate can even increase again.

Bruha et al., (2010) reported increase of the rate of corrosion by one order of magnitude when carbon steel is in direct contact with bentonite under anaerobic conditions. The average corrosion rate of carbon steel after 10 and even 20 days was over 45  $\mu\text{m/yr}$ . Only after 30 days it decreased to 26  $\mu\text{m/yr}$ . Nevertheless, these results were fraught with experimental difficulties, such as the failure of devices to avoid hydrogen leaking, so that these observations still need additional validation.

Currently, Diomidis and co-workers are studying the corrosion of carbon steel EN 10248-1 wires in presence of MX-80 bentonite compressed to 1500  $\text{kg/m}^3$  at 60°C under anaerobic conditions (ENSI Meeting, March, 2014). The obtained results up to now from this experiment are summarized in Figure 6. The corrosion rate at 60°C is initially 30  $\mu\text{m y}^{-1}$  but decreases to 0.7  $\mu\text{m y}^{-1}$  after about 24,000 hours and continues to decrease over time. An average weight loss corrosion rate of 3.3  $\mu\text{m y}^{-1}$  is reported that roughly agrees with the integral of the gas generation. More measurements and characterization of the materials are on-going.



In addition and with the aim to analyse the interface between rock and carbon steel and monitor the rate of carbon steel in the environmental context of the nuclear waste repository, an in-situ experiment (IC experiment) is being carried out since 2008 at Mont Terri. Corrosion rates measurement by using Electrochemical Impedance Spectroscopy (EIS) at 85° C have started in 2010. The experimental results show that the CR is in the range 0.6-2  $\mu\text{m yr}^{-1}$  (Figure 7). The CR values decrease over time due to the passivation of the metal surface. A good reproducibility of the results is obtained from two different carbon steels and confinement is confirmed to play an important role to maintain low corrosion rates. On-going experiments will focus on the corrosion rate measurement to check the stability of the CR over time and the impact of the chemical composition of the pore water.

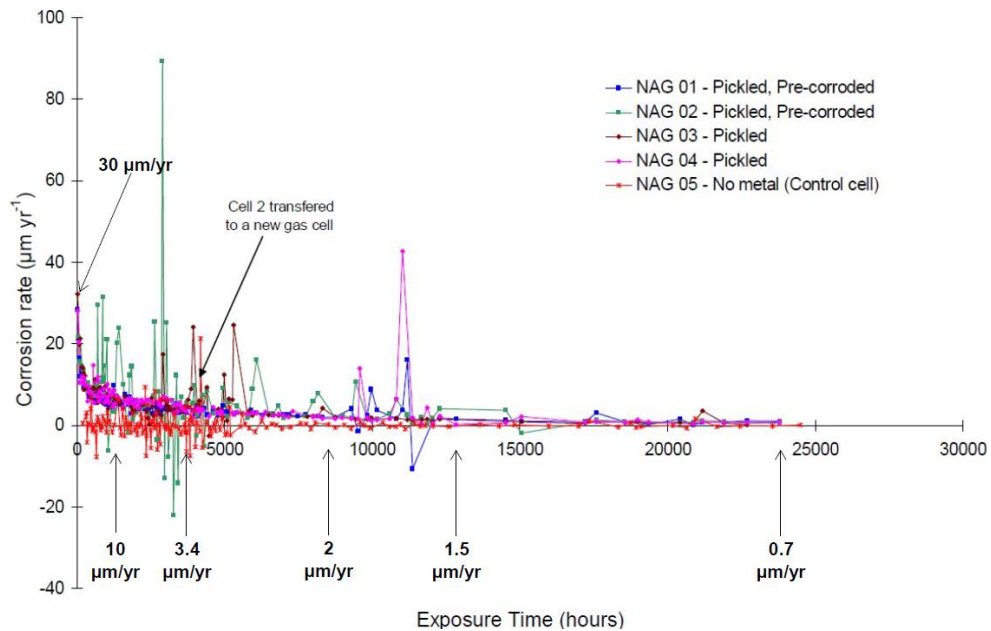


**Figure 6.** Corrosion of carbon steel in bentonite (gas cells) (from Diomidis and Johnson, 2014).

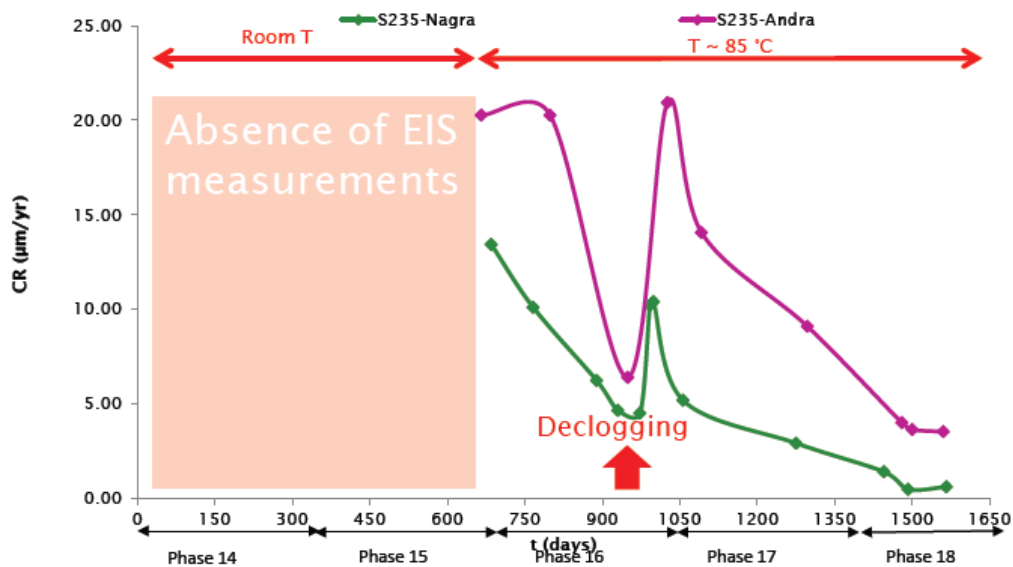


**Figure 7.** Results from the IC experiment (Mont Terri project) (Necib, 2014, ENSI Meeting, March 2014).

A conservative corrosion rate of carbon steel under anaerobic conditions in the presence of bentonite of  $2 \mu\text{m}/\text{y}$  has been selected by Diomidis (2014) arising from expert judgement. The same author derives statistically a value of  $0,43 \pm 0.23 \mu\text{m}/\text{y}$ , by giving equal weigh to all data included in the literature review. To our judgement, and as also recognised in Diomidis (2014), statistically derived rates tend to include uncertainties that can be related to the relevance of the experiments for the purpose of the assessment, so that we would recommend a value based on expert judgement. In the present study we are selecting a reference value of  $1 \mu\text{m}/\text{y}$  for this parameter, derived after examination of literature values and a sensitivity analyses is also included by varying the corrosion rate over the range of values determined in the open literature, from  $0,1 \mu\text{m}/\text{y}$  to a value of  $20 \mu\text{m}/\text{y}$ , and including a very conservative value of  $100 \mu\text{m}/\text{y}$  only for the sake of assessing the impact of this parameter on hydrogen gas generation.

#### 2.1.1.4 Corrosion rates and corrosion products under anaerobic, alkaline conditions

##### *Corrosion of steel*

An important issue in the safety assessment of low and intermediate level radioactive waste repositories is the production of  $\text{H}_2$  by metal corrosion in presence of cement grout. To this end, Nagra and the University of Toronto started a collaboration to measure the corrosion rate of

---

carbon steel foreseen in the Swiss L/ILW inventory, under conditions representative of those prevailing in a deep geological repository. The experimental measurements have been performed with a solid-state oxide probe able to detect 1 ppm H<sub>2</sub> which corresponds to a corrosion rate detection limit of 0.1 nm y<sup>-1</sup> (Newman and Wang, 2014). In that study, carbon steel is embedded in grout under 100% RH at 30 and 50 °C. The obtained long-term corrosion rates were consistent within the 1-4 nm y<sup>-1</sup> range irrespective of the environment, which is at the lower end of the values reported in the literature for similar conditions. However, blank tests with grout and no steel indicate that cement also react with water evolving hydrogen. Heating the cement up to 700°C, H<sub>2</sub> production is reduced but not eliminated in the blank tests. This fact should be carefully evaluated in future experiments.

Important differences in the corrosion rates are reported in the literature depending on the environmental conditions and the type of steels. Kursten et al., (2003) compiled the measured corrosion rates during the COBECOMA project for different steels under alkaline conditions. These results show no influence of hydrogen overpressures in the range 1 to 100 atm on the anaerobic corrosion rate of carbon steel in anoxic alkaline conditions, in agreement with Smart et al., (2002, 2002b). All these results provide an estimation of the long-term anaerobic corrosion rate of carbon steel in alkaline media on the order of less than 0.1 μm y<sup>-1</sup> at 30°C and below 1 μm y<sup>-1</sup> at 80°C. Decreasing the pH to circumneutral values resulted in an increase of a factor of 5 in the corrosion rates.

The compilation of rates of steel corrosion performed by Grauer et al. (1988) shows values in the order of 1 μm per year under anoxic and hyperalkaline conditions. Chambers et al. (1995) reported carbon steel corrosion rates below 0.1 μm per year at 30°C, and lower values below 0.01 μm per year for stainless steel. The findings of Fujiwara et al. (2001) under anoxic and hyperalkaline conditions, mention measured corrosion rates in the order of 5-10 nm per year at 35°C from experiments running for 60 days. From a compilation of experimental study, Smart and Hoch (2006) provided a value of 0.01 μm per year as the rate of corrosion of stainless steel under anoxic and hyperalkaline conditions.

The solubility of iron, as well as nature of the solid corrosion products, influences greatly the kinetics and mechanism of reaction of steel embedded in cement or concrete. At high pH, the surface of the steel is covered by the passivating layer of magnetite. However, according to Sagoe-Crentsil and Glasser (2003), at pH 13 the presence of low chloride ion concentrations are adverse

---

to spinel formation, and the solubility-limiting solid corrosion becomes “green rust”, a layer-structured hydrate containing both  $\text{Fe}^{2+}$  and  $\text{Fe}^{3+}$  and Cl. The enhanced solubility of iron, probably as an aqueous chlorocomplex, allows it to be transported and precipitated from the complex as corrosion product being disseminated within the paste.

As several discrepancies exist on determination of corrosion rates in cementitious conditions, an experiment aiming to measure gas production due to corrosion in conditions relevant for L/ILW repository is in progress in the frame of the Mont Terri project. Measurements are performed under fully saturated conditions at two different temperatures (30°C and 50°C). Hydrogen production is periodically measured with an  $\text{H}_2$  sensor which detection limit about 1 ppm  $\text{H}_2$ :  $0.1 \text{ nm y}^{-1}$ . The experimental results are shown in Figure 8 (Newman and Wang, 2014, ENSI Meeting, March 2014) where results obtained from other studies are integrated. Measured corrosion rates of carbon steel are at the lower limit of those reported in the literature ( $1\text{-}3 \text{ nm y}^{-1}$ ). Temperature appears to have a strong impact on the anaerobic corrosion of steel in grouts. At present these results are pending of confirmation and more experiments are in progress.

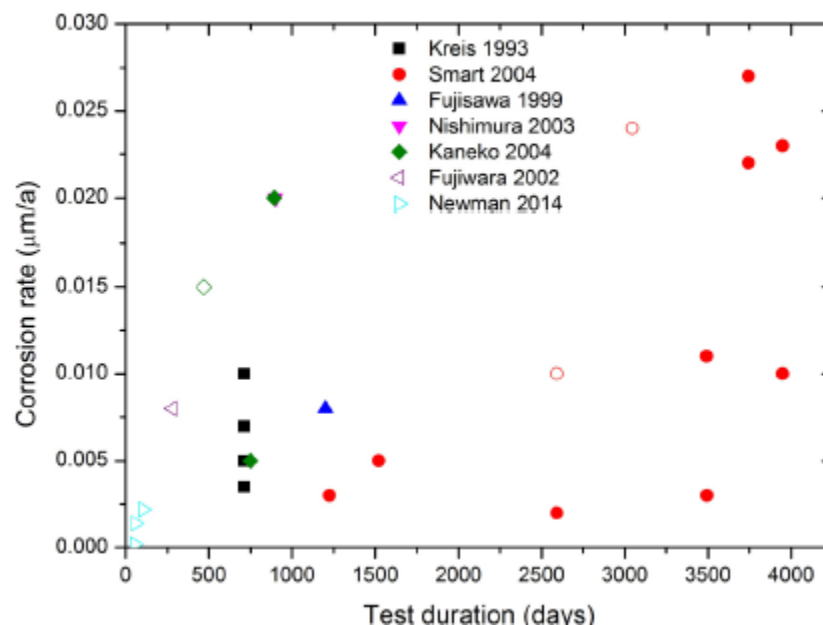


**Figure 8.** Comparative results from corrosion rates in presence of cement (Diomidis, 2014.). Open symbols correspond to cement and closed symbols to solutions.

---

### *Corrosion of other metals*

As above mentioned, hydrogen gas can be also produced by reduction of other metals present in the repository. The impact of this process will be determined by the final inventory for the waste disposal. Principal metals, other than steels, to be used and buried in repositories include: zircalloy (metal waste), Zn and Al (metal waste). They can produce H<sub>2</sub> according to the following reactions:



When aluminum is exposed to air, an oxide layer is formed, which generally provides protection to further corrosion. It can also corrode under anoxic conditions, forming also a very protective passive layer that prevents further oxidation. At high alkalinity this oxide layer re-dissolves to form soluble aluminum species thus exposing the bare metal that further corrodes to produce aluminum hydroxide, also releasing hydrogen gas (eq. 13).



In the presence of cementitious materials the product of corrosion is less dense than the metal and hence it occupies more volume. This may lead to stress within cement matrix and possibly leading to cracks.

The experimental corrosion of Al and Zn under anaerobic alkaline conditions has been performed by Fujisawa et al. (1997) Smart and Blackwood (1998). They suggested a conservative corrosion rate up to 0.1 mm·y<sup>-1</sup> because of the galvanic coupling due to the contact with steel waste. However, this value may unrealistically overestimate the actual rate.

For Zircaloy, the measured rates at a pH of 12.5 to 13 are significantly lower, down to 1 nm·y<sup>-1</sup> (Kurashige et al., 1999; Wada et al., 1999).

A summary of the corrosion rates obtained from the review of the available data for the different metals, including zircaloy is shown in Table 2-1.

**Table 2-1.** Rates of corrosion of different metals and alloys under alkaline conditions developed by the presence of cement and concrete. All corrosion rates are given in m/y. Reference value in NAB 14-21

	Reference value	Upper boundary	Upper value from:
C- steel	$2 \cdot 10^{-8}$	$1 \cdot 10^{-7}$	Based on (among others) data in Cobecoma project
Stainless steel, Ni-alloys	$1 \cdot 10^{-9}$	$1 \cdot 10^{-8}$	Based on (among others) Smart and Hoch (2006)
Aluminium	$1 \cdot 10^{-5}$	$1 \cdot 10^{-4}$	Based on Fujisawa et al. (1997) and Smart&Blackwood (1998)
Zinc	$1 \cdot 10^{-4}$	$3 \cdot 10^{-4}$	Three times safety range from data in (among others) Fujisawa et al. (1997) and Smart&Blackwood (1999)
Zircaloy	$1 \cdot 10^{-9}$	$3 \cdot 10^{-9}$	Three times safety range of data from Kurashige et al., (1999); Wada et al., (1999)

#### 2.1.1.5 Iron corrosion induced by microbial activity

Microbial activity is known to influence iron corrosion. For example, the presence of sulphate reducing bacteria (SRB) on the surface of steel may lead to increased attack by sulphide and thus affect the formation of the protective oxide layer. Moreover, iron-reducing bacteria (IRB) might be active by attachment to the magnetite layer and promoting reductive dissolution of the Fe(III) component (Kostka and Nealson 1995; Dong et al. 2000). In addition, the possibility of autotrophic methanogenic bacteria promoting degradation of inorganic carbon by using the hydrogen source could be relevant. Enning and Garrelfs (2014) provide a thorough review of bacterial mediated iron corrosion and the different findings of MIC (microbial iron corrosion). The corrosion process occurs, although there are many observations that point towards neglecting MIC as under the conditions of high level radioactive waste storage, mainly due to the presence of compacted bentonite. Motamendi et al. (1996) conducted experiments of iron corrosion by SRB under the presence of compacted bentonite. Those authors concluded that the main limitation of bacterial survival was the water activity. Indeed, bacteria can survive under high pressures, high temperatures, and scarcity of nutrients, but they could not survive under too low water activities. Motamendi et al. (1996) experiments were designed to assess the minimum water activity needed for SRB to survive. The authors found that the process of microbiologically induced sulphide corrosion in a canister in bentonite would be restrained if the water activity is below 0.96. Based on observations of archaeological analogues it can be concluded that the

---

microbial effects on corrosion rates are not expected to be very large. If SRB were active at the steel container surface, precipitation of a sulphide layer would be favoured, which would also be protective against high corrosion. However, increased pitting may also occur in this case (Johnson and King, 2003). Similarly, the build-up of  $\text{Fe}^{2+}$  by IRB on magnetite-coated steel would be limited by sulphide and siderite precipitation as well as by the slow dissolution kinetics (Dong et al., 2000).

Other studies performed in compacted bentonite showed that clays can act as an efficient filter towards microbes. As shown by Pusch (1999), sulphate-reducing bacteria (SRB) are immobile in bentonite exceeding  $1.9 \text{ Mg m}^{-3}$  saturated density. Moreover, experiments performed by Pedersen (2000) showed that the activity of SRB in bentonite ceases at dry densities higher than  $1.5 \text{ Mg m}^{-3}$  in agreement with the results by Motamendi et al. (1996) previously cited. Based on more recent studies (Stroes-Gascoyne et al. 2006), a swelling pressure criteria of  $> 2 \text{ MPa}$  for the buffer has been defined by SKB (SKB 2006a) in order to prevent bacterial activity. This swelling pressure corresponds to a buffer density of  $1.8 \text{ Mg m}^{-3}$  (SKB 2006b). Studies performed by JNC (2000) confirmed that SRB introduced into 70/30 bentonite / sand mixtures at a dry density of  $1.6 \text{ Mg m}^{-3}$  surrounding steel samples had no effect on corrosion rates and were not cultivatable after the test.

#### *2.1.1.6 Natural analogues/observation in nature*

Since experimental studies can assess only a limited time frame, natural and archaeological analogues can yield valuable information. Data from the archaeological analogues compare well with those from short-term laboratory experiments under anaerobic conditions. The studies of Johnson and Francis (1980) presented data on more than forty iron archaeological objects and estimated corrosion rates between  $0.1$  and  $10 \text{ }\mu\text{m}$  per year, in agreement with the values taken in the assessments. This suggests low and relatively uniform long-term corrosion rates in spite of very different geochemical environments. The number of observations used in this study confirms the statistical value of this estimation, which compensates for the uncertainties linked to their initial state (Féron et al., 2008).

Regarding the metallic corrosion under hyperalkaline conditions, only some analogues for cementitious environments, such as Maqarin in Jordan are recognized (Miller et al., 1994).

---

Specifically in this site, the redox conditions were not anoxic but oxidizing, so that, no analogy for metal corrosion rates of relevance for LILW repositories can be established.

Observations from archaeological objects buried in sediments (David, 2001) showed the presence of magnetite and iron sulphides and to a lesser extent of siderite, on iron surfaces. In addition to hydroxide, sulphide and carbonate, corrosion-released Fe(II) may react with dissolved silicate and the solid clay fraction. This reaction can be schematically written as:



Little is known about the details of this process, such as the nature of the iron silicate phases and the thermodynamic and kinetic constraints.

### **2.1.2 Radiolysis**

Radiation may produce gases and substances through radiolysis that can affect corrosion rates and type of corrosion products. Although this effect has been proved under high dose rates expected in high level wastes, nor evidences for, neither against the effect of radiolysis on metallic corrosion under the low dose rates expected in ILLW have been found in the literature.

The rate of production of hydrogen gas by radiolysis for the case of disposal of HLW is assumed to be a small fraction of that from corrosion of steels, principally because of the substantial wall thickness of the canister and the relatively rapid decay of the gamma intensity (Lemy et al., 2010). As a result, the production rate of gas due to radiolysis is not incorporated in calculations of gas build-up and dissipation.

## **2.2 H<sub>2</sub> consumption**

As mentioned in the previous sections, hydrogen gas will be especially produced by anaerobic corrosion of radioactive waste containers in the geological repository. As a consequence of this production, gas migration through bentonite-based buffer materials is a key issue for geological waste disposal. This processes involved mechanics and chemical changes that could affect the long-term evolution of the barriers.



The solubility limit of H<sub>2</sub> in the porewater near-field at repository hydrostatic pressure is expected to be reached within 1,000 years due to the slow diffuse transport through the Opalinus clay (Lemy et al., 2010). In Figure 9 a sketch of the expected transport mechanisms is presented in order to illustrate the evolution of the H<sub>2</sub> in the context of the HLW repository.

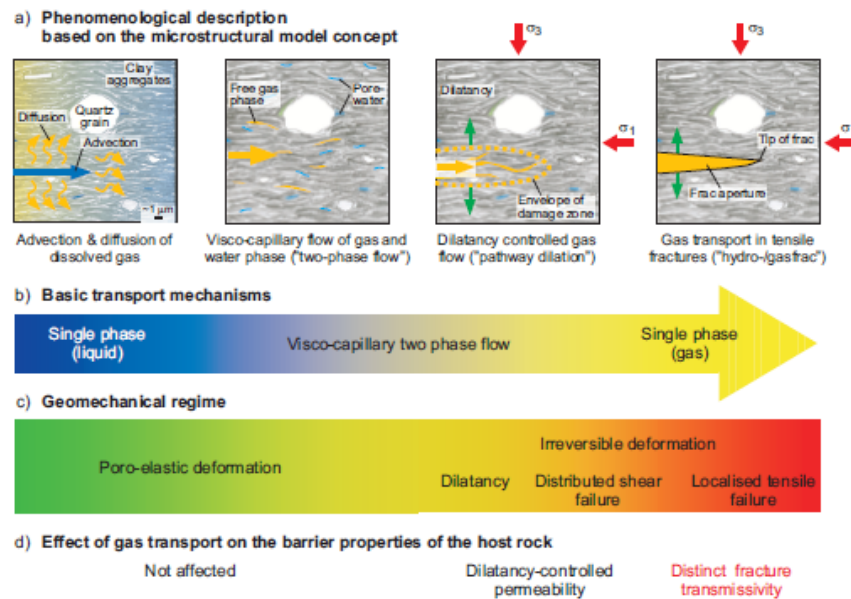


**Figure 9.** Gas transport processes in Opalinus Clay (from Nagra, 2008) ).

Due to its high reactivity and its continuous production for about 100,000 years, the interaction with gas could affect the properties of the Opalinus clay. The reductive capacity of H<sub>2</sub> could change the redox properties of the clay barrier environment, and therefore (1) its mineralogy, (2) the speciation of aqueous species and, in consequence, (3) their transfer.

Several elements such as the structural Fe(III) in the clay fraction or minerals like pyrite may react with H<sub>2</sub> and undergo chemical and mineralogical transformations. On the other hand, iron released from the corrosion process will not only precipitate as separate corrosion products, but may also interact with the clay matrix via sorption. In addition, reduction of aqueous/mineral sulphates and other oxidized species present in the porewater may induce a change in the geochemical conditions prevailing in the initial argillite.

---

In this section the main chemical reactions able to consume H<sub>2</sub> in the context of the Swiss HLW repository are summarize and discussed.

### 2.2.1 In situ H<sub>2</sub> ad/absorption

Of the total amount of H<sub>2</sub> generated by the anaerobic corrosion of C-steel, only a small fraction is absorbed by steel and can potentially degrade the container. However, the rate at which hydrogen is absorbed is related to the rate at which it is generated. In a saturated repository, therefore, the bentonite pore water will rapidly saturate with dissolved H<sub>2</sub> and a separate gas phase will be formed. The threshold pressure for the formation of the separate gas phase will be equivalent to the sum of the hydrostatic pressure at the repository depth and the breakthrough pressure in the bentonite, which in turn is approximately equal to the bentonite swelling pressure. Therefore, at a repository depth of 650 m with a bentonite dry density of 1.6 Mg·m<sup>-3</sup>, the threshold pressure would be of the order of 6-8 MPa (King and Kolar 2009). In this environment, hydrogen could be absorbed by C-steel from both the gaseous and aqueous phases.

In the case of molecular hydrogen in aqueous solution, dissolved H<sub>2</sub> and adsorbed H<sup>+</sup> (or H<sub>2</sub>O in neutral and alkaline solution) can be in equilibrium



The adsorbed H<sup>+</sup> can then lead to the absorption of H atoms from the original dissolved H<sub>2</sub> molecule. There are relatively few direct measurements of the hydrogen absorption efficiency. However, based on the data reported by Gajek and Zakroczyński (2005), it can be concluded that the efficiency of this process is extremely low and it can be neglected in calculation of H<sub>2</sub> consumption in the near field.

Hydrogen absorption from the gas phase involves three processes (King, 2009):

1. Physical adsorption (also referred to as physisorption)
2. Dissociative chemical adsorption (also referred to as chemisorption)
3. Hydrogen entry (or absorption)

The relevance of these processes as consumer of H<sub>2</sub> is widely discussed by King (2009) and conclusions point out that hydrogen adsorption/absorption from the gas phase in the frame of the

---

Swiss HLW geological disposal has an extremely low efficiency due to unfavourable environmental conditions.

## 2.2.2 Mineral transformation in clays barriers

### 2.2.2.1 Reduction of Fe(II)/Fe(III) by H<sub>2</sub>

The high specificity and reactivity of Fe determine the relevance of the interaction clay-H<sub>2</sub> from the presence of iron minerals or structural/adsorbed Fe in the barriers. Iron released from the corrosion process can precipitate as separate corrosion products or interact with the clay matrix via sorption. Under reducing conditions, Fe(II) sorption processes will be predominant (Andra 2005; Tournassat 2003; Charlet and Tournassat 2005). The whole process can be summarized as follows: under reducing conditions, sorption of Fe<sup>2+</sup> to montmorillonite occurs like other metal cations such as Ni(II) or Zn(II) (Bradbury & Baeyens 1997) by cation exchange in the interlayer and surface complexation to edge sites. In general, sorption of Fe<sup>2+</sup> was shown to be extremely strong, above pH values of 4. At low pH, Fe<sup>2+</sup> was shown to sorb via cation exchange reactions. At pH values between 4 and 7, surface complexation to edge sites was the dominant sorption process. At pH values above 7.0, the interaction process became more complex and both oxidation of Fe<sup>2+</sup> and surface precipitation of a Fe(II) silicate phase were observed.

Reduction of Fe(II) by H<sub>2</sub> is not reported in the literature. Concerning Fe (III), hydrogen gas is not commonly used to reduce ferric ions because of its slow kinetic reaction and the strong influence of temperature and pressure conditions. Lear and Stucki (1985) described a possible reduction of a nontronite (Fe(III) rich member of the smectite dioctahedral clay) at high temperature (370 °C) according to the following equation:



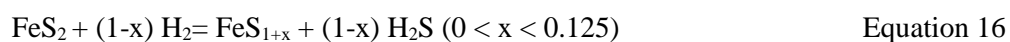
Another study has demonstrated that various oxides and iron hydroxides can be reduced by hydrogen gas, by using either pure hydrogen at 99.99% or a mixture 95% Ar-5% H<sub>2</sub> (Jozwiak et al., 2007). The temperature required for the reaction of Fe(III) depends on the reagent used. It is possible to observe partial reduction of wustite (FeO) at intermediate temperatures (<300 °C) but for total reduction, temperature must be higher (> 500 °C).

---

The reduction induced by hydrogen gas in the range of temperatures of interest for the geological disposal (25–150 °C) has not been much studied in the past. In a recent publication, Didier et al. (2012) reviewed the available information on this topic and showed a set of experiments aimed at estimating hydrogen gas interaction with clayrocks in terms of redox reactivity with structural Fe (III). The experiments were performed with several clay samples with variable Fe(III) contents. Their results evidence that the amount of consumed H<sub>2(g)</sub> in the reaction does not depend on the structural Fe(III) content of clays. In fact, the synthetic sample, which adsorbs the highest amounts of H<sub>2</sub> is one of the samples without Fe(III). Therefore, it can be concluded that the presence of structural Fe(III) in clays does not have an important impact on hydrogen gas consumption.

### 2.2.2.2 Reduction of pyrite by H<sub>2</sub>

According to the chemical composition of the Opalinus clay provided by Bosart and Wermeille (2003), pyrite contents are between 1 and 3%. This mineral is thermodynamically unstable in the presence of H<sub>2</sub> and it is reduced to pyrrhotite or troilite according to the following reaction:



Pyrite thermal degradation into pyrrhotite induced by H<sub>2</sub> has been previously investigated by thermogravimetric analysis over a temperature range of 350-700° C. However, because of dry conditions and extremely high experimental temperature these results cannot be extrapolated to the geological waste disposal context (Wiltowski et al., 1987; Lambert et al., 1998).

The kinetics of abiotic redox reactions induced by hydrogen has been reported by Truche et al., (2010). The authors present an experimental kinetics study of pyrite reduction into pyrrhotite under significant H<sub>2</sub> pressure (0-18 bar) and mid-hydrothermal conditions (90-180° C) in a pH range of 6.9 to 8.7. The results showed that pyrite is partially reduced to pyrrhotite under slightly alkaline conditions, in the presence of H<sub>2</sub> and mild hydrothermal temperatures. The reaction that kinetically controls the whole process was described as a coupled dissolution-precipitation mechanism. A rate expression is proposed for sulphide production (eq. 17) related to time (t in hours), H<sub>2</sub> partial pressure (PH<sub>2</sub> in Pa) and temperature (in K) as follows:

$$\log_{ns(-2)} = -5.22 + 0.47 \log t + 1.10 \log PH_2 - 2755/T \quad \text{Equation 17}$$

In a more recent publication, Pichler (2013) compared the results obtained from a set of simulations based on a thermodynamic model with the findings of Truche and co-workers (2010).

---

The fluid-gas-rock interaction model performed by Pichler (2013) aimed to make a quantitative assessment of the role of H<sub>2</sub> on the geochemical behaviour of a multi-mineral system. In this study, the mineralogical composition of 2 cores from the Upper Austrian Molass Basin was used to define the conceptual model. Pyrite was the only sulphur-bearing mineral found in the core samples and low concentrations of aqueous SO<sub>4</sub> were measured in the porewater. The model conditions were 80°C and 230 bar. pH was buffered by carbonate (calcite, dolomite) reactivity although the model predicts that H<sub>2</sub> injection leads to a progressive shift to alkaline conditions (from 7 to 9) .

The results of these simulations showed that only this minor amount of sulphate is converted into other sulphur bearing species and that pyrite stays stable. According to Truche and co-workers (2010), pyrite should react under the influence of hydrogen generating H<sub>2</sub>S and HS<sup>-</sup>. Two reasons have been pointed out by Pichler (2013) to explain these discrepancies: 1) Truche et al (2010) used fine grained pyrite treated with pure hydrogen at temperatures of 90 to 120°C which offered a greater surface for reactions taking place and, 2) the introduction of other minerals to the experiment could modify the pyrite behaviour. In the presence of calcite and dolomite, the reaction stopped, which suggests that carbonates work as a buffer that keeps the pyrite stable. As expected, hydrogen increases the porewater pH and leads to dissolution of dolomite, and a precipitation of calcite. Once all the carbonates had been dissolved or converted, pyrite immediately started to dissolve. The validity of these results is established for temperatures below 100 °C.

In order to solve the discrepancies between these studies, it should be useful to perform an experiment with the specific materials involved in the Swiss repository. Clearly, the results reported by Truche et al. (2010) represent an overestimation of the impact that could have this process in natural or engineered environments. Their experiments have been performed under maximum reactive conditions, with a fine-grained pure mineral (pyrite). As shown by Pichler (2013) the presence of other minerals, such as carbonate, could mitigate the reduction of pyrite and, in consequence, H<sub>2</sub> consumption. In section 4.3.2, we present the results for a numerical simulation of pyrite reduction to pyrrhothite assuming the rate proposed by Truche et al. (2010). The results of these simulations are discussed in the frame of the physicochemical conditions prescribed for the Swiss repository.

---

### 2.2.2.3 Reduction of sulphate by $H_2$

Sulphate reduction induced by  $H_2$  is another process that could be relevant in the context of clay barriers, as sulphate contents of around 2.3 g/L have been measured in Opalinus Clay pore water (Diomidis, 2014, ENSI Meeting, March 2014). This process can be induced by microbial activity, BSR (Bacterial sulphate reduction) or thermodynamically, TSR (Thermodynamic sulphate reduction). The first process is better understood than inorganic reduction and it is detailed in section 2.2.4.

Sulphate reduction by  $H_2$ , likely to occur in deep geological waste storage sites, was studied experimentally by Truche and co-workers (2009) in a two-phase system (water + gas) at 250-300° C and under 4-16 bars  $H_2$  partial pressure. The objective of this study was focused on the assessment of the nature and rate of sulphate reduction under significant  $H_2$  pressure as a function of temperature, pH, sulphate speciation and gas pressure. The experiments showed that the half-life of sulphate in the presence of  $H_2$  ranges from  $2.1 \cdot 10^5$  to  $2.7 \cdot 10^9$  years at 90 °C. The rate of sulphate reduction is not significantly affected by  $H_2$  pressure in the range of 4-16 bars in the pH interval of 2-5. In summary, extrapolation of the rate function to the temperature interval of a geological storage of nuclear waste, assure that sulphate reduction by homogeneous reaction can be neglected in the nuclear waste storage performance assessment.

### 2.2.3 $H_2$ adsorption in clays

Hydrogen could also be retained in the clay barriers because porous materials may adsorb gas due to their high surface area. In the past few years, several studies estimate the interactions between clay materials and gases like carbon dioxide or methane in terms of saturated gas diffusion and excess sorption at high pressure (Bush et al., 2008). Most of these previous works highlighted that gas sorption mainly occurs on clay fraction and varies with organic matter content due to geochemical reactions. Specifically for studies on hydrogen gas storage on clay materials, maximum concentrations of sorbed hydrogen can reach  $0.85 \text{ mmol.g}^{-1}$  for aluminum polycation intercalated montmorillonites at 77 K and 0.45 bar (Gil et al., 2009). However, the mechanisms leading to gas adsorption are not well understood at this time.

The geochemical behaviour of hydrogen in the subsurface is an issue of great concern for the nuclear waste industry. The first studies focused on hydrogen migration in the subsurface (Galle

---

et al. 1998; Ortiz et al., 2001) and the objective was to find viable solutions of preventing hydrogen escapes. Ortiz et al. (2001) have also evaluated the effects of hydrogen on clay minerals in the vicinity of the storage sites. They studied absorption of hydrogen into the Callovo-Oxfordian clays, and the effect of desaturation processes induced by the presence of hydrogen, which would make the clay brittle and lead to a higher migration rate of hydrogen gas. However, these processes could not be well described for the investigated clay minerals.

Lassin and co-workers (Lassin et al., 2011) also investigated the chemical effects of hydrogen on the reservoir fluids. Their results showed that hydrogen dissolution decreases the pH of the fluid, which in turn changes the geochemical equilibrium of the system. In the same study, the authors described possible chemical effects of hydrogen on clay minerals. However, due to insufficient thermodynamic data for clay minerals the study could not make any predictions on this issue from simulations. From laboratory experiments they concluded that the influence of hydrogen on clay minerals is negligible, but suggest further research to confirm these results.

The lack of data on hydrogen adsorption on pure clay minerals motivated the studies of Didier (2010) and Didier et al. (2012). In these studies two kinds of experiments were performed: (i) experiments run with clay suspensions, where the sample was placed in a NaCl(aq) solution (40 mM), with  $P_{H_2}$  equal to 5 bar (100%  $H_{2(g)}$ ) and  $T = 90\text{ }^\circ\text{C}$  and (ii) dry experiments, where the sample was dried before reaction, with a 0.45 bar partial pressure of  $H_{2(g)}$  (Ar/ $H_2$  (5%) mixture) and  $T = 25$  to  $120\text{ }^\circ\text{C}$ .

The amount of sorbed hydrogen on the sample was calculated as the difference between the quantity of  $H_2$  before and after the reaction. The reported adsorbed amounts of  $H_2$  in these studies for synthetic montmorillonites and Callovo-Oxfordian clayrock samples range between 0.05 and 0.11 wt% at  $90^\circ\text{C}$  in dry conditions. From the comparison of experiments performed at different temperatures, Didier (2010) concluded that temperature does not have a consistent impact on the sorption which means that  $H_{2(g)}$  could interact via either Van Der Waals or covalent binding with the surface.

An interesting comparison between the sorption capacity of various clay materials with gases like  $CH_4$ ,  $CO_2$  and  $H_2$  is included in Didier (2010) and it is reproduced in Figure 10. It can be observed that despite these different gases, the sorbed gas content is comparable. The results of Didier and coworkers (2012) estimate that up to 0.11 wt (%) of the initial hydrogen concentration in the

headspace of the experiment can be adsorbed on the clays at 90 °C under 0.45 bar of relative pressure. It means that more than 18 m<sup>3</sup> of H<sub>2(g)</sub>/m<sup>3</sup> of raw clay could be immobilized by the barriers under these physicochemical conditions. Similar results in term of H<sub>2</sub> adsorption onto clays have been reported in a more recent study by Bardelli et al. (2014) for the same Callovo-Oxfordian clay formation.

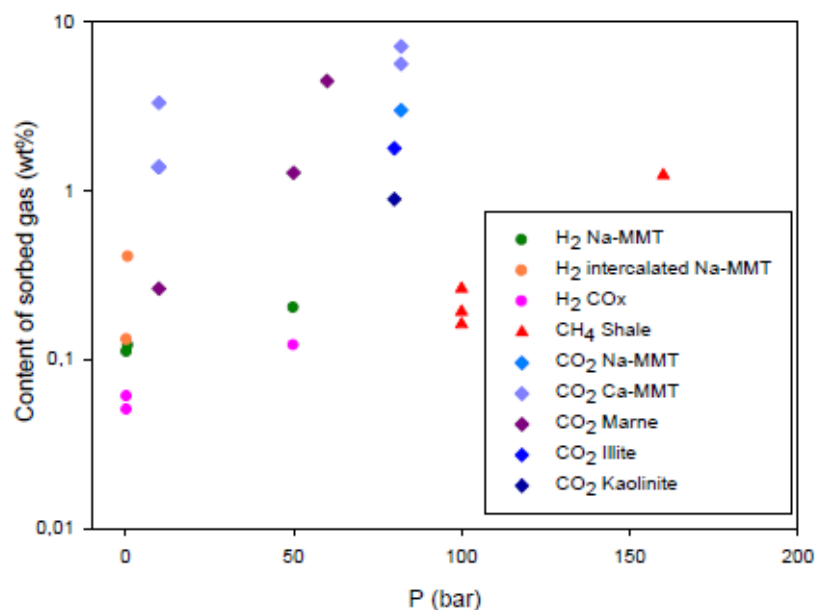


**Figure 10.** Evolution of gas sorbed content with the pressure for H<sub>2</sub>, CH<sub>4</sub> and CO<sub>2</sub> in clay materials (from Didier et al., 2010).

#### 2.2.4 Reaction catalysed by microbes

Bacteria are a large domain of microorganisms that need nutrients, energy sources and electron acceptors to survive by synthesising new biomass (bacterial growth) (Sena, 2009). The primary metabolism of bacteria is controlled by the chemical conditions of the system, although in turn, the bacterial activity triggers changes in key geochemical parameters of the environmental system. Microbial activity is varied and complex because the sources of organic carbon, electrons and energy are multiple and diverse. These processes are relevant in the frame of this study because H<sub>2</sub> is a possible energy sources for bacteria other than organic carbon, methane and other hydrocarbons or reduced inorganic molecules. During the microbial oxidation of these energy



sources, bacteria preferentially use electron acceptors in a particular order according to thermodynamic constraints:  $O_2$ ,  $NO_3^-$ , Mn, Fe,  $SO_4$ ,  $S^-$  and  $CO_2$  (Jin and Bethke, 2005).

In this study we have focused our analysis on the role of  $H_2$  as source of energy for bacterial activity and the impact of this  $H_2$  consuming process. Consumption of  $H_2$  by bacterial activity could occur under specific conditions, and this might slow down the pressure build up of hydrogen gas.

Several studies have shown that bacteria are present in most of the deep geological formations already studied, surviving even under extreme conditions (Pedersen, 2002; Stroes-Gascoyne et al., 2007). Within a nuclear repository, metallic corrosion can be considered as a source of nutritional and energetic substrate for microbial growth. The possible pathways for microbial activity in this context are presented in Figure 11.

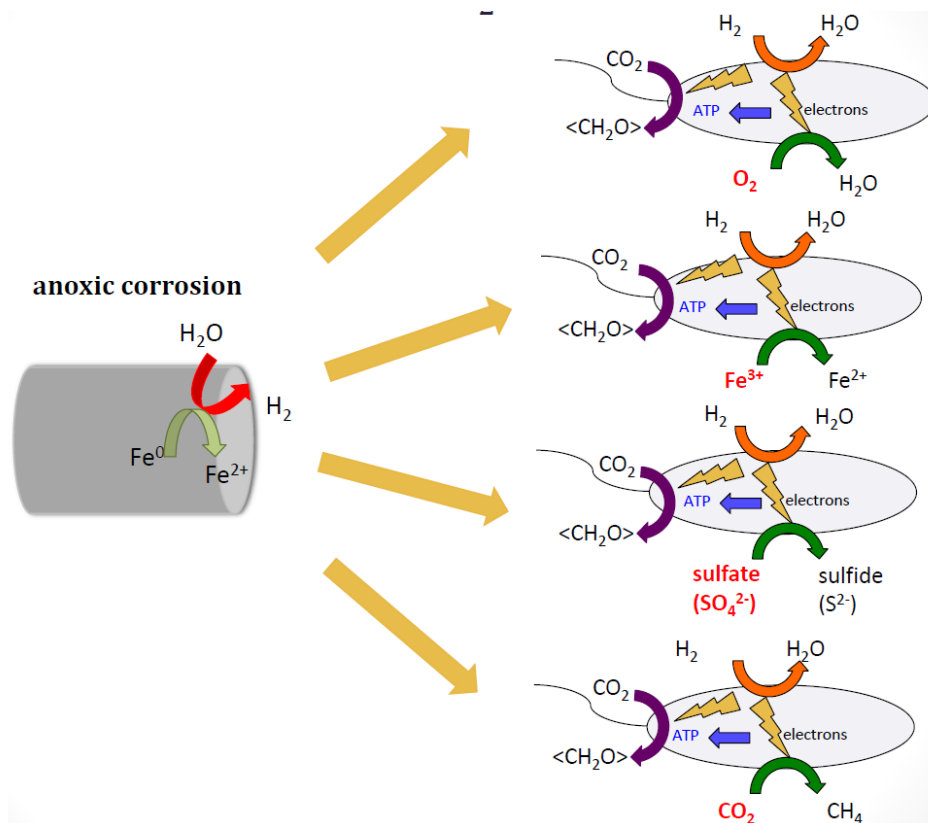


**Figure 11.** Scheme of the possible pathways for  $H_2$  oxidation in subterranean conditions (from Bernier-Latmani and co-workers, ENSI Meeting, March 2014).

The possible microbial reactions due to interaction of clay with H<sub>2</sub> are being evaluated with an *in-situ* experiment in Mont Terri by Brenier-Latmani and co-workers (ENSI Meeting, March 2014). A sophisticated experimental set-up was implemented with the objective to identify the bacterial community present in the clays and quantify biotic process induces by the presence of H<sub>2</sub> as energy source for bacterial growth (Figure 12).

The experimental data obtained up to now show that metabolism other than sulphate reduction is not evidenced and no specific iron reducing organisms have been identified (Figure 13). Based on the study of the microbial clusters, the metabolic network displayed in Figure 14 is proposed by Brenier-Latmani and co-workers. They conclude that H<sub>2</sub> in pore water will be quickly consumed by microorganism through cycling of carbon that allows the growth of organic carbon utilizing microorganisms.

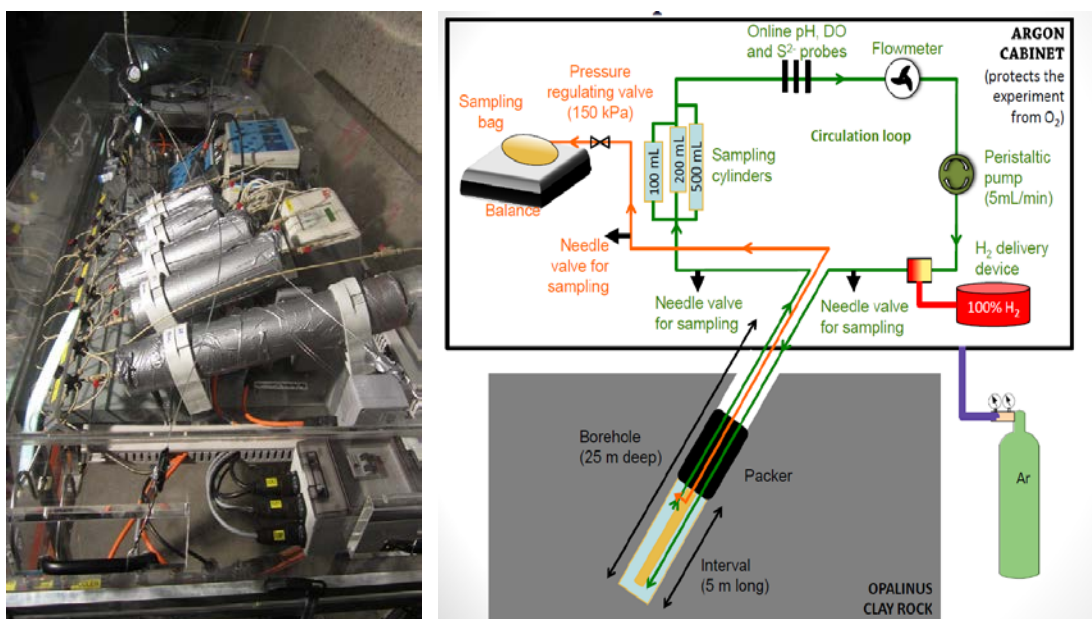


**Figure 12.** Experimental setup used in the bioreactor experiment (Mont Terri project, 2014) (from Brenier-Latmani and co-workers, ENSI Meeting, March 2014).

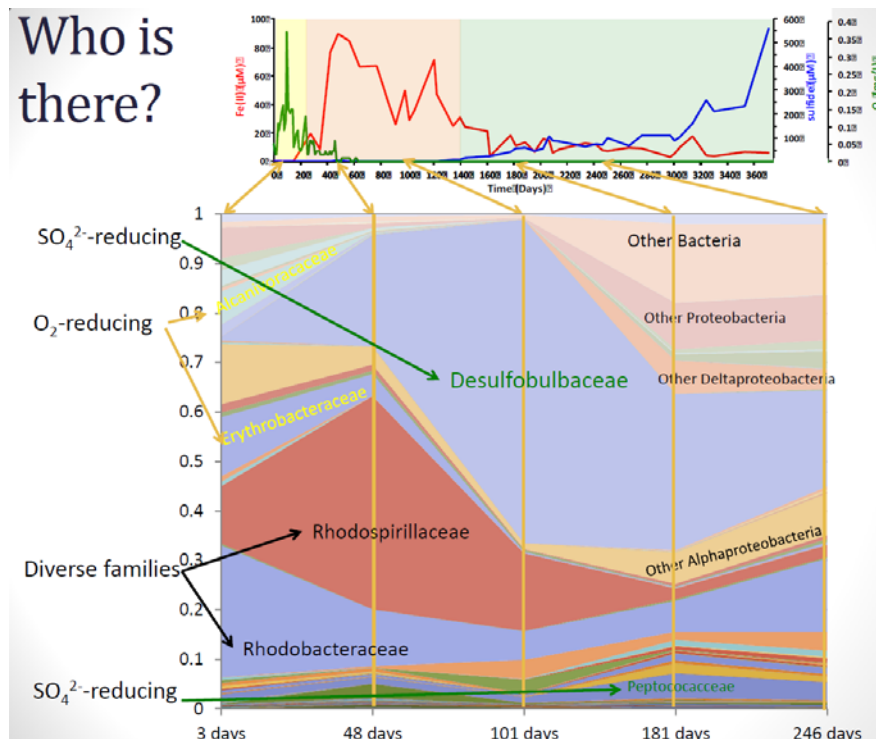


**Figure 13.** Identification of microbial community and related redox process during the bioreactor experiment (Mont Terri project 2014) (from Bernier-Latmani and co-workers, ENSI Meeting, March 2014).

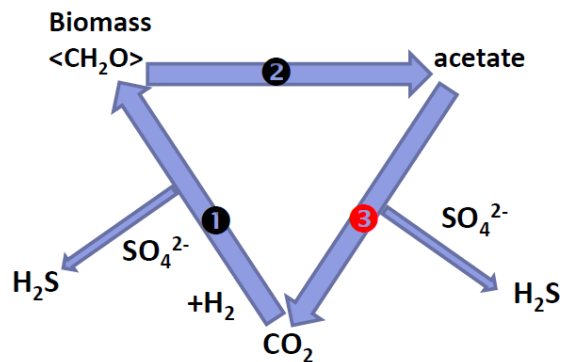


**Figure 14.** Proposed metabolic network for bacterial community in the bioreactor experiment (Mont Terri project). (From Bernier-Latmani and co-workers, ENSI Meeting 2014). 1- Autotrophic sulphate reduction, 2- Fermentation, 3- Heterotrophic sulphate reduction.

### 2.3 Gas migration in clays

Gas migration in compacted bentonite and indurated and plastic clays has been the subject of intensive experimental and modelling studies over at least the last 25 years, especially in the

---

framework of nuclear waste storage. As a result, a large body of literature is available. Even though our level of understanding of the different processes involved has substantially increased over the last years, a number of open issues still remain.

Within the framework of the European projects MEGAS (1991-1995), GASNET (2001-2003) and the more recent FORGE (Fate of Repository Gases, 2009-2013), thorough and detailed state-of-the-art reports on gas migration issues have been published (Volckaert et al., 1995; Rodwell et al., 2005; Norris, 2010). Within FORGE, a thermo-hydro-mechanical data set from the Mont Terri URL regarding gas migration has been gathered, including laboratory tests using Mont Terri's samples and in-situ tests (Marschall et al., 2013). Therefore, it is not intended in this report to include a detailed literature review on gas migration issues. Instead, a brief description of the processes analysed in the scoping calculations involving gas migration mechanisms is given. The scoping calculations performed in this study are restricted to single phase water saturated conditions, i.e. before a free gas phase is formed by the accumulation of hydrogen. Therefore, a literature review of the processes governing the system when a free gas phase is formed is out of the scope of this study.

### **2.3.1 Data for Opalinus clay**

The transport of different gases through Opalinus clay (OPA), an indurated clay, has been extensively studied over the last 20 years, under both laboratory conditions (e.g. Poller et al., 2008; Romero et al., 2012) and in-situ field conditions at Mont Terri Underground Rock Laboratory (e.g. Marschall et al., 2005; Marschall et al., 2013). Results for OPA from a borehole in the Benken area have also been obtained (Nagra, 2001; Marschall et al., 2005). As a result, NAGRA has gathered a large body of experimental and field data, and substantial process understanding has been gained (Figure 9). In addition to the studies at Mont Terri, gas migration field tests in fractured granite at Grimsel Test Site (e.g. Croise and Senger, 1996; Marschall and Lunati, 2006; Senger et al., 2008), and in Palfris marl at Wellenberg site, which is more indurated than OPA (Senger et al., 1997) have also been studied by NAGRA.

Gas transport dedicated experiments conducted at Mont Terri on OPA since 1995 include (ventilation tests are not considered in this report):

1. Gas permeability tests on core specimens,
2. Gas diffusion experiments,

- 
3. Short-term and Long-term gas injection experiments in boreholes,
  4. Gas injection experiments in microtunnels

These studies have considered both disturbed and undisturbed clay. It may be noted that the different experimental conditions considered in each test imply that the mechanisms for gas transport may be different in each case. Gas transport dedicated experiments conducted at Mont Terri have been used to determine the parameters needed for two-phase flow numerical models and also to determine:

- Gas permeability (and relative permeability curve)
- Diffusion coefficients in OPA ( $P_g < \text{gas entry pressure}$ )
- Gas entry pressure, gas breakthrough pressure (dilation), gas fracture pressure
- Anisotropy factors (angle with bedding)
- Influence of disturbance (e.g. EDZ) on gas transport properties
- Effect of path dilation or fracture on water flow properties
- Self-sealing of clay after recovery period

As mentioned above, the focus of this study is on the transport of hydrogen under single phase water saturated conditions. Under these conditions, dissolved  $H_2$  migrates essentially by diffusion through the pore network. A number of experiments have been conducted to measure diffusion coefficients of He,  $H_2$ , and other gases specifically for Opalinus Clay (Gómez-Hernández, 2000; Jacobs et al., 2013; Vinsot et al., 2014). However, data on the diffusion coefficient of hydrogen in the fully or partially saturated clay is largely missing. The most recent attempt is perhaps the HT experiment (Vinsot et al., 2014). The data produced in this experiment has not yet been used to estimate a diffusion coefficient for hydrogen. This is due to the significant rate at which hydrogen disappears from the system in the experiment, which prevents from reliably calculating a diffusion coefficient (see more details in the discussion below).

In the Mont Terri FM-C (Flow Mechanism) test (Gómez-Hernández, 2000), an in-situ in- and out-diffusion experiment with He parallel to the bedding plane on Opalinus Clay was performed. The best fit for helium effective diffusion ( $D_{\text{eff}} = 2.1 \cdot 10^{-10} \text{ m}^2/\text{s}$ ) was obtained for an out-diffusion experiment but using a porosity of 30% (which is significantly higher than the typical reported porosity values for Opalinus Clay). However, this porosity value has not been confirmed by other measurements, and therefore the validity of the fitted value for the  $D_{\text{eff}}$  may be limited.

---

In turn, Rubel et al. (2002) used the natural profile of helium obtained at Mont Terri to fit the apparent diffusion coefficient for He ( $D_{\text{app}} = 3.5 \cdot 10^{-11} \text{ m}^2/\text{s}$ ) in Opalinus Clay. In the ClayTrac Project (OECD/NEA, 2009), values for the pore diffusion coefficient ( $D_{\text{pore}}$ ) for He in Opalinus clay were also determined from natural profiles from Benken borehole and Mont Terri (which are respectively  $2.3 \cdot 10^{-10} \text{ m}^2/\text{s}$  and  $2.5 \cdot 10^{-10} \text{ m}^2/\text{s}$ ). Moreover, they critically discuss the validity of the fitted value by Rubel et al. (2002).

More recently, SCK•CEN developed a method to measure the diffusion coefficient of dissolved gases in low-permeability materials, based on the through diffusion technique (Jacops et al., 2013a). They measured the diffusion coefficient of He in samples originating from the Schlattingen borehole in northeastern Switzerland (depth 860.32 m below surface), with the sample axis oriented perpendicular to the bedding plane. By interpretation of the tests with a simple 1D Fickian diffusion model, they obtained a value for the effective diffusion coefficient of  $D_{\text{eff}} = 6.5 \cdot 10^{-11} \text{ m}^2/\text{s}$ , considering a porosity of 0.12 ( $D_{\text{pore}} = 5.4 \cdot 10^{-10} \text{ m}^2/\text{s}$ ). For comparison, the same authors also measured the diffusion of He in Boom clay (Jacops et al., 2013b) using a similar technique. They obtained values of the apparent diffusivity of  $12.2 \cdot 10^{-10} \text{ m}^2/\text{s}$  for Boom clay ( $D_{\text{pore}} = 3.30 \cdot 10^{-9} \text{ m}^2/\text{s}$ ), with an associated uncertainty of 10%. The porosity of Boom clay, around 0.37, is however much higher than that of Opalinus clay (~0.12-0.14). Diffusion coefficients of hydrogen and methane in Boom Clay have also been measured in the laboratory in Volckaert et al. (1995). The measured apparent diffusion ( $D_{\text{app}}$ ) coefficients varied over a wide range (from  $4 \cdot 10^{-12}$  to  $5 \cdot 10^{-10} \text{ m}^2/\text{s}$  for hydrogen and from  $5 \cdot 10^{-10}$  to  $2 \cdot 10^{-9} \text{ m}^2/\text{s}$  for methane) due to the complexity of the experiment. The estimated effective diffusion coefficient from re-evaluation (see Jacops et al., 2012 and references therein) is between  $1.9 \cdot 10^{-12}$  and  $1.5 \cdot 10^{-10} \text{ m}^2/\text{s}$ , i.e. a range that comprises two orders of magnitude differences.

An interesting on-going experiment of the diffusion of a gas mixture (containing 5% H<sub>2</sub>, 5% He, 5% Ne, and 85% Ar) through Opalinus clay is the in-situ HT (Hydrogen Transfer) experiment at Mont Terri (first hydrogen injection was performed in June 2011). The objectives of the HT experiment are to evaluate the effective diffusion coefficient of hydrogen in the Opalinus Clay, to identify if hydrogen consumption processes are measurable in a borehole, and to evaluate the effect of microbial activity on these processes.

A detailed description of the experimental setup may be found in Vinsot et al., 2014. The experimental setup consists of a 15-m-long and 76-mm-diameter inclined ascending borehole

---

(perpendicular to the bedding), of which the last 5 m constitute the test interval. The gas pressure in the test interval is maintained at a value of between 1.3 and 2.5 bar, which is much lower than the pore pressure in the surrounding clay. The pressure difference induces a water flow into the borehole. A water-sampling module is used to extract the water in order to maintain a constant water column height and monitor the water composition.

The largest hydrogen partial pressure value was close to 0.06 bar. Helium and neon served as reference non-reactive gases because changes in their content should only depend on dissolution and diffusion processes in the rock porewater (Vinsot et al. 2014). Up to now, two gas injection phases have been performed. Both phases have resulted in the same response of the system: whereas He and Ne seem to behave conservatively, hydrogen disappears quite fast, and after 65 days its concentration in the borehole falls below the detection limit in both injection phases. Thereafter, it was decided to inject the gas mixture constantly so that a H<sub>2</sub> partial pressure of 0.06 bar is maintained in the borehole.

The effective diffusion coefficient of the Opalinus clay calibrated with a numerical model (Vinsot et al., 2014) is  $11.53 \cdot 10^{-11}$  m<sup>2</sup>/s for helium and  $6.39 \cdot 10^{-11}$  m<sup>2</sup>/s for neon. These values are in good agreement with the known transfer properties of the rock. The drop in hydrogen concentration in the borehole indicates that other processes different from diffusion only must play an important role. The evolution of the borehole water composition suggests that hydrogen could have been consumed by reactions involving sulphate and iron reduction (Vinsot et al., 2014).

### **2.3.2 Data for bentonite**

Experiments dedicated to measuring the diffusion of hydrogen in compacted bentonite are also scarce, and only a few attempts have been published. Hydrogen diffusion in compacted bentonite under fully water saturated conditions was studied by Neretnieks and coworkers (Neretnieks, 1985; Neretnieks and Skagius, 1978), Eriksen and Jakobsson (1982), and Pusch (1983). In these different experiments, the effective diffusion coefficient for dissolved H<sub>2</sub> in bentonite was found to be in the range  $0.36$ - $3.0 \cdot 10^{-11}$  m<sup>2</sup>/s (Neretnieks, 1985). The differences are in part due to the different pressures and degrees of compaction used in each experiment.

Higashihara et al. (2001) measured helium diffusion coefficients in montmorillonite and deduced from these the dissolved hydrogen diffusion coefficients. To this end, they assumed that the tortuosity is the same for both He and H<sub>2</sub>, so that the pore diffusivities for He can be simply scaled



---

by the factor  $D_{0,\text{He}}/D_{0,\text{H}_2}$ , where  $D_0$  is the diffusion coefficient in free water. The results for Namontmorillonite indicate a pore diffusion coefficient of  $1.1 \cdot 10^{-10} \text{ m}^2/\text{s}$  for a dry density between 1500 and 1600  $\text{kg}/\text{m}^3$  (the dry density of the Swiss repository design will fall within this range). Assuming a total porosity of 0.45 for a dry density of 1500  $\text{kg}/\text{m}^3$ , the effective diffusion coefficient is  $5.0 \cdot 10^{-11} \text{ m}^2/\text{s}$ .

## 2.4 Uncertainties

### 2.4.1 Gas generation and consumption by chemical reactions

Main uncertainties for estimation of  $\text{H}_{2(\text{g})}$  production in the HLW geological disposal include: 1) the evolution of the corrosion rate with time, 2) unknown surface area for waste containers, 3) availability of water to sustain the corrosion rate over time, and 4) non-uniform corrosion processes. This last process is extremely difficult to evaluate but it can be considered negligible for gas production (Bruha et al., 2010). The corrosion rate of carbon steel is dependent on the local geochemical conditions (pH/Eh) and other important factors that could influence the corrosion rate are temperature and saturation degree. If gas generation exceeds gas evacuation through diffusion, a free gas phase will be present in the pores of the barriers. As a consequence, desaturation could occur. Corrosion rates have not been experimentally measured in many studies under partially saturated conditions, and thus lower rates might be expected under these particular conditions.

Assessment of the rate and amounts of microbially mediated gas generation/consumption is a difficult issue. For this reason, many safety assessments rely on a simple approach based on available experimental data to attempt to ensure upper limits for these reactions. A reliable prediction of the impact of biotic processes should be based on specific studies performed under similar conditions to those predicted for the geological disposal, including a good description of the microbial community present in the site. In this sense, the reported results of the Bioreactor Experiment represent a set of high quality data able to be used in the scale-up of this process.

Uncertainties in the understanding of gas generation through water radiolysis are not expected to highly influence the general process given the low relevance of this process in the overall gas formation amounts.



---

The composition of the water present in the repository will affect the corrosion process, specifically the rate and the type of secondary products formed through corrosion. For instance, the presence of high concentrations of  $\text{Cl}^-$  could favour localised corrosion under oxidising conditions. The presence of dissolved carbon dioxide could increase the corrosion rate of steel in water by decreasing the pH of the water and hence increasing corrosion rates. The presence of other complexing agents in the pore water may affect corrosion through redissolution of corrosion products. The presence of hyperalkaline conditions may cause depassivation of metallic surfaces. All these findings highlight that several relevant processes could be induced by chemicals in the pore water, thereof they should be carefully evaluated. Uncertainties linked to this point should be minimized by clearly defining the chemical composition of water in contact with carbon steel containers and clay barriers and considering the uncertainty in groundwater composition.

#### **2.4.2 Gas transport**

Regarding the transport processes of  $\text{H}_2$  in clay systems, the main uncertainties are associated with the formation of gas preferential pathways due to gas pressure build-up, and how is the effective water saturation of the pore system affected. Moreover, and may be more relevant to the present study, significant uncertainties still exist on the diffusion coefficient of dissolved  $\text{H}_2$  in bentonite and Opalinus clay.

In order to consider diffusion of dissolved gases in the liquid phase as a process that mitigates to some extent the impact of gas generation on the safety of a repository system, reliable confirmation from experimental data of the large-scale aqueous phase intrinsic diffusion coefficient for the principal gases generated in a repository is required (Norris, 2013).

Diffusion coefficients measured in experiments show considerable scatter due to the limited amount of test results and the complexity of performing such tests. This complexity is in part related to the small pore size of clays, and also to the consumption processes, which may induce a deviation of the measurements when compared to a conservative tracer. In addition, a quantitative relation between the diffusion coefficient and the degree of liquid saturation is still missing, which adds to the overall uncertainty of the diffusion process.

---

### 3. Summary of relevant geochemical processes

After evaluation of the main geochemical processes able to produce or consume H<sub>2</sub> in the HLW geological disposal the following conclusions can be highlighted:

- Regarding the production of H<sub>2</sub>, anaerobic corrosion of carbon steels can be mentioned as the dominant source of gas. For implementing this process in reactive transport models a constant corrosion rate is currently assumed. A value of 2 μm y<sup>-1</sup> is currently retained as the reference value by NAGRA under the conditions of HLW repository. Although a wide range of values has been provided by different studies, the most promising CR experiments performed in Mont Terri, in contact with bentonite, for a long-term period, support this corrosion rate, reporting a range of CR between 0.6 and 3 μm y<sup>-1</sup>. This range could be assumed for the sensitivity cases aiming to estimate an uncertainty in the rate.
- If other metals such as Al, Zn or Zr are included in the final repository inventory, CR of 0.1 μm y<sup>-1</sup> should be taken into account and included in the list of kinetically controlled processes. The relevance of these processes is determined by the final inventory of metals in the geological disposal.
- Other processes that could produce H<sub>2</sub> in a HLW disposal such as radiolysis can be neglected because their minimal impact compared to that described for anaerobic corrosion of carbon steel. The impact of H<sub>2</sub> production by radiolysis has been evaluated in several studies and, as a result, they are not included in calculations of gas build-up and dissipation.
- Among all the process described as potential consumers of H<sub>2</sub>, pyrite reduction to pyrrhotite could be relevant as bentonite and Opalinus clay contain 0.6 wt.% and 1-3 wt.%, respectively. The kinetic rate expression proposed by Truche et al. (2010) provides an estimation of H<sub>2</sub> consumption through sulphide production and can be easily implemented in the scoping calculations. Nevertheless, it is important to consider a security factor for the estimation of the impact of this process. The experimental rates have been determined at H<sub>2</sub> pressures ranging between 0 and 1.8 MPa and H<sub>2</sub> pressure of the order of 6-8 MPa are predicted at a repository depth (King and Kolar, 2009). We do not have experimental evidences that allow confirming the validation of this kinetic rate at higher pressures. Scoping calculations will be performed by assuming a multi-mineral system (Opalinus clay barrier), and the presence of carbonates (3-14% of dry weight) could control the development of this reaction, as reported by Pichler (2013).

- 
- The concentration of H<sub>2</sub> to be adsorbed/absorbed on C steel is expected to be low due to absence of H-absorption promoters (hydrides of Group VA and VIA elements) and the formation of surface oxides and mineralized films that will block hydrogen absorption.
  - Adsorption of H<sub>2</sub> in clays has been recently described and quantified at a H<sub>2</sub> partial pressure of 0.045 and 0.5 MPa (Didier, 2010; Didier et al., 2012, Bardelli et al., 2014). It is difficult to know if this process will be relevant at the predicted H<sub>2</sub> pressure for the HLW disposal (6-8 MPa). More experimental data at high H<sub>2</sub> partial pressure are needed in order to implement this process in scoping calculations. A direct extrapolation of the experimental data is not possible from the present available data because all of them are related to a H<sub>2</sub>-dry clay system.
  - Abiotic reduction of sulphate by thermodynamically driven reactions can be neglected due to slow kinetic rate at which this reaction occurs at the temperature conditions prevailing in the geological repository over time.
  - All the findings of the Bioreactor Experiment point out that sulphate reduction by SRB activity is highly relevant for the final evaluation of H<sub>2</sub> consumption by sulphate reduction reactions. The implementation of bacterial activity reactions in the scoping calculations requires the definition of several parameters (biomass concentrations, organic and inorganic carbon sources among others) that will determine the survival of the bacterial community and, in consequence, the impact of biotic redox reaction and the subsequent H<sub>2</sub> consumption.
  - Other mineralogical transformations such as reduction of structural Fe(III) by H<sub>2</sub> is not considered to be relevant as the reported studies clearly concluded that structural Fe(III) in clays can not modify the amount of H<sub>2</sub> gas to a relevant extent.

---

## 4. Scoping calculations

Following ENSI suggestions, the scoping calculations have been performed under repository conditions, i.e. with the corresponding hydrostatic pressure ( $\sim 6.5$  MPa), dimensions of canister and bentonite backfill, temperatures, materials composition, etc.

### 4.1 Calculation of the time needed to form a free gas phase

As corrosion proceeds,  $H_2$  will be generated from the corrosion reaction. Dissolved hydrogen will diffuse out through the bentonite barrier towards the Opalinus clay formation at a rate that is given by the effective diffusion coefficient in the compacted bentonite (and in the Opalinus clay, at a later stage). As long as the dissolved hydrogen concentration remains below the solubility limit, no free gas phase will form. The competition between the flux of dissolved  $H_2$  from the corrosion process into the bentonite porewater and the escape of this gas via a diffusive flux (in such a low permeability media under saturated conditions, the advective flux is much smaller than the diffusive flux) will determine whether or not a free gas phase will form.

The solubility limit of hydrogen in the pore water depends not only on the partial gas pressure but also on the temperature of the system, as given in Table 4-1.

Scoping calculations of the hydrogen generation and diffusion processes have been carried out to determine the time needed to form a free gas phase at the steel-bentonite interface after corrosion starts. The model does not consider the solubility limit to form a gas phase and is equivalent to the diffusive transport of a conservative tracer (i.e. a species that is not affected by chemical reactions), with a flux boundary condition (mass of hydrogen released during the corrosion process) at the steel-bentonite interface. This model is only valid until the solubility limit at a given temperature is reached at the steel-bentonite interface. Thereafter, the transport of dissolved hydrogen cannot be considered as a conservative tracer and the model is not valid anymore.

Different temperatures have been considered for the case with a corrosion rate of  $1\mu\text{m/a}$  (constant throughout the domain, i.e. no heat transport is modelled): 10, 25, 40, and 80 °C. Full water saturation is assumed throughout the bentonite and Opalinus clay. It is assumed that corrosion prior to water saturation will be negligible compared to the corrosion rate under full water saturation. These calculations consist of one dimensional axisymmetric numerical simulations

---

using the commercial finite element software Comsol Multiphysics. The geometry dimensions (shown schematically in Figure 15) consider a steel cylinder with a diameter of 100 cm (not explicitly represented), representative of the SF/HLW steel canisters, 105 cm for SF, and 94 cm for HLW (see Nagra, 2002). The canister is surrounded by a bentonite backfill with a diameter of 250 cm. This is in turn surrounded by the Opalinus clay formation (a sufficiently large domain, i.e. 18.75 m thickness, has been considered in the simulations so that for the analysed time frame the boundary effects are avoided). The presence of the steel is not explicitly considered but a hydrogen flux boundary condition is set at the steel-bentonite interface. The bentonite domain is discretized with linear elements with a constant size of 5 mm, while the OPA elements vary between 5 mm near the backfill and 10 mm far from the near-field.

The assumption of considering a 1D axisymmetric model is conservative in the sense that diffusion out of the hydrogen will not occur along the direction of the axis. This is due to the fact that a single disposal tunnel will host several canisters, separated by 3 m of bentonite backfill. Therefore, considering the geometry with several canisters and the corresponding backfill would lead to a higher hydrogen expulsion capacity of the bentonite barrier, and therefore a longer time would be needed to form a gas phase.

In the 1D axisymmetric model, the steel bentonite interface considered is 1 m<sup>2</sup>. Comsol then automatically scales the volume of bentonite and Opalinus clay as a function of the distance to the symmetry axis.

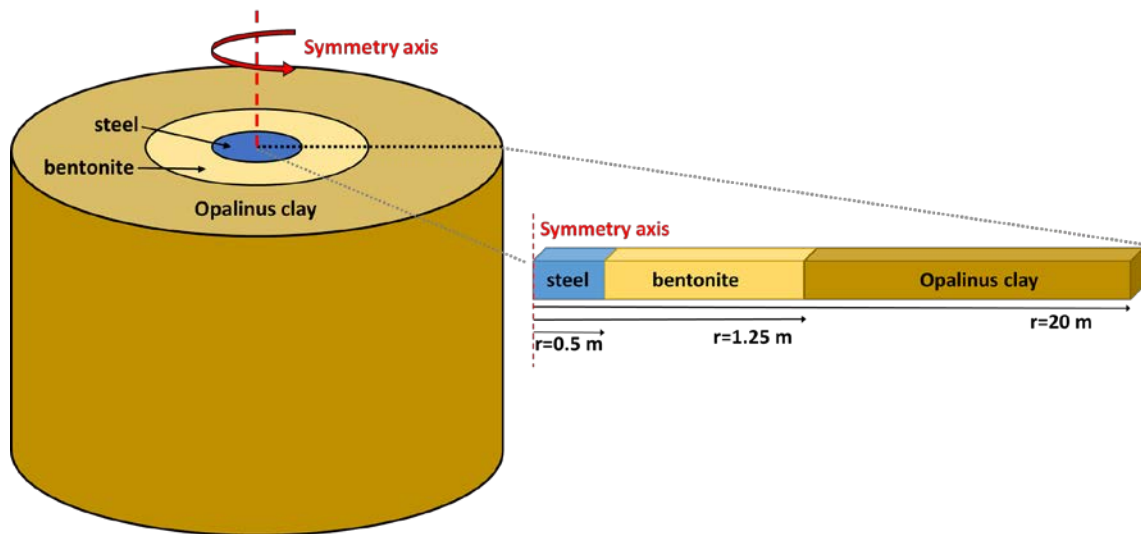


**Figure 15.** Geometry of the 1D axisymmetric calculations in Comsol Multiphysics. The steel is not considered explicitly in the simulations. Instead, a flux boundary condition is imposed at the steel-bentonite interface to mimic the effects of the corrosion process.

The corrosion rate in the reference case is 1 micron/year. Assuming that magnetite is formed according to Equations 7 and 8, 4/3 moles of H<sub>2</sub> are formed for every mol of Fe(s) consumed in the corrosion process. The amount of H<sub>2</sub> generated can be thus calculated by:

$$H_{2,generation} \left( \frac{mol}{m^2 \cdot year} \right) = corrosion\ rate \left( \frac{m}{year} \right) \cdot \frac{\rho_{steel}}{M_w^{Fe}} \cdot \frac{4}{3} \quad \text{Equation 18}$$

where the density of steel ( $\rho_{steel}$ ) is 7874 kg/m<sup>3</sup>, and the molar weight of steel ( $M_w^{Fe}$ ) is 0.055845 kg/mol. This gives a H<sub>2</sub> generation rate of 0.188 mol/(m<sup>2</sup>·year) for the reference case.

The solubility limit of dissolved hydrogen in the liquid phase can be calculated as a function of temperature and hydrostatic pressure using Henry's law or other more accurate approaches (see Section 4.3). Table 4-1 shows the Henry's constant corrected for temperature effects (following Fernández-Prini et al., 2003) and the corresponding solubility limits for two different hydrostatic pressures representative of repository conditions (6.5 MPa) and of the Mont Terri URL (3 MPa). These values have been used to determine the time needed to reach the dissolved hydrogen concentrations in the pore water corresponding to the solubility limits.

**Table 4-1.** Henry's constant and solubility for H<sub>2</sub> at different temperatures (calculated following Fernández-Prini et al., 2003) used in the scoping calculations of Section 4.1.

<i>T</i> (°C)	<i>k<sub>H</sub></i> (Mpa/x)	<i>k<sub>H</sub></i> (M/bar)	Ratio <i>k<sub>H</sub><sup>T<sub>i</sub></sup> / k<sub>H</sub><sup>25</sup></i>	Solubility at 6.5 MPa (M)	Solubility at 3 MPa (M)
10	6.33E+03	8.63E-04	1.121	0.0561	0.0259
25	7.10E+03	7.70E-04	1.000	0.0500	0.0231
40	7.59E+03	7.19E-04	0.934	0.0468	0.0216
80	7.68E+03	7.11E-04	0.924	0.0462	0.0213
100	7.23E+03	7.56E-04	0.982	0.0491	0.0227

As pointed out in Section 2.4.2, there is still a significant level of uncertainty in the diffusion process of dissolved hydrogen through compacted bentonite and OPA. Following the discussion in Section 2.3, the selected value for the effective diffusion coefficient at 25 °C ( $D_{eff,25}$ ) in the bentonite backfill (dry density of approximately 1500 kg/m<sup>3</sup>) is  $5 \cdot 10^{-11}$  m<sup>2</sup>/s (considering a porosity for bentonite of 0.455 and the diffusion data from Higashihara et al., 2001). It is noted that the available data is on the apparent diffusion coefficient for helium in compacted bentonite. It is assumed here that there is no retardation of H<sub>2</sub> in the bentonite microstructure. In this way, the apparent diffusivity is equivalent to the pore diffusivity. Then, the effective diffusion coefficient is calculated by multiplying the apparent diffusion coefficient by the total porosity.

For the Opalinus clay, given the lack of data for diffusion of hydrogen, it has been assumed that the range of values obtained for the Boom clay in the MEGAS project (Volckaert et al., 1995) can be used as a first approximation. The range of the apparent diffusion coefficient,  $D_{app}$ , is  $4 \cdot 10^{-12} - 5 \cdot 10^{-10}$  m<sup>2</sup>/s. The average of these values is  $4.5 \cdot 10^{-11}$  m<sup>2</sup>/s, which has been used in the simulations as the apparent diffusion coefficient (leading to an effective diffusion coefficient  $D_{eff} = 0.6 \cdot 10^{-11}$  m<sup>2</sup>/s when multiplying  $D_{app}$  with porosity of Opalinus clay).

To correct the diffusion coefficients for temperature effects, the empirical formula proposed by Wersin et al. (2014) for compacted bentonite has been used:

$$D_{eff,T} = D_{eff,0} \cdot e^{0.026 \cdot T} \quad \text{Equation 19}$$

where  $T$  is expressed in °C.  $D_{eff,0}$  is calculated from the known value of  $D_{eff,25}$  as  $D_{eff,25}/e^{0.026 \cdot 25}$ . Effective diffusion coefficients for different temperatures are shown in Table 4-2.

An alternative to correct the effective diffusion coefficient for temperature would be to calculate the free water diffusion coefficient,  $D_0$  (m<sup>2</sup>/s), as a function temperature according to (Appelo and Postma, 2009):

$$D_0(T) = D_0(298 K) \cdot T \cdot \mu_{298 K} / (298 K \cdot \mu_T) \quad \text{Equation 20}$$

where,  $T$  (K) is the absolute temperature and  $\mu$  is the dynamic viscosity of water (Pa·s). The dynamic viscosity of water was calculated as a function of temperature using:

$$\mu = 1.78 \cdot 10^{-3} \cdot (1 + 0.0337 \cdot T + 2.21 \cdot 10^{-4} \cdot T^2)^{-1} \quad \text{Equation 21}$$

where the temperature is expressed in °C. This free water diffusion coefficient can be used to calculate the dependence of the effective diffusion coefficient on temperature, as shown in Table 4-2.

**Table 4-2.** Effective diffusion coefficients for H<sub>2</sub> in bentonite and Opalinus clay at different temperatures, corrected for temperature following the empirical expression by Wersin et al. (2014), Approach 1, and following the theoretical value of the free water diffusion coefficient (Appelo and Postma, 2009), Approach 2.

$T$ (°C)	Bentonite		Opalinus clay	
	$D_{eff,T}$ (m <sup>2</sup> /s) Approach 1	$D_{eff,T}$ (m <sup>2</sup> /s) Approach 2	$D_{eff,T}$ (m <sup>2</sup> /s) Approach 1	$D_{eff,T}$ (m <sup>2</sup> /s) Approach 2
10	$3.38 \cdot 10^{-11}$	$1.37 \cdot 10^{-11}$	$4.14 \cdot 10^{-12}$	$2.70 \cdot 10^{-12}$
25	$5.00 \cdot 10^{-11}$	$5.00 \cdot 10^{-11}$	$6.11 \cdot 10^{-12}$	$6.11 \cdot 10^{-12}$
40	$7.38 \cdot 10^{-11}$	$1.09 \cdot 10^{-10}$	$9.03 \cdot 10^{-12}$	$1.29 \cdot 10^{-11}$
80	$2.09 \cdot 10^{-10}$	$4.13 \cdot 10^{-10}$	$2.55 \cdot 10^{-11}$	$7.81 \cdot 10^{-11}$
100	$3.51 \cdot 10^{-10}$	$6.65 \cdot 10^{-10}$	$4.30 \cdot 10^{-11}$	$1.79 \cdot 10^{-10}$

It is noted that the temperature effect on the diffusion coefficients can also be regarded as a sensitivity analysis of the uncertainty in the diffusion coefficient itself. In the simulations, the temperature dependence has been taken into account with the use of the expression proposed by Wersin et al. (2014).

The effect of the consumption of dissolved hydrogen in chemical reactions (sulphate reduction by microbial activity and reduction of pyrite into pyrrhotite) on the time needed to form a gas phase has also been assessed using the 1D axisymmetric numerical model. Two cases have been considered. In the first case, microbial activity in the bentonite is not considered, as it has been



reported that for compacted bentonite systems this process is hindered (Pedersen, 2000). The second case considers, as a limiting case, that microbial activity in the bentonite is an active process. The rates for microbial activity considered are calculated from the value 0.86 nM/h/kgw, where kgw represents kilograms of water (see Section 4.3). The rates for pyrite reduction were calculated considering the input values of  $8 \cdot 10^{-15}$  and  $5 \cdot 10^{-15}$  mol/m<sup>2</sup> pyrite/s for bentonite and OPA, respectively, and a surface area of 2.7 m<sup>2</sup>/kgw (see Section 4.3). The resulting values are given in Table 4-3.

**Table 4-3.** Rates of hydrogen consumption considered in the simulations using Comsol Multiphysics, for each domain (bentonite: MX-80, and Opalinus clay: OPA).

Bioconsumption rate (mol/m <sup>3</sup> clay/s)		Pyrite to pyrrhotite reduction rate (mol/m <sup>3</sup> clay/s)	
MX-80	OPA	MX-80	OPA
$1.08694 \cdot 10^{-10}$	$3.1056 \cdot 10^{-11}$	$9.83 \cdot 10^{-12}$	$1.76 \cdot 10^{-12}$

#### 4.1.1 Results without H<sub>2</sub> consumption by chemical reactions

The results are summarized in Table 4-4 and Table 4-5 and Figure 16 and Figure 17. Table 4-4 and Figure 16 show the time needed to form a gas phase at the steel-bentonite interface for different corrosion rates. The relation is almost linear in a log-log scale and can be approximated ( $R^2=0.99$ ) by the simple expression:

$$t_{gas} = \frac{50}{r_c^2} \quad \text{Equation 22}$$

with  $t_{gas}$  expressed in years and  $r_c$  expressed in microns/year. It is observed that the dependence of the time needed to form a gas phase on the corrosion rate is very non-linear. In the narrow range 0.5 to 2 microns/year (i.e. half or double the reference corrosion rate), the time varies between ~14 and ~280 years.

**Table 4-4.** Time needed to form a gas phase at the steel-bentonite interface for different corrosion rates, as calculated with the 1D axisymmetric model in Comsol Multiphysics. This time is valid from the moment of full water saturation reached in the whole bentonite domain.

Corrosion rate (microns/year)	Time for gas phase formation (years)
100	0.007
20	0.104
10	0.45
9	0.515
8	0.683
7	0.9
6	1.243
5	1.82
4	2.93
3	5.51
2	13.92
1	75
0.5	279
0.1	4100

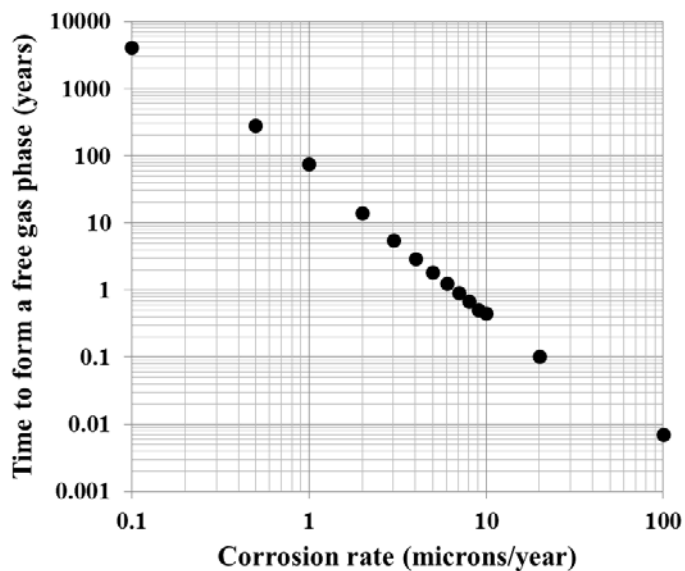


**Figure 16.** Time needed to form a gas phase at the steel-bentonite interface for different corrosion rates, as calculated with the 1D axisymmetric model in Comsol Multiphysics.

Table 4-5 and Figure 17 show the time needed to form a gas phase at the steel-bentonite interface for different near-field temperatures for the case with a corrosion rate of  $1\mu\text{m/a}$ , which affect the solubility and the diffusion coefficient. It may be observed that the time needed to form a gas phase increases with temperature. This is because the diffusion coefficient increases with temperature and therefore more hydrogen can be dissipated by diffusion, while the corrosion rate remains constant.

**Table 4-5.** Time needed to form a gas phase at the steel-bentonite interface for different temperatures for the case with a corrosion rate of  $1\mu\text{m/a}$ , as calculated with the 1D axisymmetric model in Comsol Multiphysics.

Temperature (°C)	Time for gas phase formation (years)
80	189
40	98
25	75
10	56

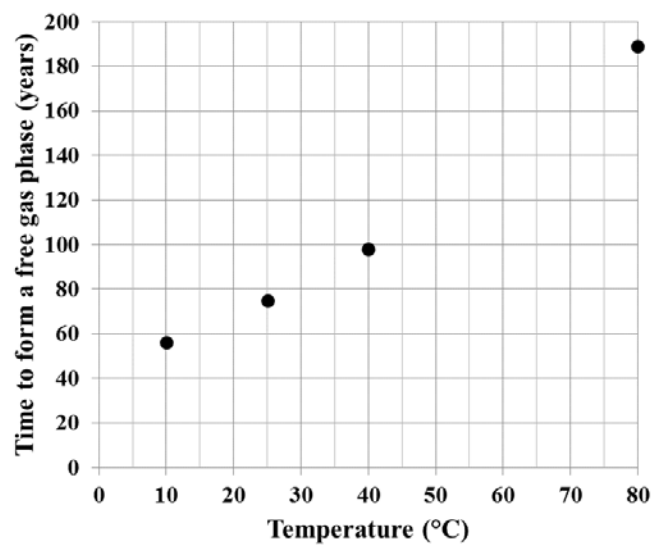


**Figure 17.** Time needed to form a gas phase at the steel-bentonite interface for different temperatures for the case with a corrosion rate of  $1\mu\text{m/a}$ , as calculated with the 1D axisymmetric model in Comsol Multiphysics.

#### 4.1.2 Results considering $\text{H}_2$ consumption by chemical reactions

The results considering  $\text{H}_2$  consumption by chemical reactions are summarized in Table 4-6 and Figure 18, showing the time needed to form a gas phase at the steel-bentonite interface for different consumption rates at  $25\text{ }^\circ\text{C}$  and for a corrosion rate of  $1\mu\text{m/a}$ . The simulation cases compared include the case with no hydrogen consumption, the reference consumption (see description above), and three more cases that test the sensitivity of the reaction rates. These cases consider that the  $\text{H}_2$  consumption rates for sulphate reducing bacteria and pyrite reduction are 2, 5, and 10 times faster than the reference consumption. All the simulations that include the

consumption of hydrogen in chemical reactions assume that both chemical processes (microbial activity and pyrite reduction) act simultaneously.

The simulations were repeated considering two different scenarios:

1. Microbial activity does not occur in the bentonite backfill (reference case, see discussion in section 2.4): this case considers pyrite reduction in the bentonite and OPA, and microbial activity in the OPA
2. Microbial activity is an active process in the bentonite backfill (sensitivity case maximising hydrogen consumption): this case considers pyrite reduction and microbial activity both in the bentonite and OPA

The results show that if the effect of microbial activity in the bentonite backfill on the consumption of hydrogen is not considered, the time needed to form a free gas phase does not significantly depend on the consumption of hydrogen by the other chemical reactions. This time is slightly longer if hydrogen consumption is considered (less than 3%). Even if microbes were also active in the bentonite backfill, the times needed to form a gas phase would not significantly change, unless the rates were 10 times higher than the reference values. In this last case, this time would increase by 35%.

**Table 4-6.** Time needed to form a gas phase at the steel-bentonite interface for different hydrogen consumption ( $r_{cons}$ ) reaction rates ( $\text{mol}_{\text{H}_2}/\text{m}^3_{\text{clay}}/\text{s}$ ) normalized with the reference consumption rate ( $r_{cons}^{ref.case}$ , see Table 3), as calculated with the 1D axisymmetric model in Comsol Multiphysics at 25 °C and for a corrosion rate of  $1\mu\text{m/a}$ .

ID simulation	$\frac{r_{cons}}{r_{cons}^{ref.case}}$	Time to form a gas phase (years)	
		With microbial activity in bentonite	Without microbial activity in bentonite
No consumption	0	75	75
Consumption ( $r_{cons}^{ref.case}$ ) (reference)	1	77	75.2
Consumption $\times 2$	2	79	75.4
Consumption $\times 5$	5	86	76.1
Consumption $\times 10$	10	101	77.2

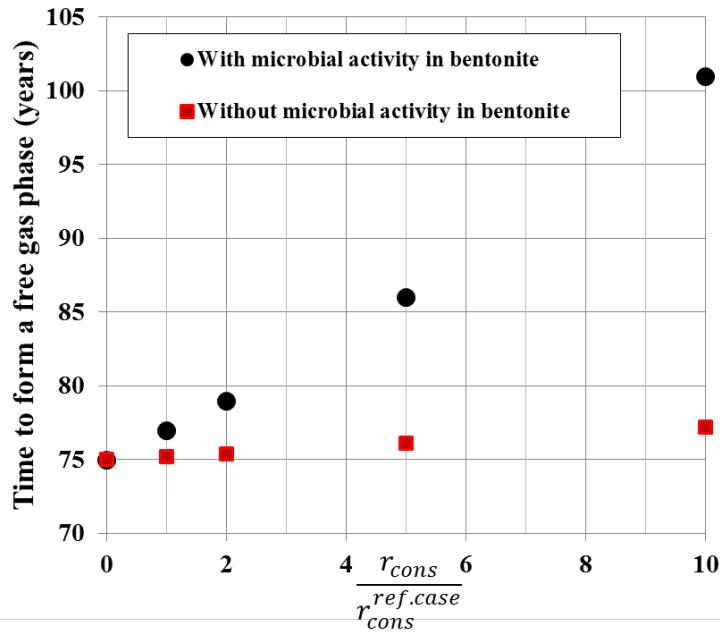


**Figure 18.** Time needed to form a gas phase at the steel-bentonite interface for different chemical reaction rates ( $H_2$  consumption due to pyrite reduction and microbial activity), as calculated with the 1D axisymmetric model in Comsol Multiphysics at 25 °C and for a corrosion rate of 1  $\mu\text{m/a}$ . Simulations with and without microbial activity in the bentonite backfill.

## 4.2 Assessment of water availability for the corrosion process

Assuming that magnetite is formed according to Equations 7 and 8, 2 moles of  $H_2O$  are consumed in the formation of  $Fe(OH)_{2(s)}$  for every mol of  $Fe(s)$  consumed in the corrosion process, while 2/3 of  $H_2O$  are generated in the formation of  $Fe_3O_4$ . Thus, the total amount of  $H_2O$  consumed in the corrosion process is 4/3 moles for every mol of  $Fe(s)$  consumed. Similarly to the previous section, the rate of water consumed in the corrosion process can be calculated as:

$$H_2O_{consumed} \left( \frac{\text{mol}}{\text{m}^2 \cdot \text{year}} \right) = r_c \cdot \frac{\rho_{steel}}{M_w^{Fe}} \cdot \frac{4}{3} \quad \text{Equation 23}$$

where  $r_c$  (m/year) is the corrosion rate, the density of steel ( $\rho_{steel}$ ) is 7874  $\text{kg/m}^3$ , and the molar weight of steel ( $M_w^{Fe}$ ) is 0.055845 kg/mol. This gives a  $H_2O$  consumption rate of 0.188 mol/( $\text{m}^2 \cdot \text{year}$ ) or 0.003384 kg/( $\text{m}^2 \cdot \text{year}$ ) for the reference case with a corrosion rate of 1 micron/year. If this quantity is normalized as per meter of canister length (SF and HLW canisters are ~5 m and ~2 m long, respectively) and considering a canister diameter of ~1 m (1.05 m for

---

SF canister, and 0.94 m for HLW canister), the water consumption rate is 0.0106 kg/(m<sub>canister</sub>·year) or 3.37·10<sup>-10</sup> kg/(m<sub>canister</sub>·s).

The consumption of water by the corrosion chemical reactions could potentially lead to a reduction in the corrosion rate if the availability of water from the surrounding bentonite and OPA formation would be limited. In this section, results are presented of scoping calculations performed with the aim of verifying whether the water flow in such low permeable porous media is high enough to keep the corrosion rate at the theoretical constant value.

The calculations have been performed in a one-dimensional axisymmetric setup, with the axisymmetric axis coinciding with the axis of the canisters, see Figure 19. It has been assumed that the bentonite is fully water saturated before corrosion starts, so that the initial state is defined by a hydrostatic pressure at repository depth, i.e. P<sub>0</sub> ≈ 6.5 MPa (or P<sub>0</sub> ≈ 3 MPa for Mont Terri URL conditions). The finite element software Comsol Multiphysics has been used to this end. Since one of the goals is to identify whether unsaturated conditions in the bentonite/OPA system can be attained or not, the Richards equation has been solved (built in equation in the Subsurface Flow Module of Comsol) in the bentonite/OPA domain:

$$\rho \left( \frac{C_m}{\rho g} + S_e S \right) \frac{\partial p}{\partial t} = \nabla \cdot \rho \left( \frac{\kappa k_r}{\mu} \nabla p \right) + Q_m \quad \text{Equation 24}$$

where the pore pressure  $p$  (Pa) is the dependent variable,  $C_m$  (1/m) is the specific moisture capacity (derivative of the retention curve with respect to the capillary pressure),  $S_e$  (-) is the effective saturation,  $S$  (1/Pa) is the storage coefficient (see below),  $\kappa$  is the absolute permeability (m<sup>2</sup>),  $k_r$  is the relative permeability,  $\rho$  (kg/m<sup>3</sup>) and  $\mu$  (Pa·s) are the density and dynamic viscosity of the fluid, respectively,  $g$  is the gravity acceleration (9.81 m/s<sup>2</sup>), and  $Q_m$  (kg/m<sup>2</sup>/s) is the fluid sink (if negative) term. Gravity effects have been neglected in the present simulations. Richards' equation can be considered as a valid approximation for the purpose of capturing the onset of unsaturated conditions in the bentonite. More rigorous calculations using a two-phase flow model would be required to analyse the behaviour under unsaturated conditions when gas pressure gradients are present, e.g. due to the generation of H<sub>2</sub> during the corrosion process.

The storage coefficient ( $S$ ) for a water saturated porous medium can be expressed, in its simplest form, as follows:

$$S = \phi \cdot \chi_f + (1 - \phi) \cdot \chi_m \quad \text{Equation 25}$$

where  $\phi$  is the total porosity and  $\chi_f$  and  $\chi_m$  are the fluid and solid matrix compressibilities (1/Pa).

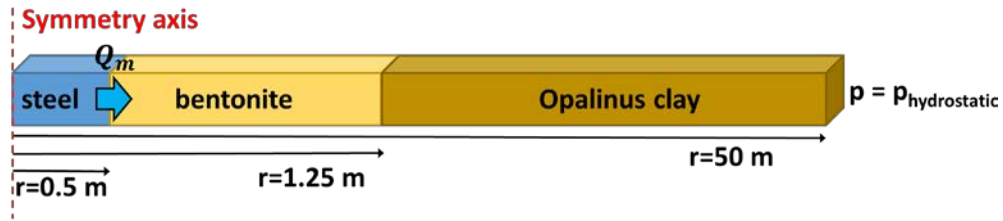


**Figure 19.** Geometry and setup of the 1D axisymmetric calculations in Comsol Multiphysics. The steel is not considered explicitly in the simulations. Instead, a water outflux boundary condition is imposed at the steel-bentonite interface to mimic the effects of the corrosion process on the water consumption rate.

The parameterisation of the model is summarized in Table 4-7 for the reference case. The water retention model used in the simulations follows the Van Genuchten formulation for the water retention curve, its derivative with respect to the capillary pressure ( $C_m$ ), and the relative permeability:

$$S_e = \left(1 + \left|\frac{\alpha p}{\rho g}\right|^n\right)^{-m} \quad (\text{if } p < 0, \text{ else } 1) \quad \text{Equation 26}$$

$$C_m = \frac{\alpha m}{1-m} (\theta_s - \theta_r) S_e^{-m} (1 - S_e^{-m})^m \quad (\text{if } p < 0, \text{ else } 0) \quad \text{Equation 27}$$

$$k_r = \sqrt{S_e} [1 - (1 - S_e^{-m})^m]^2 \quad (\text{if } p < 0, \text{ else } 1) \quad \text{Equation 28}$$

$$m = 1 - \frac{1}{n} \quad \text{Equation 29}$$

In eq. 27,  $\theta_s$  and  $\theta_r$  are respectively the saturated (total porosity) and residual liquid volume fractions.

Calculations were performed considering a hydrostatic pressure at repository depth of 6.5 MPa. This pressure is set as initial condition in the bentonite and OPA domains and also as a boundary condition in the OPA far from the canister (at a radius of 50 m away from the canister). In turn, an outflux boundary condition is set equal to 0.003384 kg/(m<sup>2</sup>·year) in the steel bentonite interface (the steel is not modelled in the simulations), corresponding to a corrosion rate of 1 micron/year.

**Table 4-7.** Parameterization of the reference case for the numerical model of water availability. All data from Senger et al. (2008b) unless otherwise stated.

Parameter	Bentonite	Opalinus clay
Porosity (-)	0.455*	0.137**
Permeability (m <sup>2</sup> )	1.00E-19	1.00E-20
Matrix compressibility (1/Pa)	3.58E-09	1.83E-09
Liquid compressibility (1/Pa)***	4.60E-10	4.60E-10
Residual liquid saturation (-)	0.3	0.5
Initial liquid saturation (-)	1	1
Van Genuchten parameter n (-)	1.82	1.67
Van Genuchten parameter $\alpha$ (1/m)	5.45E-04	5.45E-04

\*Porosity for bentonite corresponds  $1 - \rho_d/\rho_s$  to a dry density ( $\rho_d$ ) of 1500 kg/m<sup>3</sup> (Nagra, 2002) and a grain density ( $\rho_s$ ) of 2755 kg/m<sup>3</sup> (Bradbury and Baeyens, 2011)

\*\* Porosity for Opalinus clay from (Lanyon et al., 2010)

\*\*\*Liquid compressibility of water at 25 °C (e.g. Young and Freedman, 2000)

The effect of the following variables on the water availability was studied in the scoping calculations, see Table 4-8: permeability of bentonite and OPA formation, matrix compressibility, bentonite porosity, water consumption rate (a corrosion rate,  $r_c$ , of 10 microns/year has been considered as a conservative scenario), and initial (hydrostatic) pressure. The low permeability case is representative of a much higher degree of compaction of the bentonite backfill (permeability of  $1 \cdot 10^{-21}$  m<sup>2</sup>) and considers the lowest value for the Opalinus clay permeability range ( $1 \cdot 10^{-21}$  m<sup>2</sup>). With regard to the matrix compressibility, a case in which the matrix has a lower compressibility, equal to the water compressibility, has been calculated as a pessimistic scenario (a lower compressibility yields a smaller storage capacity of the porous medium, see discussion below).

**Table 4-8.** Parameters used in the sensitivity analyses.

Parameter	Reference	Alternative values
Bentonite porosity (-)*	0.455	0.300
Permeability (m <sup>2</sup> ) (bentonite/OPA)	$1.0 \cdot 10^{-19}$ / $1.0 \cdot 10^{-20}$	$1.0 \cdot 10^{-21}$ / $1.0 \cdot 10^{-20}$
Matrix compressibility (1/Pa) (bentonite/OPA)	$3.58 \cdot 10^{-09}$ / $1.83 \cdot 10^{-09}$	$4.60 \cdot 10^{-10}$ / $4.60 \cdot 10^{-10}$
Corrosion rate (microns/year)	1	10
Hydrostatic pressure (MPa)	6.5	3.0



The results are summarized in Table 4-9 and Figure 20. It may be observed from the figure that the consumption of water due to corrosion leads to a decrease in the pore pressure of the fully saturated pores of the bentonite and OPA formation. Note that during this stage water is gradually removed from the pores while the porous medium remains fully saturated. This is due to the storage capacity given by the matrix and fluid compressibilities. As pore pressure decreases, the fluid and the matrix are depressurized. As long as the pore pressure remains positive, the pores will be fully saturated. This is why the results are summarized as a pore pressure drop at the steel-bentonite interface at (almost) steady-state conditions. In all cases analysed, the pressure remains positive and therefore the porous medium is fully saturated. Under fully saturated conditions, the supply of water from the porous medium to the steel canister is not compromised.

The decrease from the hydrostatic pressure occurs at a rate that depends not only on the consumption rate itself, but also on the physical properties of the bentonite barrier, the Opalinus clay, and the fluid: permeability and matrix and fluid compressibility. This is illustrated by the pressure drop for the different cases.

**Table 4-9.** Summary of simulation cases and results of the scoping calculations of water availability for the corrosion reactions (in terms of pressure drop at the steel-bentonite interface). All cases correspond to an initial hydrostatic pressure of 6.5 MPa.

Case ID	Corrosion rate ( $\mu\text{m}/\text{year}$ )	$\kappa_{benton.}$ (m/s)	$\kappa_{OPA}$ (m/s)	$\phi_{benton.}$ (-)	$\chi_m$ (1/Pa)	$\Delta P^*$ (Mpa)
Reference case	1	1.0E-12	1.0E-13	0.455	3.58E-09	0.02
Low permeability ( $\kappa$ )	1	1.0E-14	1.0E-14	0.455	3.58E-09	0.215
Low $\kappa$ & porosity ( $\phi_{benton.}$ )	1	1.0E-14	1.0E-14	0.3	3.58E-09	0.215
Low $\kappa$ , $\phi_{benton.}$ & $\chi_m$	1	1.0E-14	1.0E-14	0.3	4.60E-10	0.24
Low $\kappa$ & $\chi_m$	1	1.0E-14	1.0E-14	0.455	4.60E-10	0.24
High $r_c$ & low $\kappa$ , $\phi_{benton.}$	10	1.0E-14	1.0E-14	0.455	4.60E-10	2.4

\* Pore pressure drop at the steel-bentonite interface after 20,000 years (steady-state reached in most of the cases)

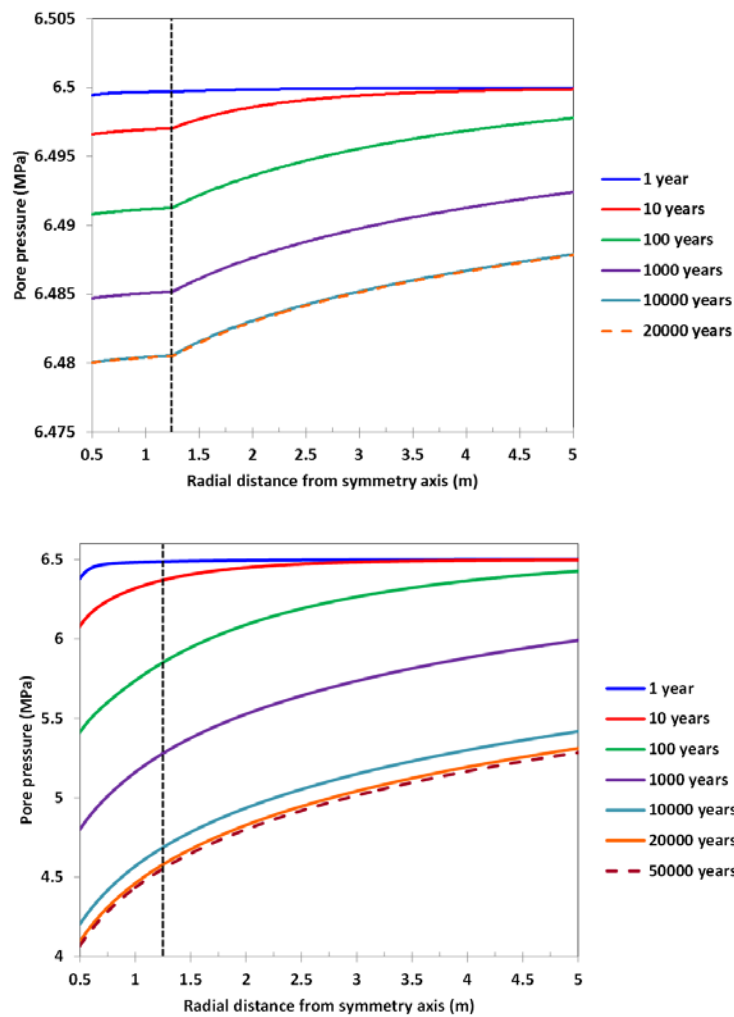


**Figure 20.** Radial profiles of the pore pressure (MPa) for different corrosion times and for two corrosion rates: (top) 1 micron/year (up to 20000 years) and (bottom) 10 microns/year (up to 50000 years). The vertical dashed line represents the bentonite-Opalinus clay interface.

The effect of different bentonite porosities has also been assessed. The reference case with a low hydraulic conductivity ( $1.0 \cdot 10^{-14}$  m/s) was used for this simulation. The results indicate that decreasing the bentonite porosity from 0.455 to 0.3 does not yield any appreciable difference. A porosity decrease is equivalent to a solid volume fraction increase. Therefore, when increasing the solid volume fraction the storage of the porous medium is increased (because the

---

compressibility of the solid is larger than that of the liquid water). However, this effect seems negligible in the present setup.

Increasing the pore compressibility has a similar effect than decreasing the porosity. This is due to the fact that both variables affect the storage term, although in an opposite direction. The storage capacity increases for larger compressibility coefficients. In this way, decreasing the pore compressibility from  $3.58 \cdot 10^{-9}$  1/Pa (Senger et al., 2008) to  $4.6 \cdot 10^{-10}$  1/Pa leads to a higher pressure drop at the steel-bentonite interface.

The simulations indicate that any influence of the water consumption due to corrosion on the corrosion rate itself can be ruled out, at least until a gas phase is formed. Once dissolved  $H_2$  concentration reaches the solubility limit, a gas phase will start to form because the  $H_2$  rate that can be expelled from the system by diffusion is lower than the generation rate (see previous scoping calculation). The presence of the gas phase will reduce the liquid degree of saturation and impact the water flow through the bentonite pore system: the suction (negative pressures) will rise and the liquid relative permeability will be lower than one, resulting in a lower permeability of the bentonite.

### **4.3 Effect of hydrogen consumption by chemical reactions**

In this section, the results of a set of scoping calculations is presented that is aimed to assess the effect of hydrogen consumption by chemical reactions on the reactive transport of hydrogen through the bentonite and Opalinus clay pore water. One dimensional (1D) reactive transport simulations have been conducted using PhreeqC version 3. The system is considered under full water saturated conditions, and transport is limited to Fickian diffusion. The hydrogen source is considered from the chemical reactions of steel corrosion, governed with a kinetic rate corresponding to a corrosion rate of 1 micron/year.

The maximum hydrogen concentration in the liquid phase is given by the solubility limit. Typically, this solubility limit has been calculated using Henry's constant (e.g. Mallants et al., 2007). However,  $H_2$  reactive transport through the bentonite and OPA under the ideal gas assumption can depart considerably from the behaviour that would be observed in practice under repository conditions, especially at high and moderately high temperatures and pressures. For a single component gas phase, the gas-liquid equilibria is given by the relation

$$\varphi P = \gamma H x \quad \text{Equation 30}$$

where  $P$  and  $\varphi$  are the pressure and the fugacity coefficient of the gas, respectively;  $H$  is the partition coefficient (Henry constant);  $\gamma$  is the activity coefficient of the dissolved species; and  $x$  is its molar fraction in the liquid phase. PhreeqC version 3 implements the Peng-Robinson equation of state (EOS) to calculate the gas-liquid equilibria (Appelo et al., 2014). The fugacity coefficient of the gas derived from this EOS is given by

$$\ln(\varphi) = \frac{Pv}{RT} - 1 - \ln\left(\frac{P(v-b)}{RT}\right) + \frac{a \cdot \alpha}{2.828 \cdot b \cdot RT} \ln\left(\frac{v+2.414 \cdot b}{v-0.414 \cdot b}\right) \quad \text{Equation 31}$$

where the EOS parameters  $a$ ,  $b$  and  $\alpha$  can be calculated in terms of the critical temperature ( $T_c$ ) and pressure ( $P_c$ ) of hydrogen, and the acentric factor, as explained by Peng and Robinson (1976) and Appelo et al. (2014). The pressure and temperature dependence of the  $H_2$  fugacity coefficient calculated through this method (dissolution of  $H_2(g)$  in pure water) is shown in Figure 21.

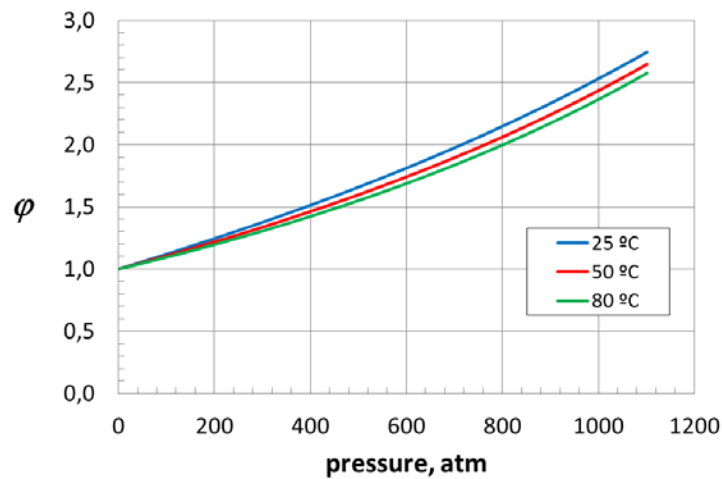


**Figure 21.**  $H_2(g)$  fugacity coefficient calculated according to the Peng-Robinson EOS.

As shown in the above figure, the  $H_2(g)$  fugacity coefficient is greater than 1.0 and increases as the pressure increases and as temperature decreases (in the range 25-80 °C). Therefore, from eq. 31 it is concluded that higher  $H_2$  solubilities will result under real gas conditions compared to the ideal gas assumption (Henry's law). For the pressures (up to 65 atm) and temperatures of interest in this work, the fugacity coefficient will not be significantly different from 1.0. Therefore it is expected that the differences in the results considering the ideal gas assumption or the Peng-Robinson EOS will be small, as shown in the next section (Section 4.3.1).

---

### 4.3.1 Base Case: no consumption

In section 2.2 a wide description of the most relevant chemical reactions contributing to H<sub>2</sub> consumption has been provided. In agreement with that, we defined a base case without H<sub>2</sub> uptake by chemical reactions, and two variant cases that take into account H<sub>2</sub> consumption by pyrite reduction to pyrrhotite and bacterial activity, respectively. Simulations were performed in a one-dimensional reactive transport setup according to the geometry shown in Figure 19. All these cases were run with the code Phreeqc (parkhurst and Appelo, 1999) and the Thermochem database v.8. The key points and assumptions prescribed for the definition of the base case are listed below:

- H<sub>2</sub> is generated in the first cell of the model by steel corrosion at a corrosion rate of 1 μm/y. Fe<sup>0</sup> is the main and only reactive component of steel. Under anoxic conditions steel corrosion proceeds at the expense of water consumption according to reaction 7. However, it is assumed that water is sufficiently available throughout the simulation (supported by the results of Section 4.2).
- Transport of dissolved H<sub>2</sub> is restricted to Fickian diffusion and under fully water saturated conditions. A  $D_{eff} = 5.0 \cdot 10^{-11} \text{ m}^2 \cdot \text{s}^{-1}$  was used in the whole domain. PhreeqC does not allow the use of different diffusion coefficients in one single simulations.
- The formation of a gas phase is allowed in the simulation when the H<sub>2</sub> concentration in the pore water reaches the solubility limit. When the solubility limit is reached in a given part of the modelled domain, the excess H<sub>2</sub> is instantaneously expelled in the gas phase at that particular location.
- The validity of the simulations relies upon the assumption that when the gas pressure build-up is high enough in the vicinity of the steel-bentonite interface, preferential pathways will form for the gas to escape the system.
- These preferential pathways imply that the large majority of the bentonite pores will still be fully water saturated, and in these water saturated pores the transport of H<sub>2</sub> is mainly governed by diffusion.
- The simulation time considered (10 ky) is much larger than the time needed to form a gas phase (10s of years).

- Initial bentonite and OPA porewater compositions are listed in the Table 4-10. They have been considered to be in equilibrium with calcite and siderite.
- The thermodynamic equilibrium between the pair S(VI)/S(-II) was decoupled.

**Table 4-10:** Reference MX-80 bentonite porewater ("D-RBPW") from Curti and Wersin (2002) and OPA porewater at the Benken site (Pearson, 2002).

	Bentonite porewater	OPA porewater
log pCO <sub>2</sub> (bar)	-2.2	-2.2
pH	7.25	7.24
pe	-3.27	-0.167
Ionic strength (eq/L)	0.323	
<b>Dissolved species (mol/L)</b>		
K	1.55·10 <sup>-3</sup>	5.65·10 <sup>-3</sup>
Na	2.74·10 <sup>-1</sup>	1.69·10 <sup>-1</sup>
Ca	1.32·10 <sup>-2</sup>	1.05·10 <sup>-2</sup>
Sr	1.90·10 <sup>-5</sup>	3.04·10 <sup>-4</sup>
Mg	7.64·10 <sup>-3</sup>	7.48·10 <sup>-3</sup>
Mn	2.34·10 <sup>-5</sup>	2.42·10 <sup>-5</sup>
Fe	4.33·10 <sup>-5</sup>	4.33·10 <sup>-5</sup>
Al	1.92·10 <sup>-8</sup>	-
Si	1.80·10 <sup>-4</sup>	1.78·10 <sup>-4</sup>
SO <sub>4</sub>	6.16·10 <sup>-2</sup>	2.40·10 <sup>-2</sup>
CO <sub>3</sub>	2.83·10 <sup>-3</sup>	2.70·10 <sup>-3</sup>
Br	2.40·10 <sup>-4</sup>	2.40·10 <sup>-4</sup>
F	1.67·10 <sup>-4</sup>	1.67·10 <sup>-4</sup>
Cl	1.66·10 <sup>-1</sup>	1.60·10 <sup>-1</sup>
Mn	-	2.42·10 <sup>-5</sup>

Before starting the base case simulation, H<sub>2</sub> diffusion through the modelled domain was checked by running a test case with pure water and no mineral reactions. In this simplified scenario, the only active processes are diffusion and hydrogen solubility limit. Two different approaches were used in order to evaluate the effect of the ideal gas assumption. In Figure 22, H<sub>2</sub> concentrations computed for four selected single cells representative of the different domains (steel-bentonite interface, bentonite, bentonite-OPA interface and OPA) are shown. The results indicate that H<sub>2</sub> saturation conditions in water are only achieved in the steel-bentonite interface. From this interface, H<sub>2</sub> diffuses through the clayey materials. By comparing both approaches, it can be concluded that both approaches yield similar results, being H<sub>2</sub> concentrations slightly higher (5-

10%) when using the Peng-Robinson approach. In all the reactive transport simulations presented in the following, the Peng-Robinson approach has been adopted using PhreeqC version 3.

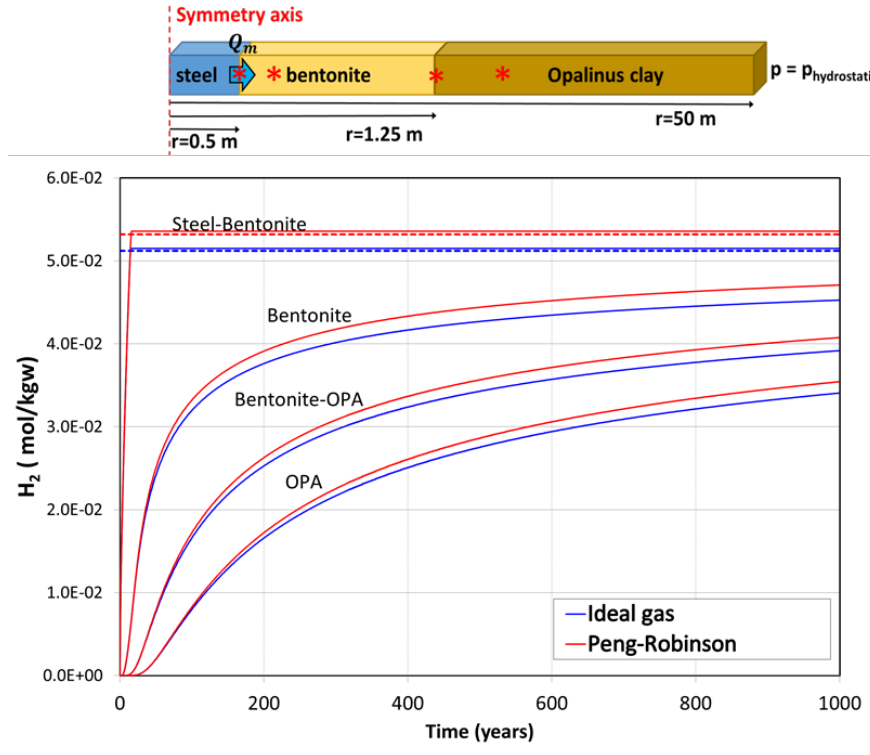


**Figure 22.** Evolution in time of dissolved  $H_2$  in the different domains (4 observation points given in the upper figure): Ideal gas vs. Peng-Robinson EOS. Corrosion rate is  $1\mu\text{m/a}$ . The observation points located in the bentonite and in the Opalinus clay are at 0.8 and 10 m from the symmetry axis, respectively.

The results of the Base Case, i.e. including the chemistry of the bentonite and Opalinus clay but excluding hydrogen consumption, are presented in Figure 23. The results are practically identical to the simplified case with pure water Figure 22. Under the prescribed conditions of our model, water composition does not influence  $H_2$  diffusion through clays. As mentioned before,  $H_2$  concentrations continuously increase in the clayey domains but the  $H_2$  solubility limit is not attained in the computed period of time (10 ky), except in the bentonite close to the steel interface. Figure 24 shows a general picture of the evolution of  $H_2$  concentrations in the whole modelled domain (concentration profiles) at different times.

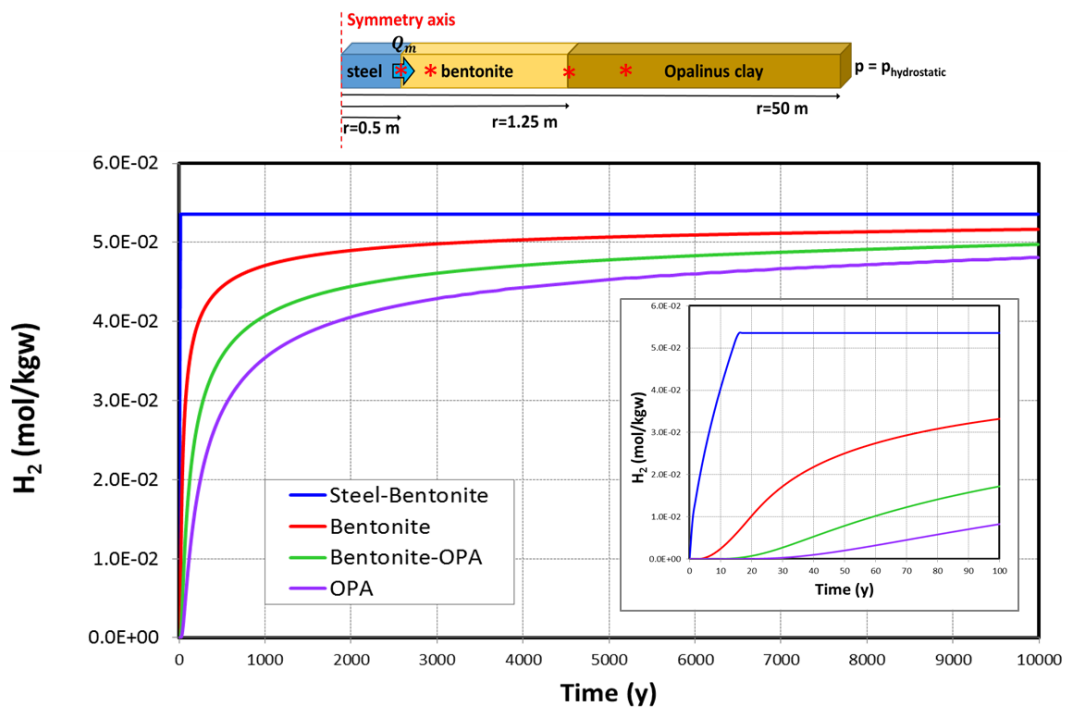


**Figure 23.**  $H_2$  concentrations in the different domains of the 1D reactive transport model. The observation points located in the bentonite and in the Opalinus clay are at 0.8 and 10 m from the symmetry axis, respectively.

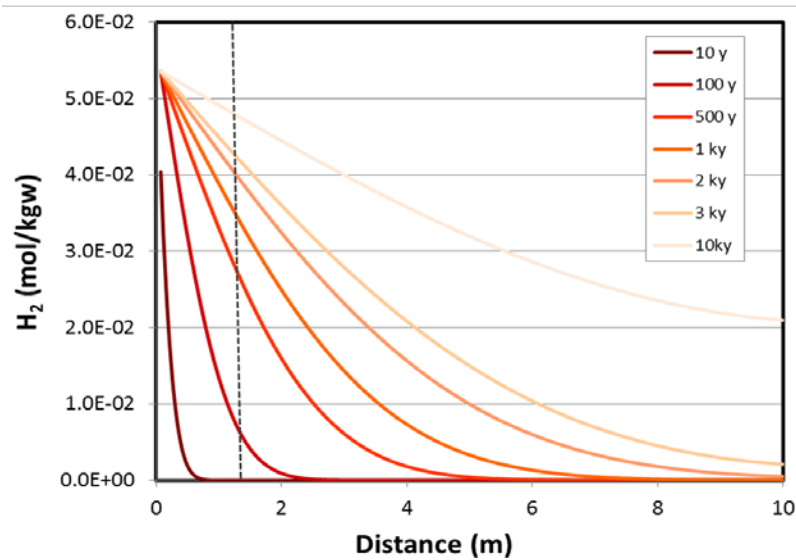


**Figure 24.**  $H_2$  concentrations in the whole domain of the 1D reactive transport model. The vertical dashed line represents the bentonite-OPA interface.



---

### 4.3.2 Hydrogen consumption by pyrite to pyrrhotite reduction

As mentioned in section 2.2.2,  $H_2$  consumption by pyrite reduction to pyrrhotite can be estimated from sulphide production according the eq. 16 and the expression rate proposed by Truche et al., (2010) (eq. 17). Thus,  $H_2$  uptake by this reaction is assumed to be equal to the sulphide production. This kinetic rate provides only an estimation of  $H_2$  consumption taking into account that  $H_2$  was not measured during the experiment and therefore, the stoichiometry of the reaction has not been experimentally established.

With the aim of implementing this process as a variant case, we included the expression rate provided by Truche et al. (2010) in the 1D model defined for the Base Case (see section 4.3.1). Prior to run any simulation, the Phreeqc reaction rate routine was checked by selecting a set of experimental data from Truche et al., (2010) and reproducing with Phreeqc a test case under the defined experimental conditions (Figure 25). A good agreement was found between experimental and modelled data.

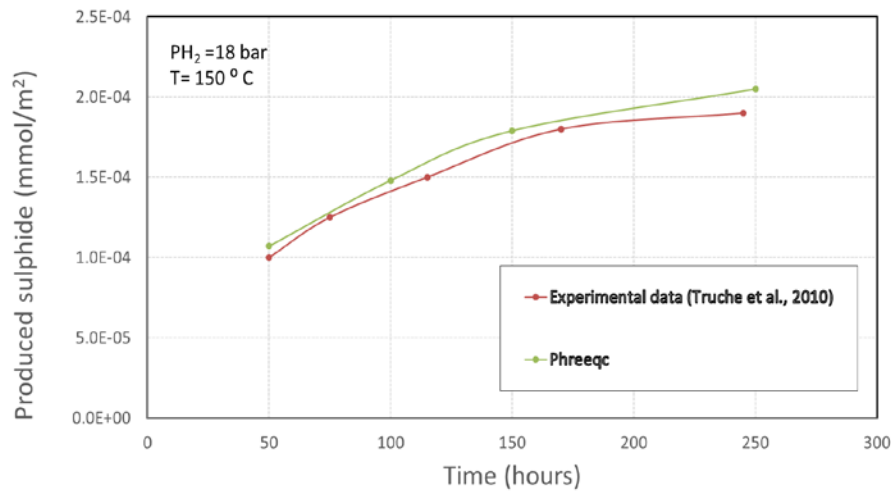


**Figure 25.** Comparison between calculated and modelled sulphide release as a function of time.

As can be seen in the rate expression (eq. 17), sulphide production depends simultaneously of hydrogen partial pressure ( $PH_2$ ) and time. In order to test the time dependence, a fixed  $PH_2$  pressure of 37 and 25 bar have been assumed for bentonite and OPA, respectively. These selected

$P_{H_2}$  correspond to maximum  $H_2$  concentrations computed in both domains at 3ky, respectively. The evolution of the kinetic rate with time is shown in Figure 26. A sharp decrease of the kinetic rate is observed at early times and the attenuation of the reaction continues at longer times. In order to avoid the highest rate values, we considered for these scoping calculations the kinetic rate at 100 ky that corresponds to  $8.0 \cdot 10^{-15} \text{ mol} \cdot \text{m}^{-2} \cdot \text{s}^{-1}$  and  $5.0 \cdot 10^{-15} \text{ mol} \cdot \text{m}^{-2} \cdot \text{s}^{-1}$  for bentonite and OPA, respectively. Surface area in  $\text{m}^2$  refers to pyrite.

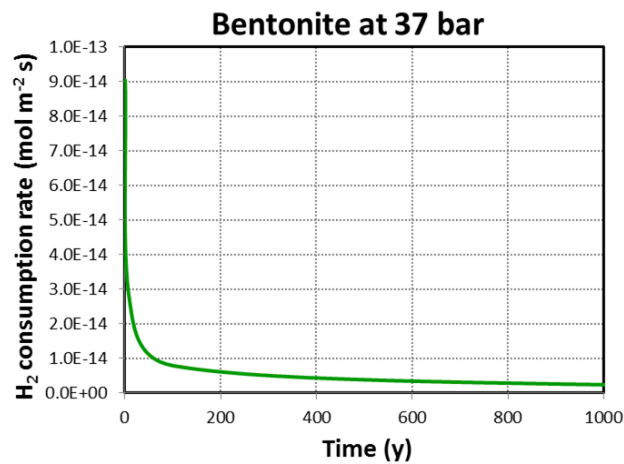


**Figure 26.** Kinetic rate evolution with time for bentonite at a partial pressure of 37 bar.

The conceptual model in which this variant case is based assumes a pyrite concentration of 0.6% wt. in the bentonite and 3 % wt. in OPA according to the mineralogical composition reported by NAGRA (2002) and a pyrite surface area of  $0.16 \text{ m}^2/\text{g}$  (Zheng et al., 2008).

Figure 27 displays the results for one single cell of bentonite as accumulated  $H_2$  consumption over time.  $H_2$  values for OPA are very similar (not shown) and practically overlap those for bentonite. Theoretical values obtained by direct calculation with eq. 17 (page 23) are added in Figure 27 for comparison purposes. In the bentonite, accumulated  $H_2$  consumption rises up to around  $6.0 \cdot 10^{-3}$  moles/kgw in 10 ky. In the OPA and for the same period time, we obtained an accumulated  $H_2$  uptake of  $5.76 \cdot 10^{-3}$  moles/kgw.

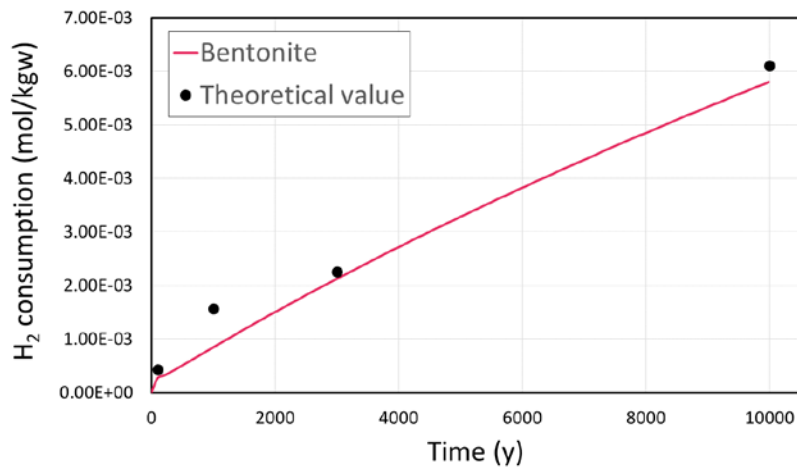


**Figure 27.** Accumulated H<sub>2</sub> consumption in a single cell of bentonite.

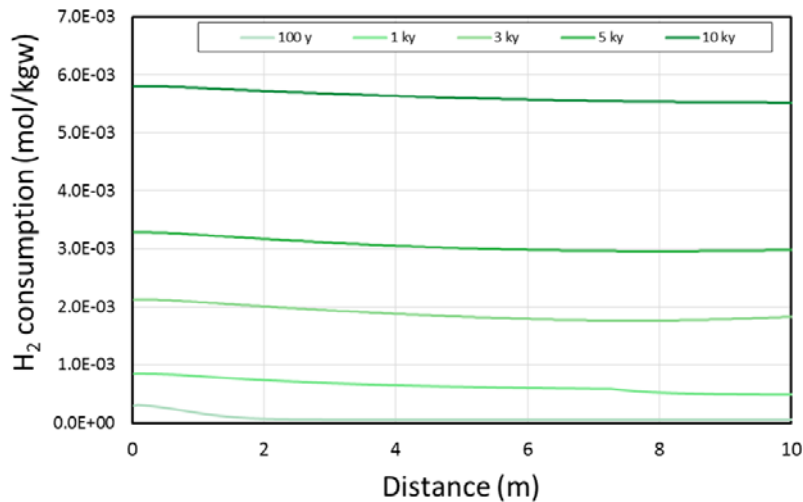


**Figure 28.** Concentration profiles of H<sub>2</sub> consumption in the modelled domain at different times.

According to the results for the whole domain (concentration profiles in Figure 28), H<sub>2</sub> uptake in the short term (<1ky) will remain below  $1 \cdot 10^{-3}$  mol/kgw, as compared to the results in Figure 24 for the Base Case. Even assuming that the reactions described by Truche et al. (2010) are valid at 25 °C and that the process will be active in the clay domain with a 100 % of the available surface area as reactive surface, H<sub>2</sub> consumption by this reaction can not be considered as an efficient sink of H<sub>2</sub> taking as reference the H<sub>2</sub> concentrations diffused from the interface steel-bentonite in the clay domains. In any case, these calculations represent a maximal estimation of H<sub>2</sub> consumption considering that the kinetic rate evolves to lower values between 0.1 and 10 ky.

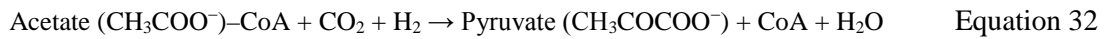
---

### 4.3.3 Hydrogen consumption by microbial activity

The relevance of this process in natural and engineered environments has been discussed in section 2.2.4. The complexity of modelling microbial processes in natural or engineered environments is linked to the lack of proper kinetic and stoichiometric parameters adequately upscaled for model implementation. In addition, in the frame of a nuclear repository, microorganism abundance and activity will be affected by factors such as the supply of nutrients, temperature, energy sources, and pore size of the clay.

The conceptual model considered for this variant case is based on the following assumptions:

- Sulphate-reducing bacteria is the unique microbial community present in porewater
- Microbial reduction of sulphate is considered according to the following reactions:



- Two scenarios were modelled by assuming the presence of sulphate-reducing bacteria in the bentonite and the OPA or only in the OPA. As mentioned in section 2.2.4, bacterial survival in compacted bentonite is questioned by several studies.
- The thermodynamic equilibrium between the pair S (VI) / S (-II) was decoupled and thus, only a kinetic reduction from S(VI) to S(-II) has been allowed.
- The biotic degradation of acetate has been controlled by the growth rate of sulphate-reducing bacteria and by the availability of sulphate following Monod type expressions as shown in Equations 34 and 35. Table 4-11 shows the values of the parameters used for these equations in the model.

$$R^{ED} = -\mu_{ED}^{Mic} \cdot [\text{Microbes}] \cdot \frac{[EA]}{K_{EA} + [EA]} \quad \text{Equation 34}$$

where:

$R^{ED}$  – rate of oxidation of electron donor (ED) due to microbial respiration (mol of ED·L<sup>-1</sup>·s<sup>-1</sup>).

$[EA]$  – concentration of electron acceptor (EA) in mol·L<sup>-1</sup> (SO<sub>4</sub><sup>2-</sup>(aq))

$\mu_{ED}^{Mic}$  – maximum rate of oxidation of ED (mol of ED·mol of biomass<sup>-1</sup>·s<sup>-1</sup>)

$K_{EA}$  – half-saturation constant of EA (mol of EA·L<sup>-1</sup>)

$$r_{net}^{Mic} = -Y^{Mic} \cdot R^{ED} - b^{Mic} \cdot [Microbes] \quad \text{Equation 35}$$

where:

$[Microbes]$  – concentration of biomass (mol of  $C_5H_7O_2N \cdot L^{-1}$ )

$r_{net}^{Mic}$  – net growth rate of microbial biomass (mol of biomass  $\cdot L^{-1} \cdot s^{-1}$ )

$Y^{Mic}$  – specific yield coefficient of microbes (mol of biomass  $\cdot$  mol of ED $^{-1}$ )

$b^{Mic}$  – decay coefficient of microbes ( $s^{-1}$ )

**Table 4-11.** Selected parameters for the Monod equations.

Parameter	Units	Value	Reference
$b^{Mic}$	$s^{-1}$	$1 \cdot 10^{-9}$	Hallberg, 2014, Maia et al., 2014
$Y^{Mic}$	mol biomass/mol <sub>acetate</sub>	$1.411 \cdot 10^{-2}$	Hallberg, 2014, Maia et al., 2014
$K_{EA}$	mol of EA $\cdot L^{-1}$	$1 \cdot 10^{-2}$	Hallberg, 2014, Maia et al., 2014
$\mu_{ED}^{Mic}$	mol $\cdot L^{-1}$	0.0102	Hallberg, 2014, Maia et al., 2014

- An unlimited amount of acetate in the clay domains is computed as the source of carbon.  $H_2$  supplied by diffusion from the interface steel-bentonite is the energy source for microbial reactions.
- Initially, the porewater compositions already used in the base case and listed in Table 4-10 are considered.

One of the most important uncertainties, other than experimental parameters, is linked to the initial amount of biomass present in the bentonite and the OPA. Biomass concentrations ranging from  $1 \cdot 10^{-8}$  to  $1 \cdot 10^{-12}$  mol/L are usually reported in contaminated and non-contaminated natural materials (Sena, 2009) but this wide range can produce contrasted results. Due to the lack of analytical determinations of biomass concentrations in the bentonite and OPA porewaters, a sensitivity analysis was performed to assess the impact of this variable in the  $H_2$  consumption in the Opalinus clay (Figure 29). As predicted, the results show that biomass concentration is a sensitive parameter with a direct impact on  $H_2$  uptake from porewater. From these calculations, an average rate of  $H_2$  consumption of 13.9 nM/h and 0.86 nM/h have been obtained for the cases with  $1 \cdot 10^{-8}$  moles of biomass/kgw and  $1 \cdot 10^{-10}$  moles of biomass/kgw, respectively. From a comparison with the range of rates reported by Harris et al. (2007) for natural environments (0.002 - 2.5nM/h) it can be concluded that a concentrations of  $1 \cdot 10^{-10}$  moles of biomass/kgw is more appropriate for this variant case and this value was used in the scoping calculations.

Figure 30 and Figure 31 display the computed  $H_2$  concentrations for a single cell representative of bentonite and OPA, respectively. The analysis of these results reveals the relevance of microbial activity as a  $H_2$  consumer. In the bentonite (Figure 30), maximal uptake of  $H_2$  is observed during the first 2 ky and then it decreases as a consequence of sulfate consumption. In the OPA (Figure 31) two different cases are shown, one of them by computing microbial activity in the bentonite and the OPA and a second one with sulphate reducing bacteria only in the OPA. Also in this case, maximal  $H_2$  uptake is observed at times shorter than 2 ky with a net  $H_2$  consumption with respect to the Base Case (Figure 30 and Figure 31). This fact can be explained by the supply of sulfate from the bentonite to the OPA domain that increases the concentration of electron acceptors in the system.

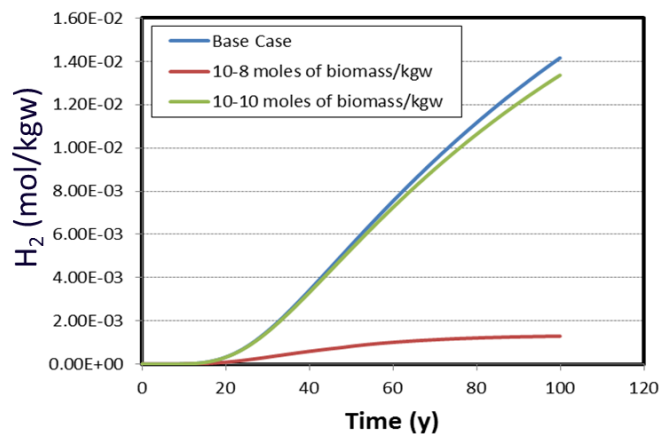


**Figure 29.**  $H_2$  consumption by sulphate-reducing bacteria in the Opalinus clay (same observation point as above). Sensitivity analysis of biomass concentration.

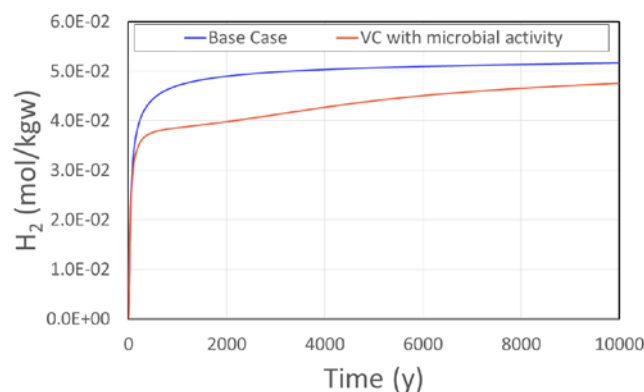


**Figure 30.**  $H_2$  concentrations over time in a single bentonite cell (same observation point as above) for: Base Case (no consumption) and Variant Case (VC, with microbial activity in the bentonite and OPA).

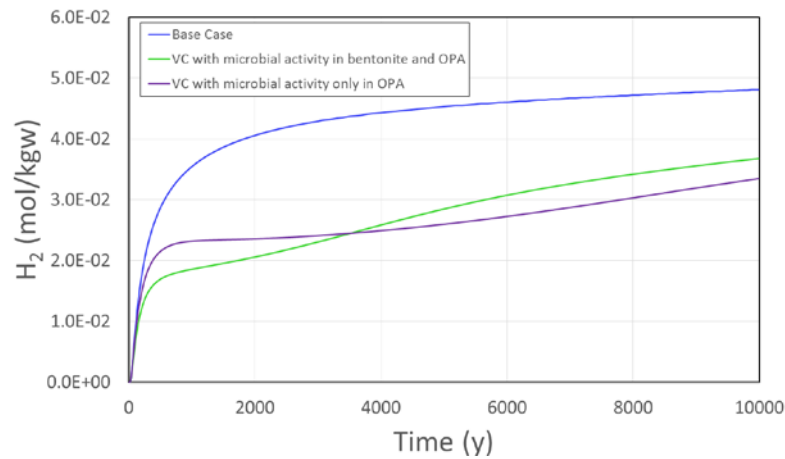


**Figure 31.** H<sub>2</sub> concentrations over time in a single cell of OPA (same observation point as above) for: Base Case (no consumption), Variant Case (VC) with microbial activity only in OPA, and Variant Case (VC) with microbial activity only in both bentonite and OPA.

By comparing the H<sub>2</sub> concentrations in the whole domain with those for the Base Case, the relevance of microbial activity is clearly visible, mainly for times longer than 100 y. It is worth noting that in this model a low concentration of biomass was considered. In consequence, these calculations represent a conservative scenario for H<sub>2</sub> uptake by microbially-mediated sulphate reduction in porewater. As we assumed a continuous bacterial activity over time, H<sub>2</sub> consumption after 2ky depends on the available sulphate concentrations and this will be the limiting factor in the long term (Figure 32).

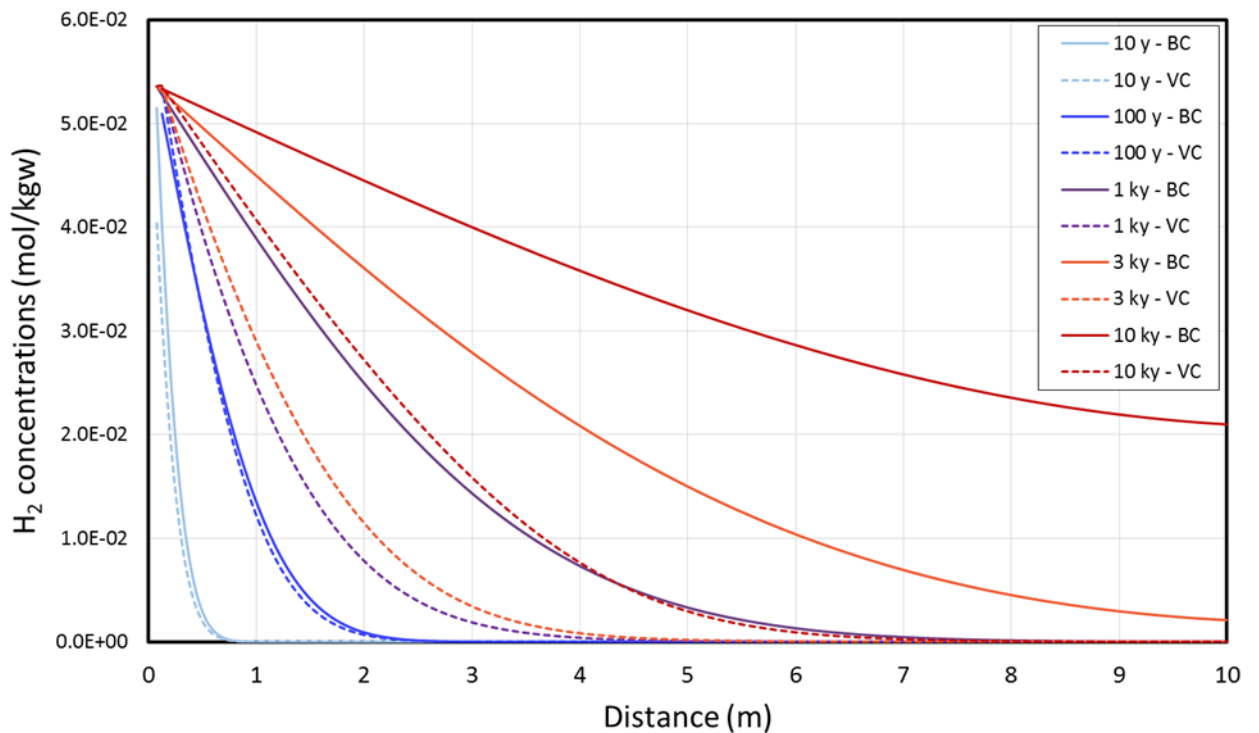


**Figure 32.** Spatial evolution of H<sub>2</sub> concentrations at different times for the Base Case (BC) and the variant case (VC) with H<sub>2</sub> consumption by microbial activity in the bentonite and OPA.

From these scoping calculations it may be inferred that biotic reactions could contribute to reduce the partial pressure of H<sub>2</sub> ( $P_{H_2}$ ) in the bentonite and OPA porewaters. However, it is important to notice that some uncertainties are implicit in our calculations. We are assuming that acetate is permanently available as carbon source and that bacterial activity is permanently maintained over a long period of time. In most of the sediments, organic matter is available for bacteria but a previous degradation process is needed to obtain acetate or lactate available for bacterial growth.

Recently, in the frame of the results obtained in the HT experiment, Vinsot et al. (2014) reported a consumption of 120 mmoles of H<sub>2</sub> and 23 mmoles of sulphate in a period of 100 days. The authors proposed sulphate reduction by microbial activity as the most plausible hypothesis to explain the observed H<sub>2</sub> sink. We have performed an estimation of this process, and this high rate of H<sub>2</sub> consumption (1.2 mmol/day) is only possible if biomass concentrations  $> 10^{-7}$  moles/L are assumed. As this range of biomass concentrations is not common in natural environments, more



---

in situ and laboratory studies are needed to define the real impact of this process in the specific context of this repository.



---

## 5. Conclusions of the scoping calculations and perspectives

The main objective of this work is the assessment of the different geochemically relevant processes able to impact on the sources and sinks of hydrogen in the context of the Swiss HLW geological disposal. To this end, a literature review and a set of scoping calculations have been performed. An important effort has been devoted to construct a sound conceptual model based on the state-of-the-art of H<sub>2</sub> behaviour in water saturated porous media. The methodological approaches used for tackling the different key points provided a quantitative assessment of the role of chemical reactions in the evolution of H<sub>2</sub> concentrations in porewater.

Three processes have been identified as potential H<sub>2</sub> consumers: (1) pyrite reduction to pyrrhotite; (2) microbial activity, and (3) H<sub>2</sub> adsorption onto clays. The first two processes have been assessed with the use of a 1D reactive transport model. The third one is not considered here because this reaction has been experimentally determined under gas saturated conditions which differs significantly from the water saturated conditions considered in this work (no data available under these conditions).

Our results indicate that H<sub>2</sub> consumption by pyrite reduction to pyrrhotite is not a relevant process, since it results in very limited H<sub>2</sub> consumption. In contrast, sulphate reduction by microbial activity may be regarded as a potential relevant consumer of H<sub>2</sub>. The impact of this process will be strongly controlled by the biomass concentration and the availability of nutrients. Our results indicate that H<sub>2</sub> could be significantly consumed by bacterial activity (as shown in Figure 32), provided the environmental conditions are favourable to maintain the reaction over time. However, more studies are needed to well establish the real impact of H<sub>2</sub> consumption by microbes upscaled to the repository conditions.

Regarding the time needed to form a free gas phase, in all the simulations analysed, the formation of a gas phase occurs in a short period of time when compared to the repository time-scale. This time depends almost linearly with the inverse of the corrosion rate in a log-log scale. The effect of higher temperatures is to increase the time needed to form a gas phase due to the enhanced diffusion of dissolved H<sub>2</sub>. The effect of consumption of H<sub>2</sub> due to chemical reactions (pyrite

---

reduction and microbial activity) on the time to form a gas phase is very limited, with an increase of less than 3% for the reference consumption case.

Water consumption due to steel corrosion has also been studied with the final aim to assess water availability for the corrosion process over a long term period. In all the simulations, the pore pressure remains positive, meaning that the liquid degree of saturation is equal to 1. Therefore, the simulations indicate that any influence of the water consumption due to corrosion on the corrosion rate itself can be ruled out, at least until a gas phase is formed. Once dissolved H<sub>2</sub> concentration reaches the solubility limit, a gas phase will start to form (the H<sub>2</sub> rate that can be expelled by diffusion is lower than the generation rate). The presence of the gas phase will reduce the liquid saturation and impact the water flow in the bentonite. As a results, the suction will rise and the liquid relative permeability will be significantly reduced, resulting in a lower permeability of the bentonite. In that scenario, the water availability for the corrosion process could be compromised.

---

## 6. References

- Agg, P. J., 1993. Modelling gas generation in radioactive waste repositories. *Nucl. Energy*, 32, 2, 81-87.
- Andra, 2005. Dossier 2005: Référentiel des matériaux d'un stockage de déchets à haute activité et a vie longue. Tome 1: Matériaux à base d'argiles gonflantes (in French). Andra report C.RP.ASCM.04.0015.A, Châtenay-Malabry, France.
- Appelo, C. A. J., Postma, D., 2009. *Geochemistry, Groundwater and Pollution*. (2<sup>nd</sup> Edition). A. A. Balkema Publishers.
- Appelo, C. A. J., Parkhurst, D. L., Post, V. E. A. 2014. Equations for calculating hydrogeochemical reactions of minerals and gases such as CO<sub>2</sub> at high pressures and temperatures. *Geochimica et Cosmochimica Acta* 125, 49–67.
- Bardelli, F., Mondelli, C., Didier, M., Vitillo, J. G., Cavicchia, D. R., Robinet, J.-C., Leone, L., Charlet, L., 2014. Hydrogen uptake and diffusion in Callovo-Oxfordian clay rock for nuclear waste disposal Technology. *Appl. Geochem.*, 49, 168-177.
- Bosart, P. Wermeille, S., 2003. The stress field in the Mont Terri Region-Data Compilation. Report of the FOWG, Geology Series, N° 4, pp 65-92.
- Blackwood, D. J., Gould, L. J. , Naish, C.C., Porter, F. M., Rance, A. P., Sharland, S. M., Smart, N. R., Thomas, M. I., Yattes, T., 2002. The localized corrosion of carbon steel and stainless steel in simulated repository environments. Report AEAT/ERRA-0318, AEA Technology.
- Bradbury, M. H., Baeyens, B., 1997. A mechanistic description of Ni and Zn sorption on Namontmorillonite. *J. Contam. Hydrol.* 27, 223-248.
- Bradbury M.H., Baeyens B., 2011. Physico-Chemical Characterisation Data and Sorption Measurements of Cs, Ni, Eu, Th, U, Cl, I and Se on MX-80 Bentonite. Nagra Technical Report 09-08.
- Bruha, P., Dovred, D., Polívka, P., Vokal, A., 2010. Preliminary results of hydrogen rate and transport properties in compacted bentonite. FORGE Report D2.2, 34 pp.
- Bush, A., Alles, S., Gensterblum, Y., Prinz, D., Dewhurst, D.N., Raven, M. D., Stanjek, H., Krooss, B. M., 2008. Carbon dioxide storage potential of shales. *Int. J. Greenhouse Gas Control*, 2, 297-308.
- Chambers, A. V., Williams, S.J. Wisbey, S.J., 1995. Nirex safety assessment research programme. Nirex near-field research: report on the current status in 1994. Nirex Science Report S/95/011.
- Charlet, L., 2006. Transfers through the reactive clay barriers in radioactive waste repositories. Surface reactions between Fe<sup>2+</sup> and smectites. In Wersin P. & Mettler S. 2006. Workshop on Fe-clay interactions in repository environments, a joint initiative by Andra, SKB and Nagra. Basel 9-10 May 2006. NAB-06-15. Nagra, Wettingen, Switzerland.
- Charlet, L., Tournassat, C., 2005. Fe(II)-Na(I)-Ca(II) cation exchange on montmorillonite in chloride medium: evidence for preferential clay adsorption of ions pairs in marine environment chemical modelling and XRD profile modelling study. *Aq Geochem* 11, 115-137.
- Croise, J., Senger, R., 1996. GTS-TPF: Analysis of extended gas threshold pressure tests at the Grimsel Test Site for determination of field-scale two-phase flow parameters in the FRI zone, Nagra Internal Report NIB 96-41, Wettingen, Switzerland.
- Curti, E., and Wersin, P., 2002. Assessment of porewater chemistry in the bentonite backfill for the Swiss SF/HLW Repository. Nagra Technical Report NTB 02-09, nagra, Wettingen, Switzerland.

- 
- David, D., 2001. Analogues archéologiques et corrosion-collection sciences et techniques-Matériaux, Publication ANDRA, ISBN 2-9510108-2-6.
- Debruyne, W., Dresselaers, J., Vermieren, P., Kelchtermans, J., Tas, H., 1991. Corrosion of container and infrastructure materials under clay repository conditions. Commission of the European Communities Report, EUR 13667 EN.
- Didier, M., 2010. Étude du transfert réactif de l'hydrogène au sein de l'argilite. Thèse doctoral (in French), Université Joseph Fourier, France.
- Didier, M., Leone, L., Greneche, J.-M., Giffaut, E., Charlet, L., 2002. Adsorption of hydrogen gas and redox processes in clays. *Environmental Science and Technology*, 46, 3574-3579.
- Diomidis, N., 2014. Scientific basis for the production of gas due to corrosion in a deep geological repository. Technical Report 14-21, Switzerland.
- Diomidis, N. and Johnson, L.H., 2014. Materials options and corrosion-related considerations in the design of a canister for the disposal of SF and HLW in deep geological repositories. *European Corrosion Congress. Eurocorr 2012. Book of abstracts*, p. 342.
- Dong, H., Fredrickson, J. K., Kennedy, D.W., Zachara, J. M., Kukkadapu, R. K., Onstott, T. C., 2000. Mineral transformation associated with the microbial reduction of magnetite. *Chem. Geol.*, 169, 299-318.
- Duro, L., Grivé, M., Domènech, C., Roman-Ross, G., Bruno, J., 2012. Assessment of the evolution of the redox conditions in SFR 1. SKB TR-12-12. Svensk Kärnbränslehantering AB.
- Enning, D. and Garrelfs, J. Corrosion of Iron by Sulfate-Reducing Bacteria: New Views of an Old Problem, *Appl. Environ. Microbiol.* February 2014 vol. 80 no. 41226-1236
- Eriksen, T., Jakobsson, A., 1982. Diffusion of hydrogen, hydrogen sulphide and large molecular weight anions in bentonite. SKB KBS TR 82-17.
- Fernández-Prini, R., Alvarez, J. L., Harvey, A. H., 2003. Henry's Constants and Vapor-Liquid Distribution Constants for Gaseous Solutes in H<sub>2</sub>O and D<sub>2</sub>O at High Temperatures, *Journal of Physical and Chemical Reference Data*, 32, 903-916.
- Féron, D., Crusset, D., Gras, J.-M., 2008. Corrosion issues in nuclear waste disposal. *J. Nucl. Mat.*, 379, 16-23.
- Fujiwara, R., Yasutomi, I., Fukudome, K., Tateishi, T., Fujiwara, K., 2001. Influence of Oxygen Concentration and Alkalinity on the Hydrogen Gas Generation by Corrosion of Carbon Steel, *Mat. Res. Soc. Symp. Proc.* 663, 497.
- Fujisawa, R., Cho, T., Sugahara, K., Takizawa, Y., Horikawa, Y., Shiomi, T., Hironaga, M. 1997. The corrosion behaviour of iron and aluminum under waste disposal conditions. *Mat. Res. Soc. Symp. Proc.* 465, Materials Research Society, Pittsburgh, 675682.
- Gajek, A., Zakroczyński, T., 2005. Long-lasting hydrogen evolution on and hydrogen entry into iron in an aqueous solution. *J. Electroanal. Chem.*, 578, 171-182.
- Galle, C., Tanai, K., 1998. Evaluation of Gas Transport Properties of Backfill Materials for Waste Disposal: H<sub>2</sub> Migration Experiments in Compacted Fo-Ca Clay” *Clays and Clay Minerals*, Vol46, No. 5, 498-508.
- García-Gutiérrez, M., Alonso de los Ríos, U., Missana, T., Mingarro, M., Granizo, N., Grivé, M., Gaona, E., Colàs, E., Duro, L., Bruno, J., 2007. Estudio bibliográfico sobre sorción y difusión de radionucleidos en cementos, hormigones y productos de corrosión en presencia de cementos. ENDESA Publicación Técnica de ENDESA 02-2007 (in Spanish).
- Gil, A., Trujillano, R., Vicente, M.A., Korili, S. A., 2009. Hydrogen adsorption by microporous materials based on alumina-pillared clays. *Int. J. Hydrogen Energy*, 34, 8611-8615.

- 
- Gómez-Hernández, J.J., 2000. Technical Note 2000-40: FM-C experiment: Part A) Effective diffusivity and accessible porosity derived from in-situ He-4 tests Part B) Prediction of HE-3 concentration in a cross-hole experiment.
- Grauer, R., Knecht, B., Kreis P., Simpson, J. P., 1991. Hydrogen evolution from corrosion of iron and steel in intermediate level waste repositories. *Mat. Res. Soc. Symp. Proc.*, 212, Eds T. A. Abrajano and Jr. L. H. Johnson, pp 295-302.
- Hallbeck, L., 2014. Determination of sulphide production rates in laboratory cultures of the sulphate reducing bacterium *Desulfovibrio aespoensis* with lactate and H<sub>2</sub> as energy sources. SKB TR-14-14. Svensk Kärnbränslehantering AB.
- Higashihara, T., Sato, S., Ohashi, H., Otsuka, T., 2001. Diffusion of helium and estimated diffusion coefficients of hydrogen dissolved in water-saturated, compacted Ca-montmorillonite. *Genshiryoku Bakuendo Kenkyu*, 7(1), 51-55.
- Harris, S. H., Richard L. Smith, R. L. and Suflita, J. M., 2007. In situ hydrogen consumption kinetics as an indicator of subsurface microbial activity. *Microbiol Ecol* 60 (2007) 220–228.
- Heusler, K.E., Landolt, D., Trasatti, S., 1988. Electrochemical corrosion nomenclature (Recommendations 1988). *Pure & Appl. Chem.*, 61, 19-22.
- Jacops, E., Volckaert, G., Maes, N., Govaerts, J., Weetjens, E., 2012. Determination of gas diffusion coefficients in undisturbed Boom clay. In *Clays in Natural and Engineered Barriers for Radioactive Waste Confinement*, Montpellier, France.
- Jacops, E., Grade, A., Govaerts, J., Maes, N., 2013a. Measuring the diffusion coefficient for He in Opalinus Clay. Mol, Belgium: SCK•CEN, 16 p. (External Report of the Belgian Nuclear Research Centre; ER-238). ISSN 1782-2335.
- Jacops, E., Volckaert, G., Maes, N., Weetjens, E., Govaerts, J., 2013b. Determination of gas diffusion coefficients in saturated porous media: He and CH<sub>4</sub> diffusion in Boom Clay. *Applied Clay Science*, 83–84, 217–223.
- Jin, Q., Bethke, C. M., 2005. Predicting the rate of microbial respiration metabolism. *Am. J. Science*, 307, 643-677.
- JNC2000. H12: Project to establish the scientific and technical basis for HLW disposal in Japan. Japan Nuclear Cycle Development institute, Supporting Report 2, Repository Design and Engineering Technology.
- Johnson, L. H., 2006. Gas production and transport in the near field of SF and HLW repositories in clay and crystalline rocks: processes, uncertainties and performance assessment aspects. D-N° 5.1.6 of the NF-PRO project. EU Contract N° F16W-CT-2003-02389.
- Johnson, A. B., Francis, B., 1980. Durability of Metals from Archaeological objects. *Metal Meteorites and Native Metals*. Report PNL-3198, Batelle Pacific Northwest Laboratory.
- Johnson, L.H., King, F. 2003. Canister options for the disposal of spent fuel. Nagra Technical Report NTB 02-11. Nagra, Wettingen, Switzerland.
- Jozwiak, W.K., Kaczmarek, E., Maniecki, T. P., Ignaczak, W., Maniukiewicz, W., 2007. Reduction behavior of iron oxides in hydrogen and carbon monoxide atmosphere. *Appl. Catal.*, 326, 17-27.
- King, F., 2008. Corrosion of carbon steel under anaerobic conditions in a repository for SF and HLW in Opalinus Clay. Technical Report 08-12. Nagra, Wettingen, Switzerland.
- King, F., 2009. Hydrogen effects on carbon steel used fuel containers. Nuclear Waste Management Organization Technical Report, NWMO TR-2009-29, Toronto, Ontario.

- 
- King, F., Stroes-Gascoyne, S., 2000. An assessment of the long-term corrosion behaviour of C-steel and the impact on the redox conditions inside a nuclear fuel waste disposal container. Ontario Power Generation Nuclear Waste Management Division Report N° 06819-REP-01200-10028.
- King, F., Kolar, M., 2009. Theory manual for the steel corrosion model version 1.0. Nuclear Waste Management Organization Technical Report, NWMO TR-2009-07, Toronto, Ontario.
- Kreis, P., Simpson, J. P., 1992. Hydrogen gas generation from the corrosion of iron in cementitious environments. In *Corrosion Problems Related to Nuclear Waste Disposal*, European Federation of Corrosion Publication Number 7 (Institute of Materials, London), 57-72.
- Kostka, J. E., Nealson, K. H., 1995. Dissolution and reduction of magnetite by bacteria. *Environ. Sci. Technol.* 29, 2535-2540.
- Kurashige, T., Fujisawa, R., Inagaki, Y., Senoo, M., 1999. Gas generation behavior of Zircaloy-4 under waste disposal conditions. *Radioactive Waste Management and Environmental Remediation*. In: ICEM Conference Proceedings, Nagoya, Japan, Sept. 26 – 30, 1999, ASME.
- Kursten B., Cornélis, B., Labat, S., Van Iseghem, P., 1996. Geological disposal of conditioned high-level and long-lived radioactive waste. In situ corrosion experiments. SCK-CEN Report R-3121.
- Kursten B., Van Iseghem, P., 1999. In situ corrosion studies on candidate container materials for the underground disposal of high-level radioactive waste in boom caly. In *Corrosion/99*, NACE Internationals (Houston, TX), paper n° 473.
- Kursten, N., Smailos, E., Azkarate, I., Werme, L., Smart, N.R., Santarini, G., 2003. COBECOMA. State-of-the-art document on the COrrOSion BEHaviour of COntainer MAterials. Final report. European Commission. Contract n° FIKW-CT-20014-20138.
- Lambert, J. M., Simkovich, G., Wlaker, P. L., 1998. The kinetics and mechanism of the pyrite-to pirrhotite transformation. *Metall. Mater. Trans. B29B*, 385-396.
- Lanyon, G.W., Gaus, I., Marschall, P., 2010. *Compilation of Existing Data (Mont Terri)*. FORGE Report D4.3 and D5.2 – VER 1.0
- Lassin A., Dymitrowska M., Azaroual, M., 2011. Hydrogen solubility in pore water of partially saturated argillites: Application to Callovo-Oxfordian clayrock in the context of a nuclear waste geological disposal”, doi:10.1016/j.pce.2011.07.092, Elsevier Ltd.
- Lear, P. R., Stucki, J., 1985. Role of structural hydrogen in the reduction and reoxidation of iron in nontronite. *Clays Clay Miner.* 33, 539-545.
- Lemy, F., Nys, V., Yu, L., Weetjens, Koskinen, K., Olas, F., Wendling, J., Caro, F., Laucoin, E., Dymitrowska, M., Pellegrini, D., Justinavicius, D., Poskas, P., Sellin, P., Altorfer, F., 2010. Summary of gas generation and migration current state-of-the-art. FORGE Milestone M15.
- Maia, F., Puigdomenech I, Roman-Ross, G. and Molinero, J., 2014. Modelling sulphide production rates from laboratory data using lactate and H<sub>2</sub> as energy sources, in preparation.
- Marschall, P., Horseman, S., Gimmi, T., 2005. Characterisation of Gas Transport Properties of the Opalinus Clay, a Potential Host Rock Formation for Radioactive Waste Disposal. *Oil & Gas Science and Technology – Rev. IFP*, Vol. 60, pp. 121-139.
- Marschall, P., Lunati, I. (editors), 2006. Grimsel Test Site – Investigation Phase V. GAM – Gas Migration Experiments in a heterogeneous Shear Zone of the Grimsel Test Site. NAGRA Technical Report NTB 03-11.
- Marschall, P., Lanyon, B., Gaus, I., Rüedi, J., 2013. Gas transport processes at Mont Terri Test Site (EDZ and host rock) – Field results and conceptual understanding of self-sealing processes. FORGE Reports D4.16. 61pp.

- 
- Masum, S. A., Vardon, P. J., Thomas, H. R., Chen, Q., Nicholson, D., 2012. Multicomponent gas flow through compacted clay buffer in a higher activity radioactive waste geological disposal facility. *Min. Mag.* 76, 3337-3344.
- Miller, W. M., Alexander, W. R., Chapman, N. A., McKinley, I. G., Smellie, J. A. T., 1994. Natural analogue studies in the geological disposal of radioactive wastes. Elsevier, *Studies in Environmental Science* 57.
- Motamedi, M.; Karland, O. And Pedersen, K. 1996. Survival of sulphate reducing bacteria at different water activities in compacted bentonite. *FEMS microbiology letters*, 141 83-87.
- Nagra, 2001. Sondierbohrung Benken – Untersuchungsbericht. Nagra Technical Report NTB 00-01, Nagra, Wettingen, Switzerland.
- Nagra, 2002. Project Opalinus Clay. Safety Report. Demonstration of disposal feasibility for spent fuel, vitrified high-level waste and long-lived intermediate-level waste TECHNICAL REPORT NTB02-05.
- Nagra, 2008. Effects of post-disposal gas generation in a repository for low and intermediate-level waste sited in the Opalinus clay of Northern Switzerland. Technical Report 08-07, Switzerland.
- Neretnieks, I., 1985. Some aspects of the use of iron canisters in deep lying repositories for nuclear waste. SKB Technical Report 85-35.
- Neretnieks, I., Skagius, K., 1978. Diffusivity measurements of methane and hydrogen in wet clay (in Swedish). SKB KBS TR 56.
- Norris, S. (ed), 2010. Summary of gas generation and migration: Current state-of-the-art, Euratom 7<sup>th</sup> Framework Project FORGE, available from [www.bgs.ac.uk/forge](http://www.bgs.ac.uk/forge).
- Norris, S. (ed), 2013. Synthesis Report: Updated Treatment of Gas Generation and Migration in the Safety Case, Euratom 7<sup>th</sup> Framework Project FORGE, available from [www.bgs.ac.uk/forge](http://www.bgs.ac.uk/forge).
- Newman, R.C. and Wang, S., 2014. Understanding and quantifying the corrosion of carbon steel in grouts relevant to the Swiss L/ILW Repository – Status Reports 2011 and 2012. Nagra Working Report NAB 12-08. Nagra, Wettingen, Switzerland. Nuclear Energy Agency (NEA), 2001. Gas generation and migration in radioactive waste disposal: safety relevant issues. Organisation for Economic Cooperation and Development, 192 pp.
- OECD/NEA, 2009. Natural Tracer Profiles Across Argillaceous Formations: The CLAYTRAC Project, Radioactive Waste Management, OECD Publishing. Available from <http://www.oecd-ilibrary.org/>.
- Ortiz L., Volckaert G., Mallants D., 2001. Gas generation and migration in Bloom Clay, a potential host rock formation for nuclear waste storage, Elsevier, Nuclear Research Center, Belgium.
- Pedersen, K., 2000. Microbial processes in radioactive waste disposal. SKB Technical Report TR-00-04., Svensk Kärnbränslehantering AB, Stockholm, Sweden.
- Pedersen, K., 2002. Microbial processes in the disposal of high level radioactive waste 500 m underground in Fenoscandian Shield rocks. In: Interactions of microorganisms with radionuclides, Elsevier, p 279-311.
- Pearson, F.J., 2002. Benken reference water chemistry. Nagra Internal Report. Nagra, Wettingen, Switzerland.
- Peng D.-Y., Robinson D. B., 1976. A new two-constant equation of state. *Ind. Eng. Chem. Fundam.* 15, 59–64.
- Pichler, 2003. Assesment of Hydrogen-rock interactions during geological storage of CH<sub>4</sub>-H<sub>2</sub> mixtures. Master Thesis, Department Mineral Resources and Petroleum Engineering, University of Leoben, Austria.



---

Poller, A., Mayer, G., Croisé, J., 2008. Hydrogeologic Analyses and Synthesis (HA) Experiment): Two-phase flow analysis of gas test in Opalinus Clay Core Specimen: Complementary Analysis. Mont Terri Project Technical Report 2007-01.

Puigdomenech, I., Ambrosi, J.-P., Eisenlohr, L., Lartigue, J.-E., Banwart, S.A., Bateman, K., Milodowski, A.E., West, J.M., Griffau, L., Gustafsson, E., Hama, K., Yoshida, H., Kotelnikova, S., Pedersen, K., Michaud, V., Trotignon, L., Rivas-Perez, J., Tullborg, E.-L., 2001. O<sub>2</sub> depletion in granitic media. The REX project. SKB TR-01-05. Svensk Kärnbränslehantering AB.

Pusch, R., 1983. Gas migration through bentonite clay. SKB KBS TR 83-71.

Pusch, R., 1999. Mobility and survival of sulphate-reducing bacteria in compacted and fully water saturated bentonite - microstructural aspects. SKB Technical Report TR-99-30. Svensk Kärnbränslehantering AB, Stockholm, Sweden.

Rivas Perez, J., Banwart, S.A., Puigdomenech, I., 2005. The kinetics of O<sub>2(aq)</sub> reduction by structural ferrous iron in naturally occurring silicate minerals. *Appl. Geochem.* 20, 2003-2016.

Rodwell, W. R., Harris, A. W., Horseman, S. T. Lalieux, P., Müller, W., Ortiz, L., Pruess, K., 1999. Gas migration through engineered and geological barriers for a deep repository for radioactive waste: status report. European Commission Report EUR 19122EN.

Rodwell, W. et al., 2003. A thematic network on gas issues in Safety Assessment of Deep repositories for radioactive waste (GASNET). European Commission, Report EUR 20620 EN, Luxembourg.

Rodwell, W., Norris, S., Cool, W., Cuñado, M., Johnson, L., Mäntynen, M., Müller, W., Sellin, P., Snellman, M., Talandier, J., Vieno, T., Vines, S., 2003. GASNET (2003). Euratom, a thematic network on gas issues in safety assessment of deep repositories for radioactive waste. Final Report on the treatment in safety assessments of issues arising from gas generation.

Romero, E., Senger, R., Marschall, P., Gómez, R., 2013. Air Tests on Low-Permeability Claystone Formations. Experimental Results and Simulations. *Multiphysical Testing of Soils and Shales* (Editors L. Laloui, A. Ferrari). Springer Series in Geomechanics and Geoengineering, pp 69-83.

Rubel, A., Sonntag, C., Lippmann, J., Pearson, F. and Gautschi, A., 2002. Solute transport in formations of very low permeability: Profiles of stable isotope and dissolved noble gas contents of pore water in the Opalinus Clay, Mont Terri, Switzerland. *Geochimica Et Cosmochimica Acta*, 66(8): 1311-1321.

Sagoe-Crentsil, K. K., Glasser, F. P., 1993. Green rust iron solubility and the role of chloride in the corrosion of steel at high pH. *Cement and Concrete Research*, 23, 785-791.

Schenk, R., 1988. Untersuchungen über die Wasserstoffbildung durch Eisenkorrosion unter Endlagerbedingungen. National Cooperative for the Storage of Radioactive Waste Technical Report, Nagra NTB 86-24.

Sena, C., 2009. Numerical modelling of radionuclide migration in near-surface systems. PhD. Thesis. Universidade de Aveiro, Portugal.

Senger, R., Marschall, P., Lavanchy, J.-M., 1997. Gas Threshold Pressure Tests in Deep Boreholes for Determining Two-Phase Flow Properties of the Host Rock at the Proposed L/ILW Repository, Switzerland. *MRS Proceedings*, 506, pp. 829-838.

Senger, R., Marschall, P., Finsterle, S., 2008a. Investigation of two-phase flow phenomena associated with corrosion in an SF/HLW repository in Opalinus clay, Switzerland. *Physics and Chemistry of the Earth*, 33, S317-S326.

Senger, R., Lanyon, B., Marschall, P., Vomvoris, S., Fujiwara, A., 2008b. Numerical modeling of the gas migration test at the Grimsel Test Site (Switzerland). *Nuclear Technology* 164, 155-168.

- 
- Simpson, J. P., 1984. Experiments on container materials for Swiss high-level waste disposal projects, Part II. National Cooperative for the Storage of Radioactive Waste Technical Report, Nagra NTB 84-01. Nagra, Wettingen, Switzerland.
- Simpson, J. P., Schenk, R., Knecht, B., 1985. Corrosion rate of unalloyed steels and cast irons in reducing granitic groundwaters and chloride solutions. *Mat. Res. Soc. Symp. Proc.* 50, 429-436.
- Simpson, J.P. and Valloton, P.-H, 1986. Experiments on container materials for Swiss high-level waste disposal projects, Part III. Nagra Technical Report NTB 86-25. Nagra, Wettingen, Switzerland.
- Simpson, J., Weber, J., 1992. Steel as a container material for nuclear waste disposal. In *Corrosion Problems Related to Nuclear Waste Disposal*. European Federation of Corrosion Publication n°7 (Institute of Materials, London), 43-56.
- SKB 2006a. Long-term safety for KBS-3 repositories at Forsmark and Laxemar – a first evaluation. Main Report of the SR-Can project. SKB TR-06-09. Swedish Nuclear Fuel and Waste Management Co (SKB), Stockholm, Sweden.
- SKB 2006b. Buffer and backfill process report for the safety assessment SR-Can. SKB TR-06-18. Svensk Kärnbränslehantering AB, Stockholm, Sweden.
- Smart, N.R., Blackwood, D.J., 1998. An investigation of the effects of galvanic coupling on the corrosion of container and waste metals in cementitious environments. AEAT-0251, issue C.
- Smart, N. R., Blackwood, D. J. and Werme, L.O., 2001. The anaerobic corrosion of carbon steel and cast iron in artificial groundwater. SKB Technical Report TR-06-44. Svensk Kärnbränslehantering AB, Stockholm, Sweden.
- Smart, N. R., D. J. Blackwood, Werme, L. O., 2002a. Anaerobic corrosion of carbon steel and cast iron in artificial groundwaters: Part 1 – electrochemical aspects. *Corrosion* 58, 547-559.
- Smart, N.R., D.J. Blackwood, Werme, L.O., 2002b. Anaerobic corrosion of carbon steel and cast iron in artificial groundwaters: Part 2 – gas generation. *Corrosion* 58, 627-637.
- Smart, N. R., Rance, A. P., Werme, L.O., 2004. Anaerobic corrosion of steel in bentonite. *Mat. Res. Soc. Symp. Proc.* 807, 441-446.
- Smart, N., Hoch, A. R., 2006. A survey of steel and zircaloy corrosion data for use in the SMOGG gas generation model. Serco report SA/ENV-0841.
- Stroes-Gascoyne, S., Hamon, C. J., Dixon, D. A., Martino, J. B., 2007. Microbial analysis of samples from the tunnel sealing experiment at AECL's Underground Research Laboratory. *Phys. Chem Earth*, 32, 219-231.
- Stumm, W., Morgan, J. J., 1996. *Aquatic chemistry, chemical equilibria and rates in natural waters*. 3<sup>rd</sup> ed., New York, Wiley.
- Taniguchi, N., Kawasaki M., Kawakami, S., Kubota, M., 2004. Corrosion behaviour of carbon steel in contact with bentonite under anaerobic condition. In *Prediction of Long Term Corrosion in Nuclear Waste Systems*. Proc. 2<sup>nd</sup> Int. Workshop, Nice, September 2004 (European Federation of Corrosion and Andra), p. 24-34.
- Taniguchi, N., Kawasaki, M. and Naito, M., 2010. Corrosion behavior of carbon steel in compacted bentonite saturated with simulated groundwater under anaerobic conditions. *Corrosion Engineering*, vol. 59, pp. 330-345.
- Tournassat, C., 2003. Cations-clays interactions: the Fe(II) case. Application to the problematic of the French deep nuclear repository field concept. PhD thesis, University of Grenoble, France, 199 p.

- 
- Truche, L. Berger, G., Destrigneville C., Pages, A., Guillaume, D., Giffaut, E., Jacquot, E., 2009. Experimental reduction of aqueous sulphate by hydrogen under hydrothermal conditions: Implications for the nuclear waste storage. *Geochimica et Cosmochimica Acta*, 73, 4824-4835.
- Truche, L. Berger, G., Destrigneville C., Guillaume D., Giffaut, E., 2010. Kinetic of pyrite to pyrrhotite reduction by hydrogen in calcite buffered solutions between 90 and 180° C: Implications for nuclear waste disposal. *Geochimica et Cosmochimica Acta*, 74, 2894-2914.
- Vinsot, A., Appelo, C.A.J., Lundy, M. Wechner, S., Lettry, Y., Lerouge, C., Fernandez, A.M., Labat, M., Tournassat, C., De Canniere, P., Schwyn, B., Mckelvie, J., Dewonck, S., Bossat, P. and Delay, S., 2014. In situ diffusion test of hydrogen gaz in the Opalinus Clay. In *Clays in Natural and Engineered Barriers for Radiactive Waste Confinement*, Norris et al (Eds.). The Geological Society of London.
- Vokál, A., Bhuha, P., Dobrev, D., Polívka, P., Silber R., 2007. A study of anaerobic corrosion of carbon steel, Deliverable 2.3.8, NF-PRO project, August 2007.
- Volckaert, G., Ortiz, L., De Cannière, P., Put, M., Horseman, S.T., Harrington, J.F., Fioravante, V., and Impey, M., 1995. MEGAS: Modelling and experiments on gas migration in repository host rocks, Final Report-Phase 1. European Commission, Report EUR 16235.
- Volckaert, G., Mallants, D., 1999. De gasproblematiek bij het Bergen van radioactief afval in een diepe geologische berging in de klei van Boom, SCK CEN-R-3287.
- Wada, R., Nishimura, T., Fujiwara, K., Tanabe, M., Mihara, M., 1999. Experimental study on hydrogen gas generation rate from corrosion of Zircaloy and stainless steel under anaerobic alkaline conditions, Radioactive Waste Management and Environmental Remediation, In ICEM Conference Proceedings, Nagoya, Japan, Sept. 26 – 30, 1999, ASME.
- Wersin, P., 2003. Geochemical modelling of bentonite porewater in high-level waste repositories. *J. Contam. Hydrol.* 61, 405-422.
- Wersin, P., Spahiu, K., Bruno, J., 1994. Time evolution of dissolved oxygen and repository conditions in a HLW repository. SKB Technical Report TR-94-02. Svensk Kärnbränslehantering AB, Stockholm, Sweden.
- Wersin, P., Birgersson, M., Olsson, S., Karnland, O., Snellman, M., 2007. Impact of corrosion-derived iron on the bentonite buffer within the KBS-3H disposal concept – the Olkiluoto Site as Case Study. POSIVA 2007-11.
- Wersin, P., Kiczka, M., Rosch, D., 2014. Safety Case for the Disposal of Spent Nuclear Fuel at Olkiluoto Radionuclide Solubility Limits and Migration Parameters for the Backfill. POSIVA 2012-40. Posiva Oy.
- Wiltowski, T., Hinckley, C., Smith, G., Nishizawa, T., A., Saporoschencko, M., Shirley, R. H., Webster, J. R., 1987. Kinetics and mechanisms of iron sulphide reduction in hydrogen and carbon monoxide. *J. Solid State Chem.* 71, 95-102.
- Young, H.D., Freedman, R.A. (editors), 2000. *Sears and Zemansky's University Physics*, 10<sup>th</sup> Edition, Addison-Wesley.
- Zheng, L., Samper, J., Montenegro, L., Mayor, J. C., 2008. Multiphase flow and multicomponent reactive transport model of the ventilation experiment in Opalinus clay. *Physics and Chemistry of the Earth*, 33, S186-S195.

ENSI 33/463

ENSI, CH-5200 Brugg, Industriestrasse 19, Telefon +41 56 460 84 00, E-Mail [Info@ensi.ch](mailto:Info@ensi.ch), [www.ensi.ch](http://www.ensi.ch)